DEVELOPING LEVITATION LASER-FUSED GLASSES AS PROXIES FOR LOWER MANTLE EXPERIMENTS: A METHODOLOGICAL APPROACH

Thomas Edwards zur Loye

Submitted to the faculty of the University Graduate School
in partial fulfillment of the requirements
for the degree
Master of Science
in the Department of Earth Sciences,
Indiana University

June 2019

Accepted by the Graduate Faculty of Indiana University, in partial fulfillment of the requirements for the degree of Master of Science.

Master's Thesis Committee

_____
Catherine Macris, PhD, Chair

_____
Andrew Barth, PhD

_____
Kathy Licht, PhD

ACKNOWLEDGEMENT

I would like to express my gratitude to my advisor, Dr. Catherine Macris, for her guidance and patience throughout the entirety of this research. Her constant support proved invaluable, for which I am forever grateful. I also extend special thanks to my committee members, Dr. Andrew Barth and Dr. Kathy Licht, for their unyielding guidance and encouragement, both with my research and during my time at IUPUI.

Thank you to the National Science Foundation, whose funding has made this research possible (NSF-EAR Grant 1664553). I would like to thank Dr. Susannah Dorfman and Alison Farmer at Michigan State University for conducting the electron probe microanalysis of the Fe-bearing samples, as well as Dr. Dorfman's guidance, advice, and use of the samples this research produced.

I am thankful to Craig Lundstrom at the University of Illinois Urbana-Champaign for both his instruction and allowing me the use of the scanning electron microscope. I would also like to thank Rick Weber, Anthony Tamalonis, and Oliver Alderman of Materials Development, Inc. for their support and advice concerning the operation of the aerodynamic levitation laser furnace, which was integral to the success of this research.

I am grateful for the unyielding support and encouragement of my family. I give special thanks to John Shukle for his friendship, as well as coding and coffee breaks along the way. Working together on Shiny applications and coding projects has been a fantastic experience so far, and will continue to be for years to come.

This research would have been impossible without the support of the IUPUI Graduate School and the IUPUI Department of Earth Sciences, and I express my gratitude to those agencies.

Preface

The following work is separated into two main sections, both of which aim to improve upon the current state of methods and available tools for their respective applications. The first chapter addresses the development of a specific methodology, finessed over the course of many iterations, each of which is described in detail. This methodology details the synthesis of glasses with the chemical compositions of the main minerals in the mantle: $(Mg, Fe)_2SiO_4$ (olivine) and $(Mg, Fe)SiO_3$ (pyroxene). This process ensures the production of compositionally accurate and homogeneous glasses using an aerodynamic levitation laser furnace. These glasses will act as lower mantle environment proxies used in high pressure experiments.

The second chapter details the creation of two different web applications, coded in the programming language R. The first application, LaserPlot, takes the output file from the aerodynamic levitation laser furnace and distills vital information, runs calculations, creates informative plots, and outputs a table of useful information and plots which enhance the efficiency and accuracy of data synthesis and regression for levitation experiments. The second application, RockR, is a collaborative project between myself, John Shukle, and Jeremiah Mickey. It was built as a teaching tool that enables the plotting of data onto a wide variety of pre-rendered classification and discrimination diagrams, which are commonly used in the geosciences. Although these plots are widely used, their free availability is limited. RockR addresses these issues, aiming to improve upon the available solutions, designed in a classroom-friendly manner that includes links to relevant literature and

explanations of plot types with the intent to improve understanding as well as functionality.

These three projects – the glass synthesis methodology, LaserPlot, and RockR – all complement each other, such that LaserPlot and RockR both enhance the methodology by distilling and detailing sample levitation conditions and facilitating the graphical representation of the semi-quantitative and quantitative compositional analyses. The tabular output file produced from each levitation experiment can be analyzed by LaserPlot, which calculates and collects important characteristics of each levitation experiment. The ternary and bivariate plotting capabilities of RockR allow for simple and streamlined plotting processes. The bivariate diagrams are used to display the Mg-pyroxene and Mg-olivine compositions, which contain SiO_2 and MgO components. The ternary diagrams enable the plotting of the Fe-bearing pyroxenes, which contain SiO_2, MgO, and Fe_2O_3 components.

Thomas Edwards zur Loye

DEVELOPING LEVITATION LASER-FUSED GLASSES AS PROXIES FOR LOWER MANTLE EXPERIMENTS: A METHODOLOGICAL APPROACH

Observations of heterogeneities in Earth's mantle motivate studies of mantle phase assemblages with variable composition. As samples cannot be directly collected from these regions, synthetic glasses can act as analogues for mantle melt and starting materials for high-pressure synthesis of stable mantle minerals in experiments. Here, I develop a specific methodology to produce homogeneous glasses that accurately span the composition space from enstatite ($MgSiO_3$) to forsterite (Mg_2SiO_4), as well as Fe-bearing enstatite ($(Mg_{0.1}Fe0_{.9})SiO_3$ and $((Mg_{0.95}Fe_{0.05})(Si_{0.95}Fe_{0.05})O_3$) with variable oxidation states. This study systematically tests and iterates upon glass synthesis methods using an aerodynamic levitation laser furnace, in which a spherical glass sample levitates on a gas stream flowing vertically through a conical nozzle, while being heated from above with a 400 W CO_2 laser. With sample diameters of 0.6-2.0 mm, shutting off the laser results in supercooling of levitated spheres at rates between 350 and 1350 °C/s. Sample preparation begins with grinding and mixing pure oxide powders in an agate mortar and pestle, followed by heating in a high temperature oven to devolatilize the mixture. Powders (0.5-7 mg aliquots) are fused into spheres in a copper hearth plate. To tune Fe valency and vitrify each sphere, samples are then levitated on flows of Ar, O_2, 5% CO in Ar, 5% CO_2 in Ar, or combinations of two of these gases, while being heated with the laser to temperatures above the liquidus for each composition for ~10 s before quenching. After x-ray diffraction (XRD)

analyses confirm vitrification, a dual polish is applied, exposing parallel flat polished surfaces for scanning electron microscope (SEM) and electron probe microanalyzer analyses (EPMA). Back-scattered electron images and energy-dispersive x-ray spectroscopy (EDS) analyses of the spheres are obtained first on the SEM to gauge compositional accuracy and homogeneity, then EPMA analyses determine quantitatively the samples' compositions. Once fully characterized, these glasses can be used in diamond anvil cell experiments, where they can act as proxies for an otherwise inaccessible area of the Earth. In addition to the development of this methodology, two web applications produced during this research aid in visualization of both data logs and analytical results.

Catherine Macris, PhD, Chair

TABLE OF CONTENTS

List of Tables

List of Figures

List of Abbreviations

BSE..... Backscatter Electron Detection

CMB..... Core-Mantle Boundary

EDS..... Energy Dispersive X-Ray Spectroscopy

EPMA..... Electron Probe Micro-Analysis

LOI..... Loss on Ignition

PID..... Proportional-Integral-Derivative

SEM..... Scanning Electron Microscopy

TAS..... Total Alkali vs Silica

WDS.....Wavelength Dispersive Spectroscopy

XRD..... X-Ray Diffraction

Chapter 1: Laser-Fused Levitation Glasses

1.1 Introduction

Deep Earth seismic wave speed variations have shown heterogeneities in the mantle, specifically near the core-mantle boundary (CMB), likely due to either compositional differences or to phase changes (Auzende et al., 2008; Lee et al., 2004; Lee et al., 2008; Murakami and Bass, 2011; Williams and Garnero, 1996). $(Mg,Fe)_2SiO_4$ (olivine) and $(Mg,Fe)SiO_3$ (pyroxene) compositions constitute approximately 85% of the upper mantle and their high pressure equivalents are believed to make up the majority of the lower mantle (Anderson, 1977). Experimental petrologists and mineral physicists working on problems in the deep Earth use these compositions for starting materials in multi-anvil and diamond-anvil cell experiments, which can reproduce pressures and temperatures equivalent to those in the lower mantle.

1.1.1 Objective

The goal of this research is to develop a specific methodology, which consistently produces homogenous glasses with the chemical compositions of the minerals enstatite ($MgSiO_3$), forsterite (Mg_2SiO_4), and Fe-bearing enstatites ($(Mg_{0.9}^{II}Fe_{0.1})SiO_3$ and $(Mg_{0.95}^{III}Fe_{0.05})(Si_{0.95}^{III}Fe_{0.05})O_3$). Glasses, rather than their crystalline counterparts, are desirable as starting materials for high pressure experiments because they maintain compositional homogeneity to a micron scale, and are easily converted to high-pressure minerals assemblages in the diamond anvil cell. By establishing a reliable and repeatable method of making these glasses,

deep Earth petrologists and geophysicists can have consistent starting materials to use in these high-pressure experiments, where they can test various theories about deep mantle processes, conditions, and materials.

1.1.2 Background

The process of creating glasses of known composition begins with oxide powders, which are fused by low-power laser heating into mm-sized spheres. These spheres are levitated in gas flows, heated above their liquidus, and cooled at fast rates to vitrify rather than crystallize the final products. Some background information is necessary in order to understand the transition between molten material and glasses versus molten material and crystalline solids. Melts can be categorized according to their 'strength.' The strength of a melt is a relative measurement of the rate of structural relaxation within the glass transition. The glass transition represents a range of temperatures during which a liquid-like structure changes to a solid-like structure or vice versa and structural relaxation theory concerns the relaxation state of the medium through this transition (Calas et al., 2006; Dingwell and Webb, 1990; Dingwell, 2006,; Moynihan et al., 1974; Mysen and Richet, 2005).

Liquid and glassy states are defined as relaxed and unrelaxed, respectively. At temperatures above the glass transition, the relaxed liquid is in equilibrium. Within the glass transition, the fluid falls out of equilibrium and achieves a partially-relaxed state. The end of the glass transition, and the beginning of the glassy state, is marked by the temperature at which the rate of structural relaxation change slows to the

degree that it effectively ceases to change on an experimental time scale (Henderson et al., 2006; Moynihan et al., 1974). The internal structure of the resultant glass mirrors that of the melt at the fictive temperature (T_f), which represents the temperature at which the melt was last in equilibrium or the instant before the melt entered the glass transition. This temperature is directly affected by the rate at which the melt cools, where slower cooling rates result in lower T_f and faster cooling rates result in higher T_f. The more gradual the cooling rates are, the more time is allowed for the melt to adjust and maintain equilibrium as cooling progresses (Calas et al., 2006; Moynihan et al., 1974).

Melts with very gradual structural relaxation changes over the course of large glass transition temperature ranges are characterized as "strong" melts, while melts with more abrupt changes in structural relaxation over the course of small glass transitions are characterized as "fragile" or "weak" melts (Tangeman et al., 2001; Kohara et al., 2004). As the temperature decreases, the internal structure is constantly rearranging itself, trying to maintain equilibrium. T_f is reached when the kinetics of the structure are no longer able to keep up with the cooling rate. The stronger melts show more gradual changes in viscosity, and T_f can be achieved at lower temperatures. Fragile melts, on the other hand, present with much faster changes in viscosity and require higher cooling rates to keep them from maintaining equilibrium, which would result in them crystallizing (devitrifying) rather than cooling to an amorphous glass (vitrifying) (Stebbins, 2016). When fragile melts are cooled at slower rates, the internal structure becomes more ordered very quickly (Fig. 1). When the structure snaps into place and crystallization is achieved, a

process called recalescence occurs, which is the release of the latent heat of crystallization when a melt becomes a crystalline solid in the glass transition (Debenedetti & Stillinger, 2001; Miura et al., 2010; Miura et al., 2011; Moynihan, 1995; Nagashima et al., 2006; Nagashima et al., 2008; Tangeman et al., 2001; Webb, 1997; Weber & Benmore, 2017). Recalescence is the primary barrier to fragile melt vitrification, avoided by achieving fast enough cooling rates, relative to the glass transition temperature range.

1.1.3 Oxygen Fugacity

The availability of free oxygen in a system is the driving factor for valency. For this research, the availability of oxygen is particularly important with respect to iron, which is the 4th most common element in the Earth's crust and occurs naturally in 3 different oxidation states: Fe^0, Fe^{2+}, and Fe^{3+} (Frost, 1991). At atmospheric pressure and assuming ideal gas behavior, this unit can be measured as the partial pressure of oxygen (x_{O2}). However, when considering geologic applications and investigating systems with pressures much greater than 1 bar, x_{O2} is no longer an accurate assessment of the oxygen availability. For such conditions, oxygen fugacity (f_{O2}) is considered. The f_{O2} variable is a unit of pressure and is often used with reference to buffers, which are represented as curves that highlight temperature-dependent f_{O2} values where specific minerals are stable in natural systems (Fig. 2). With respect to temperature, lower f_{O2} correlates with reducing Fe conditions and higher with oxidizing Fe conditions, while the lowest f_{O2} encourages the production of metallic Fe (Frost, 1991; Johannes and Holtz, 1996).

When conducting experiments synthesizing materials, f_{O2} can be controlled within a high temperature environment at atmospheric pressure. This method was developed in 1945 by Darken and Gurrey and is commonly used for iron-bearing systems. Gases like CO/CO_2 or H_2/CO_2 are mixed in specific ratios and, as the experiment occurs at atmospheric pressures and high temperatures, the partial pressures are interchangeable with f_{O2} (Holloway and Wood, 1988). As a result, the partial pressures can be controlled by the gas flow rates of the individual gases in the mix.

1.1.4 Previous Research

Prior to the use of aerodynamic levitation techniques, glass synthesis methods utilized platinum wire loops or alumina, platinum, or graphite containers to support samples, and have had three main issues (Fig. 3). First, this process caused contamination of the sample, as iron oxide reacted with the container or wire support. The result was iron and oxygen leaching from the sample and altering its intended composition (Grove, 1981; Holloway and Wood, 1988; Merrill and Wyllie, 1973; Pack et al., 2010; Roskosz et al., 2006). Second, this container problem restricted the rates of supercooling, which resulted in devitrification of weak or fragile melts like forsterite (Weber et al., 1993; Weber, 2010; Benmore and Weber, 2017). The third main issue was that contact points between the sample and the container/wire became nucleation points, which resulted in radial fan-shaped crystallization patterns extending outward (Nagashima et al., 2006).

After the development of the aerodynamic levitation laser furnace by D. A. Winborne and P. C. Nordine (Winborne et al., 1976) came the additional development of the conical nozzle laser (CNL) (Coutures et al., 1990) (the components of the model used in this research will be discussed in detail in section 1.2.2). The instrument was used primarily for materials development interests (e.g. aluminum oxides, ceramic superconductors, and reflective glass coatings) (Weber et al., 1994; Weber et al., 2002; Weber, 2010), in-situ melt structural analyses using noncontact diagnostic instruments (e.g. nuclear magnetic resonance spectroscopy (NMR), x-ray diffraction (XRD), x-ray absorption near-edge structure spectroscopy (XANES), and neutron diffraction) (Alderman et al., 2017b; Mathiak et al., 2005; Poe et al., 1992; Weber et al., 2014), chondrite and chodrule synthesis (Miura et al., 2010; Miura et al., 2011; Nagashima et al., 2006; Nagashima et al., 2008; Pack et al., 2010), and silicate glasses (Alderman et al., 2017b; Tangeman, et al., 2001; Weber et al., 2014; Wilding et al., 2004).

1.2 Methods

1.2.1 Overview

The methods section begins with a detailed description of the parts of the laser used in this research. The section continues to detail the individual steps of the glass synthesis and analysis methodology, the creation and subsequent testing of which is the primary focus of this research. Each step lead to the formation of glass spheres with specific chemical compositions. The following sections will provide a thorough explanation of the individual steps needed to begin with pure oxide powders and

end with analyzing glass samples. The glass synthesis methodology began with stock solution oxide powders, which were weighed out in stoichiometrically-determined ratios, ground down to the point that all the individual powder grains are approximately the same size, and baked (heated in a high temperature oven) to remove volatiles from the mixture.

The mixture was then portioned out into concave depressions of a copper hearth plate and heated with a laser at low power until the powder grains fused together into spheres. These spheres were levitated on gas flows and heated with the same laser to temperatures above their liquidus, and were then cooled by turning off the laser. Due to their small volumes and surface areas, the samples (mostly) supercooled and vitrified rather than crystallizing. After vitrification, parallel surfaces of the glasses were ground down to expose the interior of the spheres. The upper surface was polished to a grit size of 0.25 μm, which is optimal for semi-quantitative and quantitative analyses. XRD analyses were used to determine whether a sample was amorphous or crystalline. Semi-quantitative scanning electron microscopy (SEM) combined with energy dispersive x-ray spectroscopy (EDS) analyses were used to quantify the elemental ratios within a given area on a sample and quantitative electron probe micro-analysis (EPMA) analyses were used to do the same analysis as the SEM, but to a higher degree of accuracy and precision.

1.2.2 Aerodynamic Levitation Laser Furnace

To fully understand the processing steps of the methodology, it is important to have a detailed description of each part of the aerodynamic levitation laser furnace,

which is the primary instrument used in this glass synthesis research. The individual parts of this assemblage include: laser (Fig. 4 A), laser hearth (Fig. 5), levitation chamber (Fig. 4 B), gas mixing valves (Fig. 4 C), optical pyrometer (Fig. 4 D), and video camera (Fig. 4 E).

1.2.2.1 Laser

This system uses a Synrad i401 400 Watt continuous-wave CO_2 laser, which is an embedded class 4 laser that is configured for class 1 laser operation (Fig. 4 A). The laser beam alignment is controlled by molybdenum mirrors, which result in the beam being directed vertically down into either the laser hearth or levitation chamber and a low-power visible laser parallels this path for user tracing and alignment control during use. Adjustable focusing optics allow for different laser power densities to be directed at the sample, in addition to the laser power controlled by the user within the operational software.

1.2.2.2 Laser Hearth

The laser hearth is a chamber which is enclosed on all sides, except for a circular opening in the front and two horizontal slits opposite each other and adjacent to the opening at the front (Fig. 5). The opening at the front has a glass piece which fits onto the outside, resting on the two screws jutting outward near the base. Placement of this glass piece closes an interlock switch, which is part of the safety fault system for the laser. The slits on either side of the chamber allow two hearth rods to extend outward from a copper hearth plate (containing sample powders)

(Fig. 6) within the center of the chamber. The hearth rods give the user control of the placement of the hearth plate within the chamber while the laser is in use and a guide tracer beam, similar to what is used in laser pointers (section 1.2.2.1), shows the user where the CO_2 laser beam will strike the plate so that the user can know where the heating will begin and can move the hearth plate accordingly.

1.2.2.3 Levitation Chamber

The levitation chamber is constructed out of vacuum-grade non-magnetic steel and is an interlocked chamber, within which the user can control the atmosphere via the gas mixing valves (described in section 1.2.2.4) that pass up and through an aluminum alloy conical nozzle in the center of the chamber (Fig. 7). The chamber has six potential openings, each of which is manually sealed with either glass lenses and clamps or non-magnetic steel covers and clamps. Two of the openings extending perpendicularly from the chamber to the left and right (Figs. 4 B and 7) have 25 mm ports and could be used for external instrumentation, but neither was used at any point in this research. The two openings extending horizontally and adjacent to the 25 mm ports – facing the user and extending away from the user – have 50 mm ports. The port extending away from the user remained sealed and unused throughout this research. The port facing the user has a glass lens covering it when closed, and is the window through which the levitation experiments are viewed (through welder's glass to protect the users' eyes). When open, this port is used to insert and remove samples for the levitation experiments. The two openings directed at 45° angles to the left and right from the chamber have glass lens

covering the openings and act as windows for the optical pyrometer (section 1.2.2.5; Fig. 4 D) and video camera (1.2.2.6; Fig. 4 E).

1.2.2.4 Gas Mixing Valves

The graphical user interface allows for control over the ratio between two gas compositions (Fig. 8 A), and the flow rate to be channeled upward vertically through an aluminum alloy divergent conical nozzle, which can be seen inside the chamber in Fig. 7. Two gas inputs come through the individual gas mixing valves, before joining and directing a single gas flow mixture (Figs. 4 C and 8 B) through the conical nozzle.

1.2.2.5 Optical Pyrometer

The sample temperature during laser heated experiments is measured using an integrated Chino IR-CAS near-infrared optical pyrometer with a close-up lens attachment. This is directed at the sample location through the left 45° angle port of the levitation chamber (Figs. 4 D and 9). The device has a field of view of 0.6 mm, requiring it to be manually adjusted to be aimed at the sample prior to levitation experiments.

1.2.2.6 Video Camera

The video camera is a digital Point Grey camera, which is directed at the sample location through the right 45° angle port of the levitation chamber (Figs. 4 B and 10). The camera allows the user to view the sample during levitation. As the

temperature of the sample increases and the emitted light becomes more intense, the camera automatically adjusts the exposure and maintains sample visibility.

1.2.3 Powder Preparation

The first step in the process of synthesizing glasses with the chemical compositions of the mantle's chief constituents is powder preparation. In this study, this was achieved by combining predetermined ratios of high-purity oxide powders, such that the mixture was equivalent to the intended composition of the glass (Edgar, 1973; Holloway and Wood, 1988). Puratronic stock solution powders of SiO_2, MgO, Fe_2O_3, and ^{57}Fe doped Fe_2O_3 with respective purities of 99.995%, 99.995%, and 99.998%, were weighed out in stoichiometric ratios to recreate the desired minerals' formulas (Table 1).

Each individual powder was ground under acetone in an agate mortar and pestle using irregular and non-repeated patterns when moving the pestle (Holloway and Wood, 1988). The solution was ground into a slurry and grinding continued until all the acetone evaporated. The dry powder was then scraped back together and the process was repeated. The time from when the acetone was added and grinding commenced until all the acetone evaporated will henceforth be called one session. Each stock solution was ground for three sessions of 20 minutes, then the powders were combined, and the solution was ground for one session of 20 minutes. The resulting powder was baked in a high temperature oven to fully dehydrate/devolatilize the mixture. The oven temperature increased at 100 °C/hour until 800° C was reached, where it remained constant for 1 hour. The powder was

then stored in a desiccator to minimize absorption of water vapor from the air (Edgar, 1973).

1.2.4 Laser Fusing

The powder mixture must be fused into spheres, in order to be capable of levitating within a concentrated vertical gas flow. In section 1.3.2, the evolution of this portion of the methodology will be expanded upon. The process began with 0.5-7.0 mg aliquots of sample powder, which were each placed in one of the twelve evenly-dispersed concave depressions of a copper hearth plate (Fig. 6). This plate was then positioned within the aerodynamic levitation laser furnace's laser hearth (described in section 1.2.2.2; shown in Fig. 5). Two small rods attached to opposite sides of the hearth plate allowed the user to move the plate during the fusing process.

The powder in each depression on the hearth plate was heated with the laser at power levels of 9% to 9.5% (corresponding temperatures could not be recorded within the hearth chamber) for ~10 second intervals, while the plate was moved in small circles to facilitate formation of spheres from the powder mixture. Laser power levels of 10.5 or higher resulted in loss of sample material through vapor being release from the sample surface, while laser powers of 8.5 or lower either left the powder unaltered or merely singed it. As the powder fused together, the concavity of the depression and the movement pattern caused the hardened, fused portions to fall onto the remnant powder. This process transformed the loose

powder mixture into approximately spherical samples. Fused sphere diameters were measured with calipers to a precision of 10 microns (Table 2).

1.2.5 Levitation

The next step involved the levitation and vitrification of the fused spheres using appropriate gas compositions and temperatures. The spheres were vitrified using the levitation chamber (described in section 1.2.2.3) of the aerodynamic levitation laser furnace (Fig. 4 B). Samples were levitated on flows of Ar, O_2, 5% CO in Ar, 5% CO_2 in Ar, or combinations of two of these gases (Figs. 11 A), flowing upward through a conical nozzle (Figs. 11 B and 11 C). While being levitated and enveloped by these flowing gases, samples were heated with the laser (Figs. 11 D and 11 E) to temperatures above the liquidus (Figs. 12 A and 12 B) of each composition for approximately 10 second intervals. Quenching occurred by shutting off power to the laser which, due to the very small surface areas of the spheres, resulted in most of the samples supercooling and vitrifying rather than crystallizing (Fig. 12 C).

1.2.6 Polishing

After vitrifying the synthetic glasses, they needed to be ground down to expose the interior of the sphere, and polished to facilitate XRD, SEM, and EPMA compositional analyses, which required planar surfaces without marring or scratches. In order to achieve polished surfaces on these small spherical samples, a systematic process was developed. Details of the evolution of this process will be expanded upon in section 1.3.3, culminating in the process summarized here. Glass

spheres were adhered to carbon tape in an aluminum dish within the inner ring of a polytetrafluoroethylene washer (0.25" thick, 0.141" outer diameter, 0.062" inner diameter) (Fig. 13). The remaining vacant space around the sample was filled with Dentsply Caulk Orthodontist Powder. A single drop of Dentsply Caulk Orthodontist Resin was applied to the powder and left to sit for an hour, during which time the resin hardened and formed a temporary epoxy, holding the sample in place within the washer. Both sides of the washer/sample were ground down using silicon carbide CarbiMet abrasive pads of various grit-sizes. Following grinding to expose flat, parallel surfaces on two sides, the surfaces were polished on microcloths sprayed with diamond suspensions.

The initial grinding steps required the application of high purity deionized water to silicon carbide pads. Four abrasive pads with increasingly fine grit sizes of 240, 320, 600, and 800, and with respective approximate grain sizes of 52, 35, 15, and 13 microns were used. Between each of the abrasive pad grit sizes, the sample was sonicated in water to remove residual grit and was then dried using a compressed tetrafluoroethane gas duster spray. Smaller samples, where maintaining a controlled grip on the sample during the compressed air drying method was in question, were placed on chem wipes and allowed to dry on their own after sonicating.

Polishing steps used MetaDi Supreme polycrystalline diamond suspension grit sizes of 6 μm, 3 μm, 1 μm, and 0.25 μm. The diamond suspension solutions were each applied to separate microcloths. Of the two exposed flat surfaces on the spheres, one side received only a coarse polish of the 240 grit-sized abrasive, while

the other plane was polished with increasingly fine grit sizes culminating in 0.25 μm polycrystalline diamond suspension. As was the case with the silicon carbide pad steps, the washer/sample was sonicated in water between diamond suspension solution polishes to remove residual grit grains and debris.

After the final polish, samples were viewed with a stereoscopic binocular microscope to confirm clean, unscratched surfaces. The polished glasses were removed from the temporary epoxy by sonicating the washer/sample in acetone, which reacts with and dissolves the dental resin that was previously holding the sample within the bounds of the washer. Once free of the resin, samples were sonicated in isopropanol, as acetone residue can be a source of contamination in both SEM and EPMA.

1.2.7 X-Ray Diffraction

Two forsterite synthesis experiments yielded samples that presented with surface textural variations, giving a 'crumpled' appearance instead of smooth surfaces (Figs. 14 A and 14 B), which required XRD analyses to refute or confirm that the source of the difference was devitrification (growth of crystals upon cooling) (Edgar, 1973). This was achieved using a Bruker D8 Discover XRD. Using both Vantec and LynxEye detectors, XRD analyses identified the presence or absence of internal crystalline structures, represented in the form of Bragg's peaks. The Vantec detector assesses a larger active area and analyzes the sample more quickly than the LynxEye detector, but the latter produces a more accurate analysis. XRD analyses were performed on glasses which showed both crumpled and smooth

surfaces. The amorphous structure of the glasses was confirmed by both the absence of identifiable Bragg's peaks and a very broad and shallow background, centered near the crystalline compositional equivalent 2Θ distance (Fig. 15). XRD analyses were utilized to determine the relationships between amorphous state and smooth surfaces versus crystalline state and anomalous exterior textures.

1.2.8 Scanning Electron Microscopy

Compositional accuracy and homogeneity within each synthetic glass sample, and among samples of the same intended composition, were assessed by both backscatter electron detection (BSE) and EDS on a TESCAN VEGA3 SB SEM at the University of Illinois – Urbana-Champaign. Prior to analysis, a thin carbon layer was applied to the samples using carbon sputtering in a vacuum chamber to reduce charging by creating a conductive surface. BSE images showed compositional variations by contrast differences in grayscale images. EDS results were collected by point analysis, with 3-4 points per sample, approximately evenly spaced between the center and outer edge of each sample (Fig. 17). EDS results (Tables 3 and 4) were collected as oxide ratios, and instrumental accuracy was ensured using a Materials Research Lab block olivine standard.

1.2.9 Electron Probe Micro-Analysis

Using a Cameca SX100 EPMA from the University of Michigan, glass compositions were determined with greater accuracy than the SEM data. Si, Mg, and Fe contents were analyzed by wavelength dispersive spectroscopy (WDS). Element

counts were calibrated using synthetic standards of Al_2O_3 for O, $FeSiO_3$ for Si and Fe, and forsterite for Mg, with the Fe counts being collected on multiple spectrometers and aggregated.

1.3 Evolution of Methodology

This section will detail the various iterations of each step of the methodology outlined in section 1.2. Through the course of this research, a specific methodology was formed that consistently created compositionally accurate and homogeneous glasses. In order to finesse this process, the different steps underwent changes that ranged between subtle and significant. The following will describe the different attempts that were made, both successful and unsuccessful. These procedures shaped the evolution of the final methodology (section 1.2).

1.3.1 Powder Preparation

The powder preparation step laid the foundation for the research. It began with stock solution oxide powders (SiO_2, MgO, and Fe_2O_3), each of which was a primary constituent of the mineral compositions for Mg_2SiO_4 (olivine) and (Mg, Fe)SiO_3 (pyroxene). These powders were weighed in stoichiometric ratios according to their intended composition and the resulting mixture was used for each of the following steps of the methodology. There were three different methods used in the evolution of the powder preparation step: A, B, and C. Each of these steps will be described below.

1.3.1.1 Method A

The first mixing method used a twist action shaker. This machine functioned in a manner similar to a ball mill, except that the shaking was less vigorous and the arm holding the container in place was fashioned as a pair of vice grips. This machine was used to mix the Puratronic powders of SiO_2, MgO, Fe_2O_3, and ^{57}Fe doped Fe_2O_3, held within sealed high-density polyethylene (HDPE) wide-mouth bottles (Alderman et al., 2017). Early attempts resulted in some of the powder sticking to the side of the container. Given that the MgO powder was a slightly finer grain size than the SiO_2 powder, it seemed plausible that this sticking would be counterproductive to the goal of thorough mixing. Using a ceramic ball inside the container resulted in material becoming packed against the sides and bottom of the container, rather than continually dislodging the material and reducing the grain size variation of the mixture. Special care and attention were put into keeping the individual stock solution powders from clumping together or to the sides of the HDPE wide-mouth bottles.

The twist action shaker mixing process was put through test runs, systematically altering duration, the angle at which the container was held, and the speed of the shaker, relative to full speed. The judgment of each scenario was whether it resulted in fine material sticking together on the side or bottom of the container. Operating the shaker at speeds above ½ speed always resulted in clumping, as did runs at ½ speed for durations above five minutes. Changing the angle of the container within the grasp of the shaker had no noticeable impact. Running the machine at ¼ speed resulted in less material sticking together, improving as duration increased. The

final settings – container held upright, twist action shaker operating at ¼ of the full potential speed, and durations varying between 1 ½ minutes to 4 ½ minutes – resulted in all the material remaining loose within the container, with no preferential clumping or sticking.

1.3.1.2 Method B

The next iteration of the mixing technique aimed to address the grain size variation, which was restricting thorough mixing of the Puratronic stock solution powders of SiO_2, MgO, Fe_2O_3, and ^{57}Fe doped Fe_2O_3. This consistent grain size reduction was accomplished by grinding under acetone for 10-minute sessions in an agate mortar and pestle. To reduce the SiO_2 grains to the size of the MgO and Fe_2O_3 grains, so the SiO_2 powder underwent two grinding sessions, followed by three grinding sessions of all the Puratronic powders mixed together (SiO_2 and MgO for enstatite and forsterite; SiO_2, MgO, and Fe_2O_3 for the Fe-bearing enstatites). The final mixture was then placed in a high temperature oven under the same conditions as in methods section 1.2.4.

1.3.1.3 Method C

This method of the powder preparation step represents the final and most successful method, which is why it is the same as what is outlined in the methods section 1.2.4.

The final iteration of the powder preparation step began with the same weighing of Puratronic stock solution powders of SiO_2, MgO, Fe_2O_3, and ^{57}Fe doped Fe_2O_3 with

respective purities of 99.995%, 99.995%, and 99.998%, based on stoichiometric ratios (Table 1). Each individual stock solution powder was ground under acetone in an agate mortar and pestle moving the pestle in non-repeated patterns (Holloway and Wood, 1988). The solution was ground into a slurry, continuing until all the acetone evaporated. The dry powder was then scraped back to the middle of the mortar and the process was repeated. The time from the addition of the acetone until the evaporation of acetone represented one session. Each stock solution was ground for three sessions of 20 minutes, then the powders were combined, and the solution was ground for one session of 20 minutes. The resulting mixture was baked in a high temperature oven to fully dehydrate/devolatilize the mixture.

1.3.2 Laser Fusing

The powder mixtures (methods were described in section 1.3.1) had to be fused together into spheres, which could later be levitated within a vertical gas flow. Methods A and B of this section will expand upon the evolution of the laser fusing process, within the scope of the overall methodology. This process began with the addition sample powder into concave depressions on a copper hearth plate (Fig. 6). This plate was then positioned within the aerodynamic levitation laser furnace's laser hearth, with hearth rods fitted into slots on opposite sides of the hearth plate that facilitated the movement of the plate during the fusing process (Fig. 5). The individual allotments of powder were heated with the laser and the hearth plate was moved in small circles to encourage the formation of spheres as the powder fused together.

1.3.2.1 Method A

When fusing the powders into spheres, a range of initial powder masses were used with the expectation that the specific amounts would correlate with the diameter of the sphere produced. This was not always the case and initial powder masses greater than ~8 mg resulted in waste. Initial amounts of ~9-15 mg resulted in only a small portion of the powder fusing together, leaving behind a significant amount of residual powder in the depression of the hearth plate. Laser power during the powder fusion varied between 9% and 12% (corresponding temperatures could not be recorded within the hearth chamber), where values less than 9% did not cause the powder to fuse, but left a burnt discoloration. Using higher laser powers resulted in samples releasing tendrils of smoke, indicating loss of material, which would have altered the final composition of the samples.

The fused spheroids were seldom perfectly spherical, as was intended. They ranged between teardrop shapes, bean-like shapes, and other irregular, misshapen forms. The uneven and irregular fused samples were not stable in the gas flow, proving more likely to wobble and sometimes stick to the side of the nozzle during the levitation laser-heating process, potentially altering their final composition via loss of material due to contact with the nozzle. In an attempt to improve the sphericity of the fused samples, some were introduced into an air-driven mill, which was adapted from the original design of Bond (1951) (borrowed from John Hughes) (Nitkiewicz and Sterner, 1988). This involved placing the spheroid in a small, cylindrical chamber with interior walls that were covered in a coarse, abrasive

material (a strip of sandpaper). A small inlet to the chamber had a tube, which directed a jet of compressed air into the chamber. Gaps between the top and bottom panels and the cylinder portion of this tool allowed the incoming air to escape. This directed air flow caused the sphere to bounce along the rough cylinder walls, with the expectation that this pattern of movement would cause an evenly-dispersed abrasion and a more spherical resulting shape. The more extremely misshapen samples often became pressed against the top or bottom panels, rather than being agitated within the chamber as was intended. The abrader tool did improve the sphericity of samples which were imperfect, but already mostly spherical forms. This tool was deemed unnecessary for this process, as the mostly-spherical samples did not suffer the same difficulties during levitation as the more irregular forms.

1.3.2.2 Method B

This iteration of the laser fusing process is the same as what is outlined in the methods section 1.2.4.

This iteration of the laser fusing process began with 0.5-7.0 mg aliquots of sample powder, placed in evenly-dispersed concave depressions on a copper hearth plate (Fig. 6). This plate was then positioned within the aerodynamic levitation laser furnace's laser hearth (Fig. 5), where two guiding rods were attached to opposite sides of the hearth plate. These allowed the user the ability to move the plate in small circular motions during the fusing process, which encouraged the loose powder to fuse together into spheres. The powder in each depression on the plate was heated with the laser at power levels of 9% to 9.5% for ~10 second intervals,

where power levels of 10.5 or higher caused loss of sample material and power levels of 8.5 or lower did not have enough heat top fully fuse the powder together.

1.3.3 Polishing

The glass spheres vitrified during the levitation process (section 1.3.2) underwent a polishing before they could be analyzed with the XRD, SEM, or EPMA. The earlier methods of this process resulted in a single polished surface, which was acceptable for analysis with a low-vacuum SEM, but a dual polish was necessary for the other analysis techniques. The dual polish involved a coarse grinding step, on the opposite side from the polished surface, to create a base on which the sample rested (Fig. 18). The top surface was polished to a grit size of 0.25 μm, and being parallel to the base ground plane, ensured a level surface on which the sample could rest. This flat resting surface was necessary for the different analytical techniques. The polishing process underwent several alterations and improvements through the development of the glass synthesis methodology. The evolution of the polishing procedure stemmed from changes to the type of temporary epoxy which was used and the material (container or mold) within which the temporary epoxy was contained.

1.3.3.1 Method A

The initial temporary epoxy used for these glass samples was Crystalbond 509, which came as a soft, but solid, rod. Using the plastic handle of a screwdriver, fragments were removed by controlled blunt-force percussion. These pieces were

then placed in an aluminum dish, and then another aluminum dish was placed on top, trapping the flakes between the two layers. The same tool was then used to make small and soft taps on the base of the top dish, resulting in the powdering of the Crystalbond 509 without contamination or loss of material. A separate aluminum dish was set aside to provide a stage for the remainder of the polishing preparation. Care was taken to keep the base of the dish free from scratches or bends and a square of double-sided carbon tape adhered to the bottom of the inside of the dish. The crushed powder was poured into the inner diameter of the epoxy mold in use (which will be addressed further in this section), making sure to coat the carbon tape surface, thus avoiding the formation of bubbles or weakened structural integrity. The aluminum dish, along with the epoxy mold, Crystalbond 509, and sample, was placed on a hot plate and heated to 121° C until fully melted. It was then removed from the hot plate and left to sit for an hour. Once the Crystalbond 509 had cooled and hardened completely, the aluminum dish and carbon tape were peeled off, leaving a cylindrical puck of temporary epoxy, with the glass samples secured in place.

Epoxy molds with an inner diameter of 22.00 mm, an outer diameter of 25.30 mm, and a height of 18.90 mm, which will hence be referred to as Epoxy Mold 1, were adhered to double-sided carbon tape on an aluminum dish, with two glass samples evenly spaced within the inner diameter of the cylinder. The initial plan was to remove the puck, then to polish the top and bottom sides. The height of the cylinder made polishing both sides, without the removal of the puck, an unnecessary time drain. Cutting the cylinder to an appropriate height had the added risk of not

maintaining parallel planes, which was the primary purpose of the dual polish. Issues were encountered when removing the puck from the cylinder. Epoxy Mold 1 held tightly and stuck to the Crystalbond 509, resulting in the puck breaking in half or fracturing on the edges after pressure was applied to it. Epoxy Mold 1 was replaced by Epoxy Mold 2, with an inner diameter of 24.85 mm, an outer diameter of 29.15 mm, and a height of 30.95 mm. Assisted removal of the puck from both Epoxy Mold 1 and Epoxy Mold 2 was attempted using "PTFE Release Agent Dry Lubricant" (described as a "PTFE"-like spray), but this was counterproductive and resulted in the development of a film, which caught on and stuck to the cylinders and the puck and further hindered its removal. This cylinder allowed for the puck to be removed cleanly and without damage to the puck. However, when attempting to polish the glass sample using the uncontained puck, the heat from the friction of polishing caused the hardened temporary epoxy to warp out of shape, rendering it useless. Unable to polish parallel planes of glass sample, the top plane was polished and the sample remained secured within the puck during low-vacuum SEM analysis. This was a temporary fix to allow for sample analysis while the methodology continued to evolve, as the whole puck could not be used in high-vacuum SEM analysis or Mössbauer spectroscopy.

1.3.3.2 Method B

Brass molds with an outer diameter of 6.35 mm, an inner diameter of 4.35 mm, and a height of 6.45 mm were used to polish a single sample at a time. The brass was soft enough to be ground away during the process, and the reduction fragments did

not scratch the surface of the sample. However, this method did not allow for the polishing of parallel planes, requiring that the samples remain within the puck during SEM analysis.

After the sample received the final polish with 0.25 μm diamond suspension, the brass cylinder was placed in acetone and sonicated until the sample was released and all the Crystalbond 509 had dissolved. At this point, the sample was placed on double-sided carbon tape within the inner ring of Epoxy Mold 1 in an arrangement with other samples of the same composition. The puck was then created in the same fashion as previously mentioned in section 1.3.3.1. Once the carbon tape and aluminum dish were removed, the puck was lightly and slowly polished with the 0.25 μm diamond in suspension grit size to remove residual carbon tape, resulting in the parallel and level polished surfaces contained within the puck.

1.3.3.3 Method C

This iteration of the polishing process involved experimentation with different materials to contain the Crystalbond 509. Four different nylon flat washers (Washer A, B, C, and D) had respective outer diameter, inner diameter, and height measurements of: 19.050 mm, 12.827 mm, and 3.175 mm; 25.400 mm, 10.319 mm, and 1.588 mm; 11.113 mm, 5.080 mm, and 1.588 mm; 22.479 mm, 8.712 mm, and 1.575 mm. These were tested as potential replacements for the more 'traditional' epoxy molds. The washers' reduced height/thickness measurements relative to the molds, could allow for more efficient and direct polishing of parallel planes in the intended dual polishing method.

Washer A was deemed to be too thick, requiring excessive time added to the polishing process. More than a millimeter of washer material had to be polished away before the top portion of the glass sample was even reached. Furthermore, despite the excessive thickness, the wider inner diameter caused a weakened structure in the Crystalbond 509 and diminished its capacity to contain the sample. Washer B was of an appropriate thickness. However, like washer A, it's ratio of inner diameter to thickness resulted in increased fragility to the hardened Crystalbond 509. This caused the puck to fracture either when it was removed from the carbon tape or during the initial coarse polishing/grinding step, compromising its integrity and ability to hold the sample in place. Washer C also had a satisfactory thickness, and the inner diameter width relative to the thickness resulted in strong stability of the Crystalbond 509. The thickness of washer D was suitable, but with an inner diameter slightly wider than washer C, the hardened puck was noticeably less stable. These collective observations made washer C the temporary epoxy mold of choice, between these four nylon flat washers. Unfortunately, samples polished with these washers routinely developed scratches, varying from minor to deeper gouges in the glass surface. It was determined that the nylon material removed during polishing was hard enough to inflict damage on the sample surface. This meant that ultimately, the nylon flat washers were not an appropriate choice for the polishing process.

1.3.3.4 Method D

This method of the polishing process utilized the softer, polytetrafluoroethylene washers described in the methods section 1.2.6. Samples were adhered to double-sided carbon tape in an aluminum dish inside the inner ring of a polytetrafluoroethylene washer (0.25" thick, 0.141" outer diameter, 0.062" inner diameter) (Fig. 13). The inner ring was then filled with manually-powdered Crystalbond 509, using the process described in method A in section 1.3.3.1. This temporary epoxy was replaced in method E in section 1.3.3.5. On multiple occasions, when polishing samples that were set in Crystalbond 509 within the polytetrafluoroethylene washers, the friction of the polishing process softened the temporary epoxy enough that the samples rotated in place, which compromised attempts to achieve a dual polish.

1.3.3.5 Method E

This iteration of the polishing process is the same as what is outlined in the methods section 1.2.6.

This method utilized the same polytetrafluoroethylene washers described in section 1.3.3.4 (Fig. 13). The remaining vacant space around the sample was filled with Dentsply Caulk Orthodontist Powder, rather than the Crystalbond 509, which had been used in previous methods. One drop of Dentsply Caulk Orthodontist Resin was applied to the powder, and after an hour the resin hardened to form a temporary epoxy that encased the sample within the washer. Parallel sides of the washer and sample were ground down using silicon carbide CarbiMet abrasive pads

of decreasing grit sizes. Following grinding to expose flat, parallel surfaces on two sides, the upper surface was polished on microcloths sprayed with diamond suspensions.

High purity deionized water was applied to the silicon carbide pads during the grinding steps. Four abrasive pads with increasingly fine grit sizes of 240, 320, 600, and 800, and with respective approximate micron sizes of 52, 35, 15, and 13 were used. Between each of the abrasive pad grit sizes, the sample was sonicated in water to remove residual grit and was then dried using a compressed tetrafluoroethane gas duster spray.

Polishing steps used MetaDi Supreme polycrystalline diamond suspension grit sizes of 6 μm, 3 μm, 1 μm, and 0.25 μm, which were applied to separate microcloths. Of the two exposed flat surfaces on the spheres, one side received only a coarse polish of the 240 grit-sized abrasive, while the other plane was polished with increasingly fine grit sizes culminating in 0.25 μ polycrystalline diamond suspension. As was the case with the silicon carbide pad steps, the washer/sample was sonicated in water between diamond suspension solution polishes to remove residual grit grains and debris. After the last polish, the sample was sonicated in isopropanol to avoid leaving acetone hydrocarbon residue, which could be picked up by the high-vacuum SEM.

1.3.4 Sample-Specific Methods Used

This section will detail the specific methods used for individual samples, as well as sample-specific measurements, like diameter and mass, and calculations, like

heating rate, cooling rate, and peak temperature during levitation. Tables 2 and 5 contain this information for each sample.

1.3.4.1 Non Fe-Bearing Compositions

1.3.4.1.1 Forsterite

To synthesize forsterite, a mixture containing a 2:1 molar ratio of MgO and SiO_2 powders (MgO was adjusted for 7.2% LOI) was created using the powder mixing method described in section 1.3.1.1. Both MgO and SiO_2 powders are white, making visual estimations of homogeneity impossible. Samples 7.11.17.15, 7.11.17.20, 8.4.17.1, 8.7.17.14, 8.7.17.20, and 8.7.17.21 with diameters ranging from 1.08 - 1.25 mm (Table 2), were levitated on mixtures of 20-25% Ar and 75-80% O_2 gases using a 90°/0.7 mm nozzle (Fig. 19 A). Heating rates for these samples were between 28°C/s and 317°C/s. Upon reaching peak temperatures between 173°C -2048°C, the laser power was cut off. Cooling rates varied according to the surface area of the individual glasses, spanning a range of 637°C/s to 941°C/s. These samples were all synthesized using powder preparation method A (section 1.3.1.1) and polishing method A (section 1.3.3.1). Sample 10.6.17.20 (diameter = 0.62 mm) was levitated and vitrified using a 60°/0.7mm nozzle (Fig. 19 C) with a mixture of 10% Ar and 90% O_2 gases. After heating at a rate of 28°C/s and reaching a peak temperature 1820°C, the sample cooled at a rate of 1606°C/s. Sample 10.6.17.20 was synthesized using powder preparation method B (section 1.3.1.2) and polishing method D (section 1.3.3.4). Sample 10.6.17.20 used a different nozzle (60°/0.7mm rather than 90°/0.7mm) (Fig. 19 C) than samples 7.11.17.15, 7.11.17.20, 8.4.17.1, 8.7.17.14,

8.7.17.20, and 8.7.17.21, which was a more appropriate nozzle aperture angle for the smaller diameter and improved sample stability on the gas flow.

1.3.4.1.2 Enstatite

The enstatite mixture came from a 1:1 molar ratio of the same stock MgO and SiO_2 powders as the forsterite batch, resulting in the composition $MgSiO_3$ (also taking the 7.2% MgO LOI into account). Using a 90°/1 mm nozzle (Fig. 19 B), samples with diameters varying between 1.37 mm and 1.60 mm were vitrified in 100% argon gas flows and heat rates between 148°C/s and 300°C/s. They were held at their peak temperature of between 2005°C and 2202°C for approximately 10 seconds before shutting off the laser power. The cooling rates varied by the surface area of the individual glasses, but overall they covered a range of 456°C/s to 611°C/s. For samples 7.11.17.2, 7.11.17.4, 7.31.17.3, 7.31.17.10, and 7.31.17.11, powder preparation method A (section 1.3.1.1) and polishing method B (section 1.3.3.2) were used. For sample 11.2.17.2, powder preparation method B (section 1.3.1.2) and polishing method D (section 1.3.3.4) were used.

1.3.4.1.3 Mg-Enriched Enstatite

To synthesize a glass with a composition similar to enstatite, but having excess MgO, a mixture containing a 2.5:1 molar ratio of MgO and SiO_2 powders (MgO mass was adjusted for 7.2% LOI) was created using the powder preparation method described in section 1.3.1.1. The intended composition for this mixture was $Mg_{2.5}SiO_3$. The Mg-enriched enstatite powder was fused using the laser fusing

method outlined in section 1.3.2.2, and polished using the method outlined in section 1.3.3.2. The levitation and vitrification of these samples varied slightly from that of the forsterite and enstatite samples.

Using a 90°/0.7 mm nozzle (Fig. 19 A), two samples with diameters of 1.04 mm and 1.14 mm were vitrified with 10% Ar and 90% O_2 gas flows and heat rates of 74 °C/s and 20 °C/s, respectively. As was the case with the forsterite samples, the slower heat rates were a result of carefully maintaining sample balance on the gas flow. When the peak temperatures of 1926 °C and 1953 °C, respectively, were reached for each sample, the laser power was stopped. The cooling rates were 896 °C/s and 826 °C/s, respectively.

1.3.4.2 Fe-Bearing Compositions

1.3.4.2.1 En95

Version 2 of the En95 mixture was prepared using powder preparation method B (section 1.3.1.2), laser fusing method B (section 1.3.2.2), and polishing method D (section 1.3.3.4). Like version 1, the intended formula was $(Mg_{0.95}Fe_{0.05})SiO_3$. This En95 mixture took the MgO 7.2% LOI into account as well as a 10% LOI of the Fe_2O_3. The LOI of the Fe_2O_3 was accounted for in all later versions as well. Eight of the samples synthesized from version 2 mixtures (11.30.17.2, 11.30.17.4, 3.28.18.1, 3.28.18.5, 3.28.18.6, 3.28.18.8, 3.28.18.11, and 3.28.18.12) were analyzed by SEM. Using a 90°/1 mm nozzle (Fig. 19 B), two samples (11.30.17.2 and 11.30.17.4) with diameters of 1.19 mm and 1.24 mm, respectively, were vitrified within 100% O_2 gas flows and 11.30.17.2 was heated at a rate of 13 °C/s. When the peak temperatures of

2000 °C and 2100 °C, respectively, were reached for each sample, the laser power was stopped. The cooling rates were 687 °C/s and 335 °C/s, respectively.

An additional six samples were created using a 90°/0.7 mm nozzle (Fig. 19 A), (3.28.18.1, 3.28.18.5, 3.28.18.6, 3.28.18.8, 3.28.18.11, and 3.28.18.12) with respective diameters of 1.63 mm, 1.37 mm, 0.99 mm, 1.29 mm, 1.21 mm, and 1.01 mm. These samples were vitrified within varied gas compositions, which will be expanded upon in section 1.4.2.3, and heat rates ranging between 88 °C/s and 119 °C/s. When the peak temperatures reached between 1840 °C and 1993 °C, the laser power was stopped and the samples cooled at rates ranging between 385 °C/s and 764 °C/s. Two of the eight En95 samples analyzed with the SEM (3.28.18.8 and 3.28.18.12) stuck to the side of the conical nozzle at some point during the levitation process. These samples showed the least accurate and precise weight percentages.

Version 4 of the En95 mixture used powder preparation method C (section 1.3.1.3), laser fusing method B (section 1.3.2.2), and polishing method E (section 1.3.3.5). The intended formula was $(Mg_{0.95}Fe_{0.05})(Si_{0.95}Fe_{0.05})O_3$, and all six of the analyzed samples (6.22.18.1, 6.22.18.2, 6.22.18.3, 6.22.18.4, 6.22.18.5, and 6.22.18.6) were levitated in a gas mixture with a composition of 80% of 5% CO_2 in Ar and 20% of 5% CO in Ar, using a 90°/1 mm nozzle (Fig. 19 B). They had respective diameters of 1.51 mm, 1.51 mm, 1.50 mm, 1.47 mm, 1.39 mm, and 1.33 mm. These samples had heat rates ranging between 182 °C/s and 234 °C/s, peak temperatures reaching between 1949 °C and 2031 °C, and cooling rates ranging between 393 °C/s and 509 °C/s.

1.3.4.2.2 En90

Version 1 of the En90 mixture was prepared using powder preparation method B (section 1.3.1.2), laser fusing method B (section 1.3.2.2), and polishing method E (section 1.3.3.5). The intended formula was $(Mg_{0.9}Fe_{0.1})SiO_3$, which was the target chemical composition for all three versions of this mixture. All three versions took both a 7.2% MgO LOI into account as well as the 10% Fe_2O_3 LOI. Two samples from a version 1 mixture were analyzed by SEM. Using a 90°/1 mm nozzle (Fig. 19 B), samples 1.5.18.4 and 1.5.18.10 had respective diameters of 1.81 mm and 1.23 mm and were synthesized within 100% O_2 gas flows. The samples had respective heat rates of 23°C/s and 24°C/s, peak temperatures of 2243°C and 2250°C, and cooling rates of 446°C/s and 751°C/s (Table 2).

Version 3 of the En90 mixture was created using powder preparation method C (section 1.3.1.3), laser fusing method B (section 1.3.2.2), and polishing method E (section 1.3.3.5). The intended formula was $(Mg_{0.9}Fe_{0.1})SiO_3$, and all three of the analyzed samples (6.21.18.2, 6.21.18.3, and 6.21.18.5) were levitated within a gas flow with a composition of 100% O_2, using a 90°/1 mm nozzle (Fig. 19 B). These samples had diameters of 1.26 mm, 1.29 mm, and 1.18 mm, respectively, with heat rates ranging between 214 °C/s and 536 °C/s, peak temperatures reaching between 1948 °C and 2089 °C, and cooling rates ranging between 615 °C/s and 705 °C/s.

1.4 Results

This section will detail the results from the XRD, SEM, and EPMA analyses for each intended composition. The section is sub-divided first by the lack/presence of

iron and then by the specific composition of the samples. The non Fe-bearing samples include the forsterite, enstatite, and Mg-enriched enstatite compositions, and the Fe-bearing samples include the different versions of the En95 and En90 compositions, followed by an inspection of the visual effects of fugacity constraints on the En95 composition samples.

1.4.1 Non Fe-Bearing Compositions

1.4.1.1 Forsterite

All samples were analyzed using the TESCAN VEGA3 SEM at the University of Illinois in Urbana-Champaign as described in section 1.2.8. For samples 7.11.17.15, 7.11.17.20, 8.4.17.1, 8.7.17.14, and 10.6.17.20, multiple spots were analyzed with the EDS detector to acquire x-ray spectra and determine compositions (Fig. 17; Tables 3 and 4). The analyses were done moving from the center of the exposed surface of the sphere toward an edge to gain a better assessment of sample homogeneity from core to rim. Two of the samples (8.7.17.20 and 8.7.17.21) had large internal bubbles which were cut by the polished surface and only had room for one spot to analyze on each (Fig. 20).

(Fig. 21; Table 4) shows that from 7.11.17.15, 7.11.17.20, 8.4.17.1, 8.7.17.14, and 10.6.17.20, samples 7.11.17.15 and 10.6.17.20 had the most accurate oxide percentages, with 57.27 ± 1.05 wt% MgO and 57.69 ± 0.73 wt% MgO, respectively, and 42.73 ± 1.05 wt% SiO_2 and 42.31 ± 0.73 wt% SiO_2, respectively. Samples 8.7.17.20 and 8.7.17.21 each have one assessed spot due to limited accessible areas, with 58.76 wt% MgO and 57.12 wt% MgO, respectively, and 41.24 wt% SiO_2 and

42.88 wt% SiO_2, respectively. Samples 7.11.17.20 and 8.7.17.14 both show percentages less than the target value within 3.5%, with 54.68 ± 0.71 wt% MgO and 55.14 ± 1.96 wt% MgO, respectively, and 45.32 ± 0.71 wt% SiO_2 and 44.86 ± 1.96 wt% SiO_2, respectively. The forsterite sample with both the least accurate and the least precise MgO and SiO_2 percentages is 8.4.17.1. These spots are an average of 10.9% less than the target value, with 46.42 wt% MgO and 53.58 wt% SiO_2. Sample 7.11.17.15 was the most accurate.

Samples 10.6.17.6 and 10.6.17.8 had irregular external textures (Fig. 14), indicating that they may have crystallized (devitrified) upon quenching. These samples were analyzed on the XRD to check for devitrification. Using the Vantec detector, the interatomic spacing in the samples was assessed, seeking to discover whether there was a repeated, crystalline characteristic to the material or whether the internal structure was amorphous. The results showed a single Bragg's peak rising from a broad and shallow background (Fig. 15). The peak indicates partial devitrification, while the shallow background indicates the remainder of the sample having an amorphous structure. The peak was located at a 2-theta distance of 17.97, which correlates with an interatomic spacing for forsterite (according to the reference distances in the Bruker D8 Discover software).

Sample 10.6.17.20 was analyzed, using both the LynxEye and Vantec detectors, where the LynxEye scan was a more thorough and time-consuming analysis that fired x-rays at the sample in angle increments of 0.01° as opposed to the 1.5° of the Vantec scan. After the Vantec scan did not identify any crystallinity in the sample, the LynxEye detector was used to confirm the accuracy of the Vantec scan and the

amorphous internal structure of the sample (Fig. 16). Both scans showed broad and shallow curves with maximums centered near the forsterite 2-theta distances, but were absent of Bragg's peaks which would have been indicative of crystal growth within the sample, indicating that this sample was completely vitrified.

1.4.1.2 Enstatite

Five polished enstatite glasses mounted in Crystalbond 509 and one enstatite glass adhered to a glass slide were analyzed using the TESCAN VEGA3 SEM at the University of Illinois in Urbana-Champaign. Perfectly stoichiometric enstatite ($MgSiO_3$) should contain 40.15 wt% MgO and 59.85 wt% SiO_2, making it the target composition of these samples.

The enstatite samples generally showed greater accuracy and precision than the forsterite compositions (Tables 3 and 4). Samples 7.11.17.4, 7.31.17.10, and 7.31.17.11 were all close to the goal composition, with 41.54 ± 0.91 wt% MgO, 39.56 ± 0.68 wt% MgO, and 39.54 ± 0.54 wt% MgO, respectively, and 58.46 ± 0.91 wt% SiO_2, 60.44 ± 0.68 wt% SiO_2, and 60.46 ± 0.54 wt% SiO_2, respectively. Samples 7.31.17.3 and 11.2.17.2 were the most precise. The accuracy of 7.31.17.3 fell short of the intended composition with 35.10 ± 0.05 wt% MgO and 64.90 ± 0.05 wt% SiO_2, while sample 11.2.17.2 had 41.26 ± 0.05 wt% MgO and 58.74 ± 0.05 wt% SiO_2. The remaining enstatite sample 7.11.17.2 also showed 35.38 ± 0.61 wt% MgO and 64.62 ± 0.61 wt% SiO_2. Sample 7.31.17.10 was the most accurate sample and 7.31.17.11 was the most precise sample (Tables 3 and 4; Fig. 22).

1.4.1.3 Mg-enriched Enstatite

Like the forsterite and enstatite samples, the polished Mg-enriched glasses were analyzed using the TESCAN VEGA3 SEM at the University of Illinois in Urbana-Champaign. The samples were synthesized using powder preparation method A (section 1.3.1.1), laser fusing method B (section 1.3.2.2), and polishing method B (section 1.3.3.2) (Table 5). According to the stoichiometry of this Mg-enriched enstatite ($Mg_{2.5}SiO_3$), the glasses synthesized from this mixture should contain 62.65 wt% MgO and 37.35 wt% SiO_2. Mg-enriched enstatite samples 8.14.17.7 and 8.14.17.8 had 53.53 ± 0.37 wt% MgO and 50.62 ± 2.9 wt% MgO and 46.47 ± 0.37 wt% SiO_2 and 49.38 ± 2.9 wt% SiO_2, respectively. Sample 8.14.17.7 was the more accurate of the two samples (Tables 3 and 4).

1.4.2 Fe-Bearing Compositions

The Fe-bearing compositions described in this section include En95 and En90, with an additional section examining the effects of f_{O2} constraints on En95 compositions. The En95 samples are enstatite compositions, where the Mg cation site consists of 95% Mg versus 5% Fe. Similarly, the En90 samples are enstatite compositions, where the Mg cation site consists of 90% Mg versus 10% Fe.

1.4.2.1 En95

During the progression of this research, there were four different versions of the 95% Mg – 5% Fe enstatite (here these are referred to as En95), each of which reflected different stages of the evolution of the methodology and/or varied

intended chemical compositions. These are described below. Of the four versions, only versions 2 and 4 were analyzed with the SEM and EPMA, respectively.

1.4.2.1.1 Version 1

The first En95 mixture was prepared using powder preparation method A (section 1.3.1.1), laser fusing method B (section 1.3.2.2), and polishing method D (section 1.3.3.4) (Table 5). The intended formula was $(Mg_{0.95}Fe_{0.05})SiO_3$, and the mixtures were created from MgO, SiO_2, and Fe_2O_3 powders, accounting for a 7.2% LOI of the MgO. This version was created prior to the first semi-quantitative SEM analysis, which had showed the powder preparation process to be lacking.

1.4.2.1.2 Version 2

The intended oxide weight percentages for En95-version 2 are 37.55 wt% MgO, 58.93 wt% SiO_2, and 3.52 wt% Fe_2O_3. The samples levitated in 100% O_2 (11.30.17.2, 11.30.17.4, and 3.28.18.5) had 45.73 ± 1.3 wt% MgO, 43.34 ± 1.4 wt% MgO, and 40.78 ± 0.6 wt% MgO, 53.63 ± 1.0 wt% SiO_2, 54.83 ± 0.4 wt% SiO_2,, and 55.07 ± 0.1 wt% SiO_2,, and 0.63 ± 0.3 wt% Fe_2O_3, 1.82 ± 1.6 wt% Fe_2O_3,, and 4.15 ± 0.6 wt% Fe_2O_3,. The sample vitrified under 100% Ar (3.28.18.1) had 39.60 ± 1.2 wt% MgO, 57.16 ± 0.1 wt% SiO_2, and 3.24 ± 1.2 wt% Fe_2O_3. The sample levitated in a gas mixture of 5% CO_2 in Ar (3.28.18.6) had 40.19 ± 1.0 wt% MgO, 57.05 ± 0.1 wt% SiO_2, and 2.76 ± 1.0 wt% Fe_2O_3. The sample levitated in a gas mixture of 50% Ar and 50% O_2 (3.28.18.8) had 45.24 ± 5.2 wt% MgO, 52.81 ± 4.2 wt% SiO_2, and 1.95 ± 1.8 wt% Fe_2O_3. The sample levitated in a gas mixture of 5% CO in Ar (3.28.18.11) had 41.67 ±

2.3 wt% MgO, 56.56 ± 0.4 wt% SiO_2, and 1.77 ± 2.4 wt% Fe_2O_3,. The last sample, levitated in a gas mixture of 50% of 5% CO_2 in Ar and 50% of 5% CO in Ar (3.28.18.12) had an MgO percentage of 59.98 ± 6.2%, an SiO_2 percentage of 39.99 ± 6.2%, and an Fe_2O_3 percentage of 0.03 ± 0.0%. The most accurate sample was 3.28.18.1 (Fig. 23).

1.4.2.1.3 Version 3

This En95 mixture was prepared using powder preparation method C (section 1.3.1.3), laser fusing method B (section 1.3.2.2), and polishing method E (section 1.3.3.5). The intended formula was $(Mg_{0.95}Fe_{0.05})SiO_3$. The products of this version were being polished when the intended formula was altered in what is version 4.

1.4.2.1.4 Version 4

This mixture was analyzed with the EPMA which evaluated the elemental composition of each sample at between 35 and 48 individual spots (Tables 6 and 7). The six samples, listed in ascending order (6.22.18.1, 6.22.18.2, 6.22.18.3, 6.22.18.4, 6.22.18.5, and 6.22.18.6), had 36.92 ± 0.2 wt% MgO, 37.06 ± 0.1 wt% MgO, 37.37 ± 0.1 wt% MgO, 36.88 ± 0.2 wt% MgO, 37.11 ± 0.1 wt% MgO, and 36.69 ± 0.1 wt% MgO, with a target 37.05 wt% MgO. They had, respectively, 54.73 ± 0.4 wt% SiO_2, 54.83 ± 0.3 wt% SiO_2, 55.26 ± 0.3 wt% SiO_2, 54.75 ± 0.4 wt% SiO_2, 54.86 ± 0.3 wt% SiO_2, and 54.37 ± 0.3 wt% SiO_2, with a target 55.23 wt% SiO_2. They had, respectively, 8.34 ± 0.1 wt% Fe_2O_3, 8.37 ± 0.1 wt% Fe_2O_3, 8.38 ± 0.1 wt% Fe_2O_3, 8.37 ± 0.1 wt%

Fe_2O_3, 8.37 ± 0.0 wt% Fe_2O_3, and 8.38 ± 0.0 wt% Fe_2O_3, with a target 7.73 wt% Fe_2O_3. The most accurate sample was 6.22.18.6 (Fig. 24).

1.4.2.2 En90

During the progression of this research, there were three different versions of the 90% Mg – 10% Fe enstatite (En90), each of which reflected different stages of the evolution of the methodology. Of these versions, only versions 1 and 3 were analyzed with the SEM and EPMA, respectively.

1.4.2.2.1 Version 1

The intended oxide weight percentages for En90 are 34.76 wt% MgO, 57.58 wt% SiO_2, and 7.65 wt% Fe_2O_3. Samples 1.5.18.4 and 1.5.18.10 had 40.02 ± 1.8 wt% MgO and 37.70 ± 2.5 wt% MgO, 59.98 ± 1.8 wt% SiO_2 and 62.30 ± 2.5 wt% SiO_2, and 1.71 ± 1.5 wt% Fe_2O_3 and 4.12 ± 2.6 wt% Fe_2O_3. The most accurate sample was 1.5.18.10 (Fig. 25).

1.4.2.2.2 Version 2

This En90 mixture was prepared using powder preparation method C (section 1.3.1.3), laser fusing method B (section 1.3.2.2), and polishing method E (section 1.3.3.5). The intended formula was $(Mg_{0.9}Fe_{0.1})SiO_3$. Before these samples could be analyzed, the calculations determining the initial mass ratios of the oxide powders for the powder preparation method was changed. The products of this version were being polished when the initial stock solution masses were reevaluated (Table 5).

1.4.2.2.3 Version 3

Version 3 was assessed with the EPMA, resulting in elemental analyses of each sample at between 41 and 72 individual spots (Tables 6 and 7). The three samples, (6.21.18.2, 6.21.18.3, and 6.21.18.5), had 57.10 ± 0.4 wt% SiO_2, 56.79 ± 0.7 wt% SiO_2, and 56.96 ± 0.4 wt% SiO_2, respectively, with a target 57.58 wt% SiO_2. The samples had 34.90 ± 0.1 wt% MgO, 34.82 ± 0.5 wt% MgO, and 35.38 ± 0.1 wt% MgO, respectively, with a target 34.76 wt% MgO. The samples had 8.18 ± 0.1 wt% Fe_2O_3, 8.19 ± 0.1 wt% Fe_2O_3, and 8.22 ± 0.1 wt% Fe_2O_3, respectively, with a target 7.65 wt% Fe_2O_3. The most accurate sample was 6.21.18.3 (Fig. 26).

1.4.2.3 Visual Effects of Fugacity Constraints

Twelve En95 samples with an intended composition of $Mg_{0.95}Fe_{0.05}SiO_3$, created using the methods outlined in section 1.2, were synthesized in various gas environments, as described in previous sections, to determine correlations between f_{O2} of the levitation gas mixture and visual characteristics of the glasses (Figs. 27 A-M (levitated glasses)). For six different gas mixture scenarios that were heated to 1800 °C, one sample was held at peak temperature for 30 seconds and one sample was held at peak temperature for 60 seconds. As a result, for each of the six gas mixtures used, two glass samples were created. Four of these f_{O2} conditions involved levitation using a pure gas, or a premixed batch of two gases contained in a single gas cylinder: pure Ar, pure O_2, a premixed cylinder of 5% CO in Ar, and a premixed cylinder of 5% CO_2 in Ar.

The remaining two f_{O2} conditions involved combining/mixing (in the levitation furnace) gases from either the gas cylinders containing a pure gas or from the cylinders with the premixed gases; the combinations investigated here were: (1) 50% Ar plus 50% O_2 and (2) 50% of the 5% CO in Ar plus 50% of the 5% CO_2 in Ar. Levitation experiments were run using the same proportional-integral-derivative (PID) conditions, except for holding time, which was either one of two durations: 30 seconds or 60 seconds. The PID settings were chosen to achieve a consistent heating rate of 100 °C/s. The measured heating rates varied between 85 °C/s and 120 °C/s, with the exception of sample 3.28.18.13 which had a heat rate of 285 °C/s. The gas flow rates on which the samples levitated were varied between different samples, as the flow rates were dependent on the sample size, mass, and shape variations. The diameter of each sample can be found in Table 2. Each of the 30 second hold-time samples was polished and analyzed with the SEM.

The samples synthesized in pure O_2 (3.28.18.4 and 3.28.18.5) had a brown color after levitation and vitrification (Figs. 27 D and 27 E), while the samples synthesized in 50% Ar and 50% O_2 (3.28.18.8 and 3.28.18.9) had a brownish-green coloration (Figs. 27 H and 27 I). Sample 3.28.18.3 was also synthesized in O_2, however this sample stuck to the side of the nozzle during levitation and nucleated on contact (Fig. 27 C). The remaining glasses all had varying shades of green. The 100% Ar samples (3.28.18.1 and 3.28.18.2) (Figs. 28 A and 28 B), the samples that were entirely 5% CO_2 in Ar (3.28.18.6 and 3.28.18.7) (Figs. 27 F and 27 G), and the 50/50 mix of 5% CO_2 in Ar plus 5% CO in Ar sample held at temperature for 60 seconds (3.28.18.13) presented with pale green colors (Fig. 27 M). The samples that were

entirely 5% CO in Ar (3.28.18.10 and 3.28.18.11) had a blue-green color (Figs. 27 J and 27 K), as did the 50% of the 5% CO_2 in Ar and the 50% of the 5% CO in Ar sample held at temperature for 30 seconds (3.28.18.12) (Fig. 27 L).

The SEM results from the six samples held at peak temperature for 30-second intervals (3.28.18.1, 3.28.18.5, 3.28.18.6, 3.28.18.8, 3.28.18.11, and 3.28.18.12) were detailed in the En95 section 1.4.2.1 (Tables 3 and 4).

1.5 Discussion

1.5.1 Non Fe-Bearing Compositions

1.5.1.1 Forsterite

The forsterite glasses were the most difficult to synthesize, due primarily to the fragility of the melt for this composition. As mentioned in section 1.1.1, forsterite requires fast cooling rates in order to vitrify and avoid recalescence (Debenedetti & Stillinger, 2001; Miura et al., 2010; Moynihan, 1995; Nagashima et al., 2008; Tangeman et al., 2001; Webb, 1997; Weber & Benmore, 2017). The samples are cooled by cutting off the laser power, rather than via controlled cooling by gradually lowering the laser power over time, which leads to the fastest possible quenching for a given sample diameter. However, by fusing smaller samples, we were able to reduce the amount of surface area by reducing the sample diameter. This led to slightly faster cooling rates for smaller spheres. Diameters less than or close to 1 mm can achieve high enough cooling rates to exceed the structural relaxation rate and avoid crystallization. Previous research determined that the minimum cooling rate for forsterite vitrification in pure O_2 was 700 °C/s, as samples with cooling

rates between 250 °C/s and 700 °C/s resulted in crystallization (Tangeman et al., 2001). The glasses synthesized in this research, which were levitated in varying combinations of Ar and O_2 gases, recorded cooling rates of between 637 °C/s and 1606 °C/s for sample diameters ranging between 0.62 mm and 1.25 mm (Fig. 28).

Smaller samples were difficult to levitate with stability within the gas flows. These balance issues were directly tied to the heating rate for smaller samples. Slower heating rates were utilized to keep the molten spheres centered in the gas flow. Heating too quickly caused the samples to wobble within the flow and then stick to the side of the nozzle, causing them to significantly lose their form and often nucleate on contact. By incrementally increasing the laser power and decreasing the gas flow, the smaller samples were able to maintain stability. This progression resulted in lower heating rates with longer heating durations. Larger samples were less affected by the passing gas flows and were able to be heated more rapidly.

The six forsterite samples analyzed by SEM using powder preparation method A (section 1.3.1.1) showed a lack of consistent accuracy and homogeneity, though half of them did achieve oxide percentages close to the intended target. Two of those samples were only analyzed with a single spot analysis, due to the presence of vesicles intersecting the polished surface. The forsterite sample that used powder preparation method B (section 1.3.1.2) (10.6.17.20) showed a tight grouping of accurate spot analyses (Fig. 21).

The internal structure for three of the forsterite samples (10.6.17.6, 10.6.17.8, and 10.6.17.20) was assessed by XRD, successfully confirming that an amorphous internal structure of a glass could be visually determined by smooth external

textures and transparency. Two samples (10.6.17.6 and 10.6.17.8) had exterior textures like crumpled paper (Fig. 14) (discussed in sections 1.2.7 and 1.4.1.1), though the material was transparent and the temperature vs time data from the levitation run showed no evidence of recalescence. The results from the XRD's Vantec detector showed a single crystalline peak for each sample, above an otherwise broad and shallow background. Bragg's peaks are clear indicators of crystalline structure, whereas the low-intensity curves that extend across a wide variety of interatomic spacing distances are evidence of an amorphous structure. The combination of these two features indicated that the samples had each nucleated on the inside and, rather than crystallizing completely, had collapsed inward resulting in the crumpled exterior texture. This resulted in primarily amorphous internal structures, with microcrystalline inclusions. This could have been caused by dust particles in the levitation chamber that interacted with the cooling sample and provided contact points from which nucleation began to occur. As no other samples that were transparent presented with varied exterior textures, this theory was not tested and is only speculation. Sample 10.6.17.20, which was transparent with a smooth surface, was analyzed with both the Vantec detector and the LynxEye detector of the XRD, and showed a complete lack of crystalline peaks, confirming an amorphous structure.

1.5.1.2 Enstatite

As opposed to forsterite, the enstatite composition yields a very strong melt. So, barring contact with the nozzle or some other contact nucleation site, the samples

easily vitrified upon cooling within a wide range of cooling rates. As extreme cooling rates were not required, the enstatite samples were able to have greater diameters than the forsterite samples, which granted them better stability within the gas flows. The six enstatite samples analyzed with the SEM (7.11.17.2, 7.11.17.4, 7.31.17.3, 7.31.17.10, 7.31.17.11, and 11.2.17.2) were all levitated in pure Ar, using powder preparation method A (section 1.3.1.1) and laser fusing method B (section 1.3.2.2). Polishing method B (section 1.3.3.2) was used for samples 7.11.17.2, 7.11.17.4, 7.31.17.3, 7.31.17.10, and 7.31.17.11. Powder preparation method B (section 1.3.1.2), laser fusing method B (section 1.3.2.2), and polishing method D (section 1.3.3.4) were used for sample 11.2.17.2.

Samples 7.31.17.10, 7.31.17.11, and 11.2.17.2 were all within 1.11% of the target weight percentages with minimal variation between individual spots of less than 0.68% (Tables 3 and 4; Fig. 22). However, the remaining two samples were created from the same batch and though they showed tight grouping of the individual spot analyses, accuracy was poor. For sample 7.11.17.2, multiple vitrification attempts were made on the same sample. Contact nucleation with the nozzle on earlier attempts could account for the compositional inconsistencies. This does not explain the inaccuracy of sample 7.31.17.3, which vitrified on its first run and had oxide weight percentages more than 5.5% from the intended value. Sample 11.2.17.2, which employed the more rigorous powder preparation process, was very accurate and precise.

1.5.1.3 Mg-enriched Enstatite

Enriched enstatite samples were synthesized with the intention of achieving the composition $Mg_{2.5}SiO_3$. They were prepared using the same methods as the bulk of forsterite and enstatite samples, using powder preparation method A (section 1.3.1.1), laser fusing method B (section 1.3.2.2), and polishing method B (section 1.3.3.2). The two samples (8.14.17.7 and 8.14.17.8) were levitated with a gas mixture of 90% O_2 and 10% Ar, with relatively low heating rates due to stability within the gas flow and high cooling rates, which were possible because they had relatively small diameters of 1.04 mm and 1.14 mm, respectively. The SEM spot analyses of the samples showed them both to be significantly depleted in MgO, by 9.1% and 12.0%, respectively. The MgO values were even less than the 57.29% intended for the forsterite composition, revealing them to not be Mg-enriched glasses. As powder preparation method A (section 1.3.1.1) was employed for these samples, the initial mixing was less rigorous and could have been the cause of compositional heterogeneities within the individual samples.

1.5.2 Fe-Bearing Compositions

1.5.2.1 En95

Four different En95 versions were created: (1) Version 1; (2) Version 2; (3) Version 3; (4) Version 4. Version (1) glasses did not undergo SEM analysis before the next version of the methodology was in effect. Version (2) glasses, samples 11.30.17.2, 11.30.17.4, 3.28.18.1, 3.28.18.5, 3.28.18.6, 3.28.18.8, 3.28.18.11, and 3.28.18.12, were synthesized using powder preparation method B (section 1.3.1.2),

laser fusing method B (section 1.3.2.2), and polishing method D (section 1.3.3.4), and had varied oxide weight percentages, the majority of which were depleted in Fe_2O_3. Samples 3.28.18.1, 3.28.18.5, 3.28.18.6, 3.28.18.8, 3.28.18.11, and 3.28.18.12 were each levitated within different gas mixes, with the goal of determining correlations between the color of the glasses produced and their environments during vitrification. The three samples vitrified under 100% O_2 (11.30.17.2, 11.30.17.4, and 3.28.18.5) showed a range of weight percentages, with MgO and SiO_2 values more than 3% from the intended composition, and inconsistent Fe_2O_3 percentages. Samples 3.28.18.1, 3.28.18.6, 3.28.18.8, 3.28.18.11, and 3.28.18.12 were each synthesized under different gas environments, with the most accurate results coming from the sample vitrified in 100% Ar, though the spot analyses showed heterogeneities within the sample. The least accurate and precise results came from the two samples which came in contact with the side of the conical nozzle during levitation. Contact with the metal clearly resulted in leaching of material, significantly reducing the weight percentage of Fe_2O_3 and causing the ratio of MgO and SiO_2 to vary dramatically across each of the samples.

Version (3) glasses were being polished for SEM analysis when the methodology was changed and the intended formula changed from $(Mg_{0.95}Fe_{0.05})SiO_3$ to $(Mg_{0.95}Fe_{0.05})(Si_{0.95}Fe_{0.05})O_3$. Version (4) glasses showed consistently accurate weight percentages, with clear homogeneity across the six samples (6.22.18.1, 6.22.18.2, 6.22.18.3, 6.22.18.4, 6.22.18.5, and 6.22.18.6). These glasses were made using powder preparation method C (section 1.3.1.3), laser fusing method B (section 1.3.2.2), and polishing method E (section 1.3.3.5). These quantitative EPMA results

are from approximately 10 times as many spot analyses as the semi-quantitative SEM results, and show accuracy and precision across each sample. All the samples are within 1% of the intended weight percentage with a variability of 0.4% or less within each sample. The Fe_2O_3 results were consistent across the samples and within each sample, all of which were slightly enriched around 8.37% relative to the intended 7.73%. This could be due to an overestimation of the LOI for the Fe_2O_3 powder, where more of the stock solution than necessary was added in the powder preparation step described in section 1.2.4. If less material than expected was actually lost, the unanticipated residual could account for the excess in the EPMA results.

1.5.2.2 En90

Three different En90 versions were created: (1) Version 1; (2) Version 2; (3) Version 3. The oxide weight percentages of two glasses (1.5.18.4 and 1.5.18.10) from version (1) were determined by SEM multiple spot analyses. Both samples showed excessive MgO and SiO_2 weight percentages, with depleted Fe_2O_3 percentages. In addition to sufficiently lacking in accuracy, both had margins of error between 1.5% and 2.5%, showing an inconsistent composition both within the prepared batch of powder as well as within the individual samples.

Version (3) glasses (6.21.18.2, 6.21.18.3, and 6.21.18.5) were assessed by EPMA from between 41 and 72 individual spot analyses. These results showed the glasses to be very accurate and precise, with oxide weight percentages all falling within 1% of the target amounts and with a maximum margin of error of 0.7%. All of the Fe_2O_3

weight percentages were higher than intended, by approximately 0.5%. As was the case for the En95 glasses, this is likely due to an overestimation of the LOI for the initial Fe_2O_3 stock solution powder.

1.6 Summary and Conclusions

Throughout the course of this research, and after myriad iterations of the various steps involved in synthesizing homogeneous glasses with accurate compositions, a rigorous methodology evolved, to consistently create compositionally accurate and precise materials. Early versions of the different intended chemical compositions showed inaccuracies and imprecisions, which fundamentally altered and drove the methodology changes. Increasing the thoroughness with which the initial stock solutions were mixed and making adjustments to the intended chemical composition have resulted in consistently accurate and homogeneous Mg-Fe enstatite glasses. The quantitative results of this research show that the intended compositions were achieved with minimal error, and defend the claim that the final methodology presented in section 1.2 consistently produces compositionally accurate and homogeneous glasses. The final version of this methodology will be used to vitrify ^{57}Fe-bearing Mg-Fe enstatites in oxidizing and reducing environments, with the goal of producing samples with a range of ferric $(Mg_{0.95}{}^{III}Fe_{0.05})({}^{III}Fe_{0.05}Si_{0.05})O_3$ and ferrous $(Mg_{0.9}{}^{II}Fe_{0.1}SiO_3)$ iron.

The success of this methodology has direct implications for deep Earth petrology and geophysics. The ability to produce accurate and homogeneous glasses with the chemical compositions of the mantle's primary minerals ensures consistent starting

materials for simulations of the lower mantle environment. Where natural mineral samples exhibit compositional variations, glasses preserve accuracy and homogeneity to a micron scale. Having these starting materials allows experiments simulating the pressure and temperature conditions near the core-mantle boundary to be replicated, without the need to account for compositional heterogeneities within each sample or between samples of the same intended composition.

1.7 References

Alderman, O. L. G., Lazareva, L., Wilding, M. C., Benmore, C. J., Heald, S. M., Johnson, C. E., Johnson, J. A., Hah, H. -Y., Sendelbach, S., Tamalonis, A., Skinner, L. B., Parise, J. B., & Weber, J. K. R. (2017). Local structural variation with oxygen fugacity in Fe_2SiO_{4+x} fayalitic iron silicate melts. *Geochimica et Cosmochimica Acta*, *203*, 15-36.

Alderman, O. L. G., Wilding, M. C., Tamalonis, A., Sendelbach, S., Heald, S. M., Benmore, C. J., Johnson, C. E., Johnson, J. A., Hah, H. -Y., & Weber, J. K. R. (2017). Iron K-edge X-ray absorption near-edge structure spectroscopy of aerodynamically levitated silicate melts and glasses. *Chemical Geology*, *453*, 169-185.

Anderson, D. L. (1977). Composition of the mantle and core. *Annual Review of Earth and Planetary Sciences*, *5*(**1**), 179-202.

Angell, C. A. (1991). Relaxation in liquids, polymers and plastic crystals - strong/fragile patterns and problems. *Journal of Non-Crystalline Solids*, *131-133*, 13-31.

Ballhaus, C., Berry, R. F., & Green, D. H. (1990). Oxygen fugacity controls in the Earth's upper mantle. *Nature*, *348*(6300), 437.

Behrens, H. and Gaillard, F. (2006). Geochemical aspects of melts: volatiles and redox behavior. *Elements*, *2*, 275-280.

Benmore, C. J. & Weber, J. K. R. (2017). Aerodynamic levitation, supercooled liquids and glass formation. *Advances in Physics: X*, *2*(3), 717-736.

Birnie, D. P. & Kingery, W. D. (1985). Quenching of solid samples for high temperature equilibrium measurement. *Journal of Materials Science*, *20*(6), 2193-2198.

Birnie, D. P. & Dyar, M. D. (1986). Cooling rate calculations for silicate glasses. *Journal of Geophysical Research: Solid Earth*, *91*(B4), 509-513.

Briggs, D. (Director) (2018, October 15) Dark Origins of the Moon. [Television series episode] In D. Briggs (Producer), *Space's Deepest Secrets.* The Science Channel.

Calas, G., Henderson, G. S., & Stebbins, J. F. (2006). Glasses and melts: linking geochemistry and materials science. *Elements*, *2*, 265-268.

Catalli, K., Shim, S. H., Prakapenka, V. B., Zhao, J., Sturhahn, W., Chow, P., Xiao, Y., Liu, H., Cynn, H., & Evans, W. J. (2010). Spin state of ferric iron in $MgSiO_3$ perovskite and its effect on elastic properties. *Earth and Planetary Science Letters*, *289*(1-2), 68-75.

Coutures, J. P., Massiot, D., Bessada, C., Echegut, P., Rifflet, J. C., & Taulelle, F. (1990) Etude par RMN ^{27}Al d'aluminates liquides dans le domaine 1600-2100 °C. *C R Academie Sci Paris*, *310*, 1041-1045.

Darken, L. S. & Gurrey, R. W. (1945). The system iron-oxygen. I. The wustite field and related equilibria. *Journal of the American Chemical Society*, 68, 798-816.

Debenedetti, P. G. & Stillinger, F. H. (2001). Supercooled liquids and the glass transition. *Nature*, *410*(6825), 259.

Dingwell, D. B., & Webb, S. L. (1990). Relaxation in silicate melts. *European Journal of Mineralogy*, (4), 427-449.

Dingwell, D. B. (2006). Transport properties of magmas: diffusion and rheology. *Elements*, *2*, 281-286.

Dorfman, S. M., Badro, J., Rueff, J. P., Chow, P., Xiao, Y., & Gillet, P. (2015). Composition dependence of spin transition in (Mg,Fe)SiO_3 bridgmanite. *American Mineralogist*, *100*(10), 2246-2253.

Edgar, A. D. (1973). *Experimental petrology basic principles and techniques*. London, Oxford University Press.

Frost, B. R. (1991). Introduction to oxygen fugacity and its petrologic importance. *Reviews in Mineralogy and Geochemistry*, *25*(1), 1-9.

Grove, T. L. (1982). Use of FePt alloys to eliminate the iron loss problem in 1 atmosphere gas mixing experiments: Theoretical and practical considerations. *Contributions to Mineralogy and Petrology*, *78*(3), 298-304.

Gu, T., Li, M., McCammon, C., & Lee, K. K. (2016). Redox-induced lower mantle density contrast and effect on mantle structure and primitive oxygen. *Nature Geoscience*, *9*(9), 723.

Henderson, G. S., Calas, G., & Stebbins, J. F. (2006). The structure of silicate glasses and melts. *Elements*, *2*, 269-273.

Holloway, J. R. & Wood, B. J. (1988). *Simulating the Earth experimental geochemistry*. Boston, MA: Unwin Hyman.

Johannes, W. & Holtz, F. (1996). *Petrogenesis and experimental petrology of granitic rocks*. Berlin, Germany: Springer-Verlag.

Kohara, S., Suzuya, K., Takeuchi, K., Loong, C. K., Grimsditch, M., Weber, J. K. R., Tangeman, J. A., & Key, T. S. (2004). Glass formation at the limit of insufficient network formers. *Science*, *303*(5664), 1649-1652.

Lee, K. K. M., O'Neill, B., Panero, W. R., Shim, S. H., Benedetti, L. R., & Jeanloz, R. (2004). Equations of state of the high-pressure phases of a natural peridotite and implications for the Earth's lower mantle. *Earth and Planetary Science Letters*, *223*, 381-393.

Lee, S. K., Lin, J. F., Cai, Y. Q., Hiraoka, N., Eng, P. J., Okuchi, T., Mao, H. K., Meng, Y., Hu, M. Y., Chow, P., Shu, J., Li, B., Fukui, H., Lee, B. H., Kim, H. N. & Yoo, C. S. (2008). X-ray Raman scattering study of MgSiO3 glass at high pressure: Implication for triclustered MgSiO3 melt in Earth's mantle. Proceedings of the National Academy of *Sciences*, *105*(**23**), 7925-7929.

Lucas, P., Coleman, G. J., Cantoni, C., Jiang, S., Luo, T., Bureau, B., Boussard-Pledel, C., Troles, J., & Yang, Z. (2017). Chalcogenide glass sensors for bio-molecule detection. In *Optical Fibers and Sensors for Medical Diagnostics and Treatment Applications XVII* (Vol. 10058, p. 100580Q). International Society for Optics and Photonics.

Mathiak, G., Egry, I., Hennet, L., Thiaudière, D., Pozdnyakova, I., & Price, D. L. (2005). Aerodynamic levitation and inductive heating – a new concept for structural investigations of undercooled melts. *International Journal of Thermophysics*, *26*(**4**), 1151-1166.

Merrill, R. B. and Wyllie, P. J. (1973). Absorption of iron by platinum capsules in high pressure rock melting experiments. *American Mineralogist*, *58*, 16-20.

Miura, H., Yokoyama, E., Nagashima, K., Tsukamoto, K., & Srivastava, A. (2010). Phase-field simulation for crystallization of a highly supercooled forsterite-chondrule melt droplet. *Journal of Applied Physics*, *108*(11), 114912.

Miura, H., Yokoyama, E., Nagashima, K., Tsukamoto, K., & Srivastava, A. (2011). A new constraint for chondrule formation: condition for the rim formation of barred-olivine textures. *Earth, Planets and Space*, *63*(10), 8.

Moynihan, C. T., Easteal, A. J., Wilder, J., & Tucker, J. (1974). Dependence of the glass transition temperature on heating and cooling rate. *The Journal of Physical Chemistry*, *78*(26), 2673-2677.

Moynihan, C. T. (1995). Structural relaxation and the glass transition. *Reviews in Mineralogy and Geochemistry*, *32*(1), 1-19.

Mysen, B. O. & Richet, P. (2005). *Silicate glasses and melts properties and structure*. Amsterdam, Netherlands: Elsevier.

Nagashima, K., Tsukamoto, K., Satoh, H., Kobatake, H., & Dold, P. (2006). Reproduction of chondrules from levitated, hypercooled melts. *Journal of Crystal Growth*, *293*, 193-197.

Nagashima, K., Moriuchi, Y., Tsukamoto, K., Tanaka, K. K., & Kobatake, H. (2008). Critical cooling rates for glass formation in levitated Mg_2SiO_4-$MgSiO_3$ chondrule melts. *Journal of Mineralogical and Petrological Sciences*, *103*(3), 204-208.

Nitkiewicz, A. M. & Sterner, S. M. (1988). An improved Bond air mill for the preparation of spherical single crystals. *American Mineralogist*, *73*, 662-666.

Pack, A., Kremer, K., Albrecht, N., Simon, K., & Kronz, A. (2010). Description of an aerodynamic levitation apparatus with applications in Earth sciences. *Geochemical Transactions*, *11*(1), 4.

Poe, B. T., McMillan, P. F., Coté, B., Massiot, D., & Coutures, J. P. (1992). SiO_2-Al_2O_3 liquids: in-situ study by high-temperature ^{27}Al NMR spectroscopy and molecular dynamics simulation. *Journal of Physical Chemistry*, *96*, 8220-8224.

Roskosz, M., Luais, B., Watson, H. C., Toplis, M. J., Alexander, C. M. O'D., & Mysen, B. O. (2006). Experimental quantification of the fractionation of Fe isotopes during metal segregation from a silicate melt. *Earth and Planetary Science Letters*, *248*, 851-867.

Stebbins, J. F. (2016). Glass structure, melt structure, and dynamics: Some concepts for petrology. *American Mineralogist*, *101*(4), 753-768.

Tangeman, J. A., Phillips, B. L., Navrotsky, A., Weber, J. K., Hixson, A. D., & Key, T. S. (2001). Vitreous forsterite (Mg_2SiO_4): Synthesis, structure, and thermochemistry. *Geophysical Research Letters*, *28*(13), 2517-2520.

Webb, S. (1997). Silicate melts: Relaxation, rheology, and the glass transition. *Reviews of Geophysics*, *35*(2), 191-218.

Weber, J. R., Hampton, D. S., Merkley, D. R., Rey, C. A., Zatarski, M. M., & Nordine, P. C. (1994). Aero-acoustic levitation: A method for containerless liquid-phase processing at high temperatures. *Review of Scientific Instruments*, *65*(2), 456-465.

Weber, J. R., Tangeman, J. A., Key, T. S., Hiera, K. J., Paradis, P. F., Ishikawa, T., Yu, J., & Yoda, S. (2002). Novel synthesis of calcium oxide–aluminum oxide glasses. *Japanese journal of applied physics*, *41*(**5R**), 3029.

Weber, J. K. R. (2010). The containerless synthesis of glass. *International Journal of Applied Glass Science*, 1(*3*), 248-256.

Weber, J. K. R., Benmore, C. J., Skinner, L. B., Neuefeind, J., Tumber, S. K., Jennings, G., Santodonato, L. J., Jin, D., Du, J., & Parise, J. B. (2014). Measurements of liquid and glass structures using aerodynamic levitation and in-situ high energy x-ray and neutron scattering. *Journal of Non-Crystalline Solids*, *383*, 49-51.

Wilding, M. C., Benmore, C. J., Tangeman, J. A., & Sampath, S. (2004). Coordination changes in magnesium silicate glasses. *Europhysics Letters*, *67*(**2**), 212-218.

Williams, Q., & Garnero, E. J. (1996). Seismic evidence for partial melt at the base of Earth's mantle. *Science*, *273*(**5281**), 1528-1530.

Winborne, D. A., Nordine, P. C., Rosner, D. E., & Marley, N. F. (1976). Aerodynamic levitation technique for containerless high temperature studies on liquid and solid samples. *Metallurgical and Materials Transactions B*, *7*(**4**), 711-713.

Chapter 2: R Shiny Applications

2.1 LaserPlot

2.1.1 Introduction

When interpreting and analyzing the data output files from levitation experiments using the aerodynamic levitation laser furnace, there were many difficulties and steps required. The relevant data for plotting didn't appear until after 121 lines of the spreadsheet. At this point the data recording began, but the experiment began a variable amount of time later. Initial efforts to filter these data and retrieve necessary conditions of the experiment required sizeable manual user input for each file. This involved the creation of an Excel file, which was able to produce quality plots and synthesize information, but required significant time and energy. As a solution to these complications, LaserPlot was created.

LaserPlot is a browser application built specifically for the Microsoft Excel 97-2003 formatted data output from the aerodynamic levitation laser furnace. The coding is in the language of R and it employs the Shiny package, which runs the code in the background and displays a clean graphical user interface in the browser page. The full source code can be viewed via the hyperlink in Appendix A. The application has the capability to produce high-quality plots of temperature vs time and laser power vs time, in addition to automatically running derivation calculations, linear regressions, and pulling important information from the loaded Excel file. All this information is then sorted and available to download as a CSV file, and the plots are available as either PDF or PNG files.

2.1.2 Motivation

The structure of the output file from the aerodynamic levitation laser furnace includes a lot of detail, which makes it time consuming to extract and assess the relevant information. In order to reduce the processing time, LaserPlot was developed. The first 121 rows of the file consists of machine information, including but not limited to: a list of Boolean vectors for specific machine settings, PID settings, the gases used during levitation and their relative percentages, the gas flow rate, and the date. After these lines, the data fall within eight variables, though only the time, corrected temperature, and laser power variables are of analytical importance. The file begins recording data from the time that it is manually initiated in the Materials Development Inc. laser software until the moment that it is manually stopped. This means that the relevant information within the file is contained within a range that begins where the corrected temperature readings are above the pyrometer's minimum operational range of 600°C and ends after both the laser has been shut off and the temperature has dropped below 600°C. This range of time is dependent on when heating actually began, which means that the significant row numbers vary between experiments.

When attempting to plot and extract information from each data file without LaserPlot, some of the extraction is achievable within Excel, but there are a few features which are essentially irreproducible. The calculations of the heating rates in LaserPlot utilize the user-defined time at which the heating curve transitions into the holding curve, which can be accurately viewed and updated fluidly in real time.

Attempting to reproduce the finessing capability in a program like Excel would result in significant time loss, as the program lacks the smooth user interface that comes with such a specifically tailored program. Along those same lines, LaserPlot's aesthetic controls are quickly and easily accessible, where everything that is needed is already available. It's not that other programs would be incapable of producing the plots or running the calculations. LaserPlot was built for this purpose, making the process easier and faster, with consistent output formats.

2.1.3 Functionality

The capabilities of LaserPlot can be broken down into 5 main sections: data loading, plot controls, heating duration determination, cooling and heating rate calculations, and output options. Each of these categories has screenshot-aided instructions detailing their operation in the information tab of the application, specifically within the Levitation Laser tab.

The data loading section is portrayed in an easy-to-follow display and is the first visible item on the Levitation Laser tab. Selecting Browse (Fig. 29) opens a loading window into the user's PC. Selecting the file provides the program with a pathway from which the data will be read. Upon selection of a file, five areas on the page become instantly populated with information from the file: the time variable, the temperature variable, the laser power variable, the "Input Data" section, and the "Levitation Laser Data" section. The time, temperature, and laser power variables are automatically selected, using the time, corrected temperature, and laser power columns from the file format. The "Input Data" section is displayed in the center of

the screen and shows the tabular layout of the data, as it is read directly from the file. The “Levitation Laser Data” section, on a selectable tab to the right of “Input Data”, displays only four columns. The temp, time, and laser power columns reflect the previously selected variables. The remaining column is titled “Laser” and shows the specific instances when the laser was turned on and when it was turned off. These distinctions are necessary for both plot controls and cooling and heating rate calculations.

The plot controls section allows the user the opportunity to determine plot aesthetics and to manually adjust two items which will be part of the tabular output: gas flow and additional notes (Fig. 30). The gas flow is recorded in the Excel file that is being read by LaserPlot, but if the flow rate was adjusted after that point, it will need to be manually adjusted in the labelled text box. The additional notes feature offers the user a text box, which will occupy its own column in the tabular output file and has no character length limit. The editable plot aesthetics are the plot titles, the colors of the laser on and off sections, the visibility of the cooling and heating rate regression equations, and the line thicknesses for each plot. The plot titles are shown in text boxes to the right of their respective plots, as well as at the top of each plot, and will update in real time as they are changed.

The “Laser” column mentioned in the data loading section consisted of a binary determination of whether the laser was turned on or off in each measured instance. This is visible in the temperature vs time plot and will be expanded upon later in this section. The user has color control over both the “On” and “Off” segments, as well as the Laser Power vs Time curve, using a pop-up color palette, which allows

for the full range of hexadecimal colors and transparency selection (Fig. 31). The cooling and heating rate regression equations can be toggled on and off using a checkbox next to their labels. The last of these controls is the thicknesses of the curves in each plot. This input box defaults to a value of 1.5, but it allows for the user to type in desired values or use vertical arrows to incrementally increase or decrease the thickness in steps of 0.5. The thickness feature of the plot only recognizes increments of 0.5, so inputted values beyond that scope are rounded to the nearest acceptable value within the program and a message appears requesting that a valid value be entered, including the two nearest valid values. Even though an invalid entry does not cause an error in the program, the user is alerted that their selected value is not the one represented in the plot.

The next section is also an adjustable control, but does not fall under the realm of an aesthetic. It is a user input marking the transition from the sample heating to being held at temperature. Using a hover functionality, the program identifies and displays the x and y coordinates of the cursor, which would show either both time and temperature or both time and power. This allows the user to locate the specific time at which the experiment transitions from heating toward holding the sample at an intended temperature in the temperature vs time plot. (Fig. 32) This time can then be inputted into the text box on the right, titled as “Input time where heating becomes holding (s)”. This value defaults to the time at which the laser turns off. Entering an illogical value does not terminate the program; rather, it shows NA values. If the value is deleted completely, the plot will disappear. This can be remedied with no loss of progress by changing the input to a rational value. This

input box also has an incremental selection tool associated with it, which allows the user to tick up or down by increments of 0.1°C. Coupling this option with the R^2 value of the heating rate's linear regression allows for optimization of this equation's fit to the data's heating rate.

The calculation of the heating and cooling rates is achieved by two separate methods, both of which are visible in the application and are included in the tabular output file. The first method is linear regression. For a majority of the levitation experiments, the heating rate was either manually kept as constant as possible or a predetermined intended heat rate was selected within the PID settings before the experiment began. This means that the heat rate for a majority of cases should be generally linear in nature. The cooling rate is largely linear in nature as well, though it does decrease with time to a variable degree. The linear regression model shows the best fit line within the data segment, reflecting the greatest R^2 value which explains the highest percentage of the data variability. The second method is an averaging of derivatives. These calculations are based on the exact same time range as the linear model, but the rate at every instance is taken into account.

After optimizing the linear regression model for the heat rate and adjusting the aesthetic controls, there are three different output buttons: the temperature vs time plot, the laser power vs time plot, and a table. Each of these can be downloaded by selecting "Download Temp vs Time Plot", "Download Power vs Time Plot", and "Download Table", respectively. (Fig. 33) The plots can be saved as either PDF or PNG file types. If the file is in a PDF format, every feature of the plot is editable. This means that everything acts as individual objects and can be moved, deleted, or text

font types, colors, and sizes can be changed freely. On the other hand, if all the plot aesthetics and positioning are as desired, downloading a static PNG image allows for easy placement within a document or publication.

The output data table (Table 8) is a single row of data for the plot, covering sixteen different variables that have either been calculated within the program, pulled from the original file loaded into the program, or were generated by the user in the "Additional Notes" or "Gas Flow" input boxes. The calculated variables include the heating duration, the holding duration, the mean holding temperature, the peak temperature, the heating and cooling rates determined by linear regression, and the heating and cooling rates determined by averaged derivative. The heating duration represents the time between where the sample temperature exceeds 600°C and the user-defined point at which the heating curve transitions into holding. From this point and continuing until the laser is turned off represents the holding duration. The mean holding temperature is the average temperature calculated during this time span and the peak temperature is the maximum temperature value recorded during the entire levitation experiment. The variables that were taken from the original file include the sample name, the date of the experiment and the time that the recording began, the composition and relative percentage of Gas A, the composition and relative percentage of Gas B, and the gas flow. The gas flow variable is listed as being taken from the original file and as a user-generated input value. The reason is that the file records the gas flow setting in place when the recoding log initiates, but if the gas flow is adjusted during the course of the

experiment, it is not reflected in the log. If there are changes during levitation, the user's input will overwrite the initially recorded value.

2.1.4 Summary and Limitations

The Shiny web application LaserPlot uses the data output from the aerodynamic levitation laser furnace to produce two bivariate plots of temperature vs time and laser power vs time and a table. The plot aesthetics can be adjusted in the application, including coloring, line thicknesses, and the presence of linear regressions and their equations. As the plots can ultimately be downloaded as PDF files, text type, size, color, and location can be further adjusted in editing software applications. The table output downloads as a CSV file, and is populated by machine conditions pulled from the data file, user inputs in the application, and calculations of heating rate, cooling rate, maximum temperature, and mean holding temperature. LaserPlot contains everything necessary to provide a fast, fluid, and easy-to-use data analysis experience.

The program does have certain conditions which must be met in order to function properly. These relate to characteristics of the actual levitation experiment. Based on how the program interprets the data in order to run the various calculations, the following two conditions must be met: the file must represent a single levitation experiment and the laser power must be shut off before recording of the data file ceases.

For the first condition, this means that after the experiment has been completed and the laser has been shut off, the recording must also stop, preserving the single

experiment in the data file. If, rather than ceasing recording at this point, another levitation experiment were to begin in the same file, the program would interpret the entire duration of time until the laser was shut off for the last time as a single run. This means that everything in between the first heating and the last cooling would be recognized by LaserPlot as a single experiment. The calculations for the first heating rate and the last cooling rate would still be accurate, but everything in between would be compromised.

For the second condition, this means that the last row in the data file must have a laser power value of zero. This is necessary because of the manner in which the laser "on" and "off" portions of the curve are recognized by LaserPlot. The "on" portion is determined as the range of values from when the temperature rises above 600°C, which is the minimum pyrometer reading temperature, until the last row where the laser power does not equal zero. The "off" portion is then determined by the difference between the last row of data in the file and the last row where the laser power does not equal 0. If these two values are the same, and the laser "off" portion effectively becomes null, then the program identifies it as a missing variable and cannot function.

With the two requisite conditions for LaserPlot's functioning obeyed, this tool contains everything necessary to analyze the aerodynamic levitation laser furnace output in a straightforward and fast manner. The computation of several key variables, the allocation of variables from the loaded file, and the option to input additional information offers a seamless compilation of information. Coupled with

the tidy analysis collection, the plot outputs are both of a publication quality and able to be further customized as PDF files with any editing software options.

2.2 RockR

2.2.1 Introduction and Motivation

RockR is a web application, designed to act as a tool for classroom and lab environments. It was created with the intent to provide plotting capabilities wrapped within an easy-to-use user interface. It came about at the request of one of the professors in a collaborative venture between three R-savvy geology master's students: myself, John Shukle, and Jeremiah Mickey. The initial request was for an application that could provide the functionality to create ternary plots, which are triangular plots comprised of three separate axes, each of which is driven by its own variable. Building such a program in R offered the potential and the opportunity to include much more functionality than merely creating ternary plots, which could improve upon plotting capabilities and ease of plotting. It was at this point that the application began to grow and evolve.

RockR's design was educationally-driven, providing the user with instruction, links to relevant literature, and geoscientific examples spliced into the application itself. The provided instruction includes descriptions of how to navigate and operate the various sections of RockR. But it also includes overviews of the different plot types, along with the original papers with which they are associated, and even an interactive model illustrating the mechanics of point location calculations using ternary diagrams. Explanations of how to best organize and format datasets prior to

loading them into the application are also included, using both written and visual descriptions, as well as a link to an R-focused publication on "tidy data" (Wickham, 2014).

While RockR has the capability of plotting data onto blank ternary and bivariate plots, it goes beyond that to include underlying diagrams from which data patterns and relationships can be drawn. Within the geosciences, there are numerous discrimination and classification diagrams utilized in conjunction with data from rocks, minerals, and soils, in addition to numerous other applications (Figs. 34 and 35). However, despite the commonality and frequency with which these plots are used, at this point in time there was not a readily available, easily accessible, and free method by which they could be generated. Some programs do exist, but they either have user costs or require downloading and installation in the form of software packages. RockR aimed to specifically fit the niche of an easy to use and free tool. Perhaps its greatest advantage over other programs is its accessibility. Rather than the alternatives, RockR does not require installation of any kind, as it runs in any browser window. It does not expect programming knowledge or any awareness of coding languages. Even so, the full source code can be viewed via the hyperlink in Appendix B. The web application has streamlined functionality, which provides a fast and fluid experience that can be accessed from any device with browser capabilities (e.g. PC, laptop, tablet, mobile device), and is not operating system dependent.

2.2.2 Functionality

The home page opens to a brief introduction, with an overview of the application layout and organization. The middle portion of the home page contains a detailed table with pictures describing the various discrimination and classification diagrams as well as the additional curves in the metamorphic facies section. The last portion of the home page is the credits information, which includes app authors, RockR presence on various social media outlets, the preferred method of citing the app, a link to the GNU General Public License v3.0 under which the application is licensed, and citations from the various R packages as well as the primary literature references connected via hyperlinks and used as the base for discrimination and classification diagrams.

The resources page contains useful links for data acquisition, American societies, additional resources, and open source publications. Within each of these categories, there are labeled images that hyperlink to the source material. Every one of the websites shown is free to use and contain information useful to both students and professionals.

As the name would suggest, the help page offers additional information concerning data loading and plot creation, with stepwise instructions and screenshots highlighting certain features of the program. At the top of the opening page, sample files can be downloaded for each of the plot types. As the purpose of the application is to streamline and enhance plotting efficiency, it is an open-source project. As a result, the help page also offers a link to the application's GitHub page. This page includes everything that exists in RockR, and can be downloaded directly

or, if the user has their own GitHub account, they can fork the entire repository. Once the files have been downloaded, the entire application could be run locally through RStudio. This also means that, if desired, anyone could take the code and alter it to their own purposes, as long as they adhered to the GNU General Public License v3.0 agreement.

Beyond the home and help pages, the application is broken into three primary sections: the bivariate section, the ternary section, and the metamorphic facies section. The organizational scheme within each section is the same, insofar as the different tabs used to navigate around the section. They each open to a background information page, which outlines the general purpose and highlights original authors and useful publications. The other tab options are the input data page and the create plot page, both of which have some generic similarities present in all the primary sections and some unique characteristics. The input data page consists of functionality facilitating the loading of data files and selection of variables, and the create plot page displays the respective plots with varied aesthetic and functional options.

2.2.3 Teaching tool

The different plot sections open to basic explanations, as well as example diagrams produced using RockR. Within the explanation are links to original publications and author information, offering further background for students. Ternaries are not intrinsically understood conceptual plots, so the ternary section offers multiple avenues by which the user can achieve a more thorough

understanding of the plot purpose and capabilities. As opposed to bivariate diagrams with two axes, with which most people are familiar, ternary diagrams have three different axes. As written explanations are not the optimal method of learning for every student, there is an interactive ternary example within the ternary section. Further along, figure and text combinations detail how to read and interpret these diagrams. And finally, a series of basic equations show how data are normalized, so that each variable is shown relative to the summation of all three variables. The concepts of deciphering plots and normalizing data points are brought together in an interactive ternary diagram (Fig. 36). The input boxes to the left can be adjusted by the user and, as changes are made, the equations next to the input boxes and the ternary diagram both update in real time. This enhances conceptual understanding through the visualization of the effective relationship between the equation and the plotted point. As ternary diagrams are more difficult to understand than bivariate diagrams, it is the most involved information page between the different plot type sections. Within the information sections of the individual plot types, RockR offers hyperlink access to useful and freely accessible resources, which can help improve conceptual learning.

2.2.4 Ease of use

In addition to offering instruction and external resource links, RockR provides an easily navigable user interface that enables quality plot creation. The application is designed such that the process of loading data, creating plots, and manipulating aesthetic controls is fluid and simple. The final product can be quickly downloaded

in a variety of formats at the click of a button. The data loading step offers simple functionality to assist the user in variable selection and combination, without having to parse through their entire data file. These data are then sent to each plot type ready to go, with no adjustments necessary. When dropped into the ternary plot, the data points are automatically normalized, and the various groups are given distinct colors. The aesthetic alterations update in real time, allowing for fast customization of the plot. Additionally, if a discrimination diagram is selected, the individual polygon regions within the diagram can be colored to highlight patterns in the data. By having a specific and purposeful design, RockR is capable of a streamlined plotting ability, with a clean and professional finish. This application was not designed to be revolutionary or unique in its creation. It is not the first application capable of making these plots, nor does it lay claim to any of the plots, diagrams, or curves contained within it. RockR improves upon the plotting processes which already exist, making them fast, easy to use, and free.

2.2.5 Summary

RockR was designed as a tool for both classroom and laboratory environments. It does not claim ownership of any of the discrimination or classification plots and is entirely open-source. It is intended to help facilitate the fluid and expedient production of publication quality plots, including those that overly specific discrimination and classification diagrams. Moreover, this application offers the user fundamental instruction to the different plot types, as well as hyperlinks to

additional information. While other products do exist that can enable plotting onto these sorts of diagrams, RockR is free and requires no installation of software.

The bivariate section has plotting capabilities and aesthetic controls which can be replicated with a wide variety of software applications. However, the controls for these plot characteristics are more immediately available and streamlined and the plotted data can be correlated with numerous varieties of TAS diagrams from publications as far back as 1979 (Fig. 37). The ternary section optimizes the plotting process, which would otherwise be timely and painstaking. This section also includes the most discrimination diagrams, covering a wealth of possible applications. Lastly, the metamorphic facies section is a more unique section. Having two different interactive pressure and temperature-determined plots, this section allows for the plotting of pathways in the context of the different metamorphic facies. The pathways generally follow either intrusion origins or collision origins, showing burial and heating followed by exhumation or vice versa, respectively. In addition this section has the option to toggle on or off mineral phase boundaries and specific gradients.

Being an open-source project, RockR is continuously evolving and improving, with new diagrams being added as requested. RockR simplifies and improves upon existing plotting capabilities, but it also incorporates underlying discrimination and classification diagrams with the plotted data. With the information about the plotting sections, coupled with the hyperlinks to original papers and the interactive ternary example, RockR is able to wrap together necessary functionality and aesthetic control, while excess adjustment potentials. This allows such a browser

application to function as a very structured and efficient plotting tool for the classroom and laboratory environments.

2.3 References

Aramaki, S. & Roy, R. (1962). Revised phase diagram for the system Al_2O_3-SiO_2. *Journal of the American Ceramic Society*, *45*(*5*), 229-242.

Attali, D. (2017). colourpicker: A Colour Picker Tool for Shiny and for Selecting Colours in Plots. R package version 1.0. https://CRAN.R-project.org/package=colourpicker

Auguie, B. (2016). gridExtra: Miscellaneous Functions for "Grid" Graphics. R package version 2.2.1. https://CRAN.R-project.org/package=gridExtra

Chang, W., Cheng, J., Allaire, J. J., Xie, Y. and McPherson, J. (2017). shiny: Web Application Framework for R. R package version 1.0.5. https://CRAN.R-project.org/package=shiny

Cox, K. G., Bell, J. D., & Pankhurst, R. J. (1979). The interpretation of igneous rocks. London, GB: Unwin Hyman Ltd.

Dickinson, W. R. & Suczek, C. A. (1979). Plate tectonics and sandstone compositions. *AAPG Bulletin*, *63*(*12*), 2164-2182.

Eskola, P. (1920). The Mineral Facies of Rocks. *Norsk. Geol. Tidsskr. 6*, 143-194.

Folk, R. L. (1954). The distinction between grain size and mineral composition in sedimentary-rock nomenclature. *The Journal of Geology*, *62*(**4**), 344-359.

Guzman, R. G. (2015). NORRRM: Geochemical Toolkit for R. R package version 1.0.0. https://CRAN.R-project.org/package=NORRRM

Hamilton, N. (2017). ggtern: An Extension to ggplot2, for the Creation of Ternary Diagrams. R package version 2.2.1. https://CRAN.R-project.org/package=ggtern

LeBas, M.J., Le Maitre, R.W., Streckeisen, A., Zanettin, B. (1986). A Chemical Classification of Volcanic Rocks Based on the Total Alkali-Silica Diagram. *Journal of Petrology*, *27* (*3*), 745-750.

Middlemost, E. (1994). Naming materials in the magma/igneous rock system. *Earth-Science Reviews*, *37*, 215-224

Möbius, A. F. (1827). Der barycentrische Calcul ein neues Hüsmittel zur analytischen Behandlung der Geometrie dargestellt und insbesondere auf die Bildung neuer Classen von Aufgaben und die Entwickelung mehrerer Eiegnschaften der Kegelschnitte. Leipzig: J. A. Barth

Morimoto, N., Fabries, J., Ferguson, A. K., Ginzburg, I. V., Ross, M., Seifert, F. A., Zussman, J., Aoki, K., & Gottardi, G. (1988). Nomenclature of pyroxenes. *American Mineralogist*, *73*, 1123-1133.

O'Connor, J. T. (1965). A classification for quartz-rich igneous rocks based on feldspar ratios. *US Geological Survey Professional Paper B*, *525*, 79-84.

Peacock, S. M. (1993). The importance of blueschist- eclogite dehydration reactions in subducting oceanic crust. *Geological Society of America*, *105*, 684-694

R Core Team (2017). R: A language and environment for statistical computing. R Foundation for Statistical Computing, Vienna, Austria. URL https://www.R-project.org/.

Shepard, F.P. (1954). Nomenclature based on sand-silt-clay ratios: *Journal of Sedimentary Petrology*, *24*, 151-158.

Streckeisen, A. (1976). To each plutonic rock its proper name. *Earth-science reviews*, *12*(*1*), 1-33.

Streckeisen, A. (1980). Classification and nomenclature of volcanic rocks, lamprophyres, carbonatites and melilitic rocks IUGS Subcommission on the systematics of igneous rocks. *Geologische Rundschau*, *69*(*1*), 194-207.

Turner, F.J., (1948). Mineralogical and Structural Evolution of the Metamorphic Rocks. *Geol. Soc. Am. Mem.*, *30*, 1-342.

Urbanek, S. (2013). png: Read and write PNG images. R package version 0.1-7. https://CRAN.R-project.org/package=png

Wickham, H. (2009). ggplot2: Elegant Graphics for Data Analysis (2nd ed.). New York, NY: Springer-Verlag.

Wickham, H. (2014). Tidy data. *The Journal of Statistical Software, 59*, http://vita.had.co.nz/papers/tidy-data.html.

Wickham, H, Hester, J., and Francois, R. (2017). readr: Read Rectangular Text Data. R package version 1.1.1. https://CRAN.R-project.org/package=readr

Wickham, H. & Bryan, J. (2017). readxl: Read Excel Files. R package version 1.0.0. https://CRAN.R-project.org/package=readxl

Wilson, B.M. (2007) Igneous petrogenesis: a global tectonic approach. Berlin, DE: Springer-Verlag.

Xie, Y. (2014) knitr: A Comprehensive Tool for Reproducible Research in R. In Victoria Stodden, Friedrich Leisch and Roger D. Peng, editors, Implementing Reproducible Computational Research. Chapman and Hall/CRC. ISBN 978-1466561595

Xie, Y. (2015) Dynamic Documents with R and knitr. 2nd edition. Chapman and Hall/CRC. ISBN 978-1498716963

Xie, Y. (2017). knitr: A General-Purpose Package for Dynamic Report Generation in R. R package version 1.17.

Tables

Table 1. Oxide ratios of SiO_2 : MgO : Fe_2O_3 for glass compositions.

Composition	SiO_2 (mol)	MgO (mol)	Fe_2O_3 (mol)
$MgSiO_3$	1	1	0
Mg_2SiO_4	1	2	0
$(Mg_{0.9}^{II}Fe_{0.1})SiO_3$	1	0.9	0.05
$(Mg_{0.95}^{II}Fe_{0.05})SiO_3$	1	0.95	0.025
$(Mg_{0.95}^{III}Fe_{0.05})(Si_{0.95}^{III}Fe_{0.05})O_3$	0.95	0.95	0.05

Table 2. List of all synthetic glasses' characteristics of levitation experiments.

Composition	Sample	Diameter (mm)	Mass (before polish) (g)	Cool Rate (°C/s)	Polished	SEM	Gas Flow	Peak Temp (°C)	% Ar	% O_2	Ox/Red	% CO_2	% CO
Forsterite	7.11.17.15	1.08		734.96	Y	Y	135	2000	25	75	NA	NA	NA
Forsterite	8.7.17.14	1.25		688.20	Y	Y	155	2000	20	80	NA	NA	NA
Forsterite	8.4.17.1	1.09		699.56	Y	Y	175	1800	25	75	NA	NA	NA
Forsterite	7.11.17.20	1.16		694.92	Y	Y	160	2000	25	75	NA	NA	NA
Forsterite	8.7.17.21	1.17		916.91	Y	Y	150	1950	20	80	NA	NA	NA
Forsterite	8.7.17.20	1.20		599.16	Y	Y	150	2000	20	80	NA	NA	NA
Forsterite	7.11.17.18	1.28		699.28	Y	N	135	2200	25	75	NA	NA	NA
Forsterite	8.7.17.16	1.35		559.33	Y	N	160	2000	20	80	NA	NA	NA
Enstatite	7.31.17.9	1.20		605.69	Y	N	175	2000	100	0	NA	NA	NA
Enstatite	7.31.17.6	1.17		722.60	Y	N	175	2000	100	0	NA	NA	NA
Enstatite	7.31.17.5	1.08		691.76	Y	N	175	2000	100	0	NA	NA	NA
Enstatite	7.31.17.4	1.36		383.09	Y	N	175	2000	100	0	NA	NA	NA
Enstatite	7.31.17.3	1.49		507.44	Y	Y	175	2000	100	0	NA	NA	NA
Enstatite	7.31.17.11	1.40		558.03	Y	Y	175	2150	100	0	NA	NA	NA
Enstatite	7.31.17.10	1.37		580.39	Y	Y	175	2100	100	0	NA	NA	NA
Enstatite	7.31.17.8	1.50		506.33	Y	N	175	2000	100	0	NA	NA	NA
Enstatite	7.11.17.4	1.72		441.21	Y	Y	230	2000	100	0	NA	NA	NA
Enstatite	7.11.17.2	1.60		362.52	Y	Y	175	2000	100	0	NA	NA	NA
Enstatite	7.31.17.1	1.65		400.66	Y	N	175	2000	100	0	NA	NA	NA
$MgO_{2.5}SiO_2$	8.14.17.7	1.04		820.91	Y	Y	150	1950	10	90	NA	NA	NA
$MgO_{2.5}SiO_2$	8.14.17.8	1.14		718.29	Y	Y	200	1950	10	90	NA	NA	NA
Enstatite	9.11.17.1	1.24		969.92	N	N	76	1250	100	0	NA	NA	NA
Enstatite	9.11.17.4	1.11		409.40	N	N	110	1250	100	0	NA	NA	NA
Enstatite	9.11.17.7	1.18		469.42	N	N	112	1300	100	0	NA	NA	NA

Table 2. Continued.

Composition	Sample	Diameter (mm)	Mass (before polish) (g)	Cool Rate (°C/s)	Polished	SEM	Gas Flow	Peak Temp (°C)	% Ar	% O_2	Ox/Red	% CO_2	% CO
Enstatite	9.11.17.8	1.16		425.23	N	N	103	1300	100	0	NA	NA	NA
Enstatite	9.11.17.3	1.00		847.59	N	N	78	1500	100	0	NA	NA	NA
Enstatite	9.11.17.5	1.13		938.96	N	N	78	1050	100	0	NA	NA	NA
Enstatite	9.11.17.6	1.03		801.99	N	N	68	1050	100	0	NA	NA	NA
Forsterite	10.6.17.13	0.85		855.58	N	N	113	2075	10	90	NA	NA	NA
Forsterite	10.6.17.20	0.62		1606.16	Y	Y	91	1800	10	90	NA	NA	NA
Enstatite	11.2.17.1	1.12		599.56	N	N	109	1200	100	0	NA	NA	NA
Enstatite	11.2.17.2	1.38		565.90	N	Y	115	1560	100	0	NA	NA	NA
Enstatite	11.2.17.3	1.06		641.50	N	N	112	1350	100	0	NA	NA	NA
Enstatite	11.2.17.4	1.30		560.32	N	N	86	1300	100	0	NA	NA	NA
Enstatite	11.2.17.5	1.27		690.90	N	N	104	1700	100	0	NA	NA	NA
Enstatite	11.2.17.6	1.09		552.43	N	N	83	1260	100	0	NA	NA	NA
En95	11.30.17.1	1.84		436.67	Y	N	300	2500	0	100	oxidized	NA	NA
En95	11.30.17.2	1.19		686.82	Y	Y	280	2000	0	100	oxidized	NA	NA
En95	11.30.17.3	1.65		489.28	Y	N	300	2400	0	100	oxidized	NA	NA
En95	11.30.17.4	1.24		NA	Y	Y	180	2100	0	100	oxidized	NA	NA
En95	11.30.17.5	1.75		452.88	Y	N	285	2350	0	100	oxidized	NA	NA
En95	11.30.17.6	1.63		437.23	Y	N	285	2000	0	100	oxidized	NA	NA
En95	11.30.17.7	1.47		552.11	Y	N	285	2100	0	100	oxidized	NA	NA
En95	11.30.17.8	1.33		623.21	Y	N	250	2000	0	100	oxidized	NA	NA
En90	1.5.18.1	1.38		618.71	Y	N	260	2250	0	100	oxidized	NA	NA
En90	1.5.18.2	1.33		627.54	N	N	278	2200	0	100	oxidized	NA	NA
En90	1.5.18.3	1.36		646.26	N	N	286	2200	0	100	oxidized	NA	NA
En90	1.5.18.4	1.81		432.37	Y	Y	356	2250	0	100	oxidized	NA	NA

Table 2. Continued.

Composition	Sample	Diameter (mm)	Mass (before polish) (g)	Cool Rate (°C/s)	Polished	SEM	Gas Flow	Peak Temp (°C)	% Ar	% O_2	Ox/Red	% CO_2	% CO
En90	1.5.18.5	1.36	0.00575	515.63	N	N	291	2250	0	100	oxidized	NA	NA
En90	1.5.18.6	1.66		526.74	N	N	346	2235	0	100	oxidized	NA	NA
En90	1.5.18.7	1.69		505.59	N	N	377	2230	0	100	oxidized	NA	NA
En90	1.5.18.8	1.35		586.93	N	N	233	2200	0	100	oxidized	NA	NA
En90	1.5.18.9	1.14		560.22	Y	N	219	2200	0	100	oxidized	NA	NA
En90	1.5.18.10	1.23	0.00280	710.75	Y	Y	231	2250	0	100	oxidized	NA	NA
En90	1.5.18.11	1.51		503.60	N	N	241	2200	0	100	oxidized	NA	NA
En95	EN5Fe_O2_10p1mg_60s	1.92		no log data	Y	N	no log data	no log data	0	100	oxidized	NA	NA
En95	EN5Fe4_1CO2_CO_5p3mg_60s	1.49		no log data	Y	N	no log data	no log data	NA	NA	reduced	80	20
En95	EN5Fe4_1CO2_CO_6p0mg_10s	1.55		no log data	Y	N	no log data	no log data	NA	NA	reduced	80	20
En95	EN5Fe4_1CO2_CO_6p3mg_60s	1.59		no log data	N	N	no log data	no log data	NA	NA	reduced	80	20
En95	3.6.18.1	1.47	0.00454	367.91	N	N	165	2000	100	0	NA	NA	NA
En95	3.6.18.2	1.56	0.00539	381.74	N	N	210	2010	100	0	NA	NA	NA
En95	3.6.18.3	1.28	0.00302	457.21	N	N	160	2000	100	0	NA	NA	NA
En95	3.6.18.4	1.05	0.00173	540.91	N	N	146	1800	100	0	NA	NA	NA
En95	3.6.18.5	1.06	0.00176	579.35	N	N	120	2000	100	0	NA	NA	NA

Table 2. Continued.

Composition	Sample	Diameter (mm)	Mass (before polish) (g)	Cool Rate (°C/s)	Polished	SEM	Gas Flow	Peak Temp (°C)	% Ar	% O_2	Ox/Red	% CO_2	% CO
En95	3.6.18.6	0.93	0.00122	707.44	N	N	160	1750	0	100	oxidized	NA	NA
En95	3.6.18.7	0.96	0.00128	682.17	N	N	171	1710	0	100	oxidized	NA	NA
En95	3.6.18.8	0.86	0.00097	756.54	N	N	124	1750	0	100	oxidized	NA	NA
En95	3.6.18.9	0.94	0.00123	676.31	N	N	141	1750	0	100	oxidized	NA	NA
En95	3.6.18.10	1.02	0.00154	577.35	N	N	148	1700	0	100	oxidized	NA	NA
En95	3.6.18.11	0.92	0.00114	739.02	N	N	140	1800	0	100	oxidized	NA	NA
En95	3.6.18.12	0.89	0.00106	765.63	N	N	147	1750	0	100	oxidized	NA	NA
En95	3.28.18.1	1.63	0.00483	376.21	Y	Y	144	1800	100	0	NA	NA	NA
En95	3.28.18.2	1.46	0.00430	376.36	Y	N	115	1800	100	0	NA	NA	NA
En95	3.28.18.4	1.36	0.00280	558.55	Y	N	150	1800	0	100	oxidized	NA	NA
En95	3.28.18.5	1.37	0.00386	478.70	Y	Y	160	1800	0	100	oxidized	NA	NA
En95	3.28.18.6	0.99	0.00140	593.04	Y	Y	80	1800	NA	NA		100	0
En95	3.28.18.7	1.49	0.00440	390.36	Y	N	136	1800	NA	NA		100	0
En95	3.28.18.8	1.29	0.00318	475.09	Y	Y	152	1800	50	50	NA	NA	NA
En95	3.28.18.9	0.96	0.00132	704.82	Y	N	95	1800	50	50	NA	NA	NA
En95	3.28.18.10	1.17	0.00226	495.30	Y	N	100	1800	NA	NA		0	100
En95	3.28.18.11	1.21	0.00247	493.53	Y	Y	100	1800	NA	NA		0	100
En95	3.28.18.12	1.01	0.00149	568.52	Y	Y	80	1800	NA	NA		50	50
En95	3.28.18.13	1.41	0.00418	375.52	Y	N	150	1800	NA	NA		50	50
En90	5.16.18.4	1.33	0.00333	457.22	N	N	150	2071	NA	100	oxidized	NA	NA
En90	5.16.18.5	1.35	0.00334	483.02	N	N	155	2079	NA	100	oxidized	NA	NA
En90	5.16.18.7	1.31	0.00286	593.94	N	N	160	2059	NA	100	oxidized	NA	NA
En90	5.16.18.10	1.37	0.00382	400.96	N	N	160	2199	NA	100	oxidized	NA	NA
En90	5.16.18.11	1.22	0.00373	540.84	N	N	225	2067	NA	100	oxidized	NA	NA

Table 2. Continued.

Composition	Sample	Diameter (mm)	Mass (before polish) (g)	Cool Rate (°C/s)	Polished	SEM	Gas Flow	Peak Temp (°C)	% Ar	% O_2	Ox/Red	% CO_2	% CO
En90	5.18.18.2	1.33	0.00526	413.43	N	N	175	2128	NA	100	oxidized	NA	NA
En90	5.18.18.5	1.49	0.00485	513.47	N	N	310	2216	NA	100	oxidized	NA	NA
En90	5.21.18.1	1.28	0.00314	539.27	N	N	200	2070	NA	NA	reduced	80	20
En90	5.21.18.2	1.40	0.00444	558.07	N	N	300	2098	NA	100	oxidized	NA	NA
En90	5.21.18.3	1.49	0.00550	547.47	N	N	330	2000	NA	100	oxidized	NA	NA
En90	5.21.18.7	1.49	0.00395	577.19	N	N	290	2033	NA	100	oxidized	NA	NA
En90	5.21.18.10	1.48	0.00508	535.82	N	N	305	1998	NA	100	oxidized	NA	NA
En95	5.30.18.1	1.67	0.00672	459.87	N	N	315	2171	NA	100	oxidized	NA	NA
En95	5.30.18.2	1.63	0.00665	451.28	N	N	315	2093	NA	100	oxidized	NA	NA
En95	5.30.18.10	1.62	0.00592	493.66	N	N	315	2094	NA	100	oxidized	NA	NA
En95	5.30.18.11	1.42	0.00401	405.64	N	N	155	1951	NA	100	oxidized	NA	NA
En95	5.30.18.12	1.53	0.00506	576.28	N	N	300	2149	NA	NA	reduced	80	20
En95	5.30.18.13	1.43	0.00409	378.77	N	N	155	1977	NA	NA	reduced	80	20
En95	5.30.18.14	1.42	0.00438	372.21	N	N	160	2253	NA	NA	reduced	80	20
En90	6.11.18.1	1.48	0.00452	401.97	N	N	167	1977	NA	NA	reduced	80	20
En90	6.11.18.2	1.43	0.00435	420.36	N	N	160	1984	NA	NA	reduced	80	20
En90	6.11.18.6	1.35	0.00424	407.09	N	N	194	1923	NA	NA	reduced	80	20
En90	6.11.18.7	1.25	0.00362	422.00	N	N	165	1955	NA	NA	reduced	80	20
En90	6.11.18.9	1.37	0.00353	443.90	N	N	160	2024	NA	NA	reduced	80	20
En95	6.15.18.3	1.38	0.00352	460.27	N	N	180	2074	NA	NA	reduced	80	20
En95	6.15.18.5	1.39	0.00367	422.26	N	N	155	2031	NA	NA	reduced	80	20
En95	6.18.18.1	1.54	0.00523	532.35	N	N	290	1962	NA	NA	reduced	80	20
En95	6.18.18.2	1.57	0.00539	520.80	N	N	290	1950	NA	NA	reduced	80	20
En95	6.18.18.5	1.48	0.00459	501.39	N	N	250	1936	NA	NA	reduced	80	20

Table 2. Continued.

Composition	Sample	Diameter (mm)	Mass (before polish) (g)	Cool Rate (°C/s)	Polished	SEM	Gas Flow	Peak Temp (°C)	% Ar	% O_2	Ox/Red	% CO_2	% CO
En95	6.18.18.6	1.34	0.00342	481.36	N	N	185	2046	NA	NA	reduced	80	20
En95	6.18.18.7	1.33	0.00352	521.58	N	N	185	2037	NA	NA	reduced	80	20
En95	6.18.18.8	1.30	0.00311	471.19	N	N	160	1932	NA	NA	reduced	80	20
En95	6.21.18.1	1.26	0.00283	665.65	N	N	225	1948	NA	100	oxidized	NA	NA
En95	6.21.18.2	1.26	0.00297	615.38	N	N	250	1951	NA	100	oxidized	NA	NA
En95	6.21.18.3	1.29	0.00320	658.82	N	N	250	2028	NA	100	oxidized	NA	NA
En95	6.21.18.5	1.18	0.00240	705.34	N	N	245	2089	NA	100	oxidized	NA	NA
En90	6.22.18.1	1.51	0.00513	415.82	N	N	245	1949	NA	NA	reduced	80	20
En90	6.22.18.2	1.51	0.00514	393.45	N	N	250	2031	NA	NA	reduced	80	20
En90	6.22.18.3	1.50	0.00502	412.33	N	N	212	2025	NA	NA	reduced	80	20
En90	6.22.18.4	1.47	0.00462	425.45	N	N	225	1997	NA	NA	reduced	80	20
En90	6.22.18.5	1.39	0.00407	449.00	N	N	180	1956	NA	NA	reduced	80	20
En90	6.22.18.6	1.33	0.00315	508.60	N	N	170	1977	NA	NA	reduced	80	20
En90	6.22.18.7	1.11	0.00249	551.60	N	N	160	1937	NA	NA	reduced	80	20
En90	6.22.18.8	1.26	0.00268	551.10	N	N	170	1969	NA	NA	reduced	80	20
En95	7.2.18.1	1.10	0.00186	550.96	Y	N	190	2141	NA	100	oxidized	NA	NA
En95	7.2.18.6	1.48	0.00468	503.05	Y	N	290	2051	NA	100	oxidized	NA	NA
En95	7.2.18.7	1.50	0.00452	503.60	Y	N	280	1955	NA	100	oxidized	NA	NA
En90	7.2.18.8	1.15	0.00224	550.96	Y	N	165	2141	NA	NA	reduced	80	20
En90	7.2.18.13	1.18	0.00246	560.01	Y	N	170	2009	NA	NA	reduced	80	20
En90	7.2.18.14	1.15	0.00229	567.56	Y	N	155	1973	NA	NA	reduced	80	20
En90	7.2.18.15	1.46	0.00458	394.76	Y	N	165	1967	NA	NA	reduced	80	20
En90	7.2.18.16	1.37	0.00400	437.55	Y	N	165	2102	NA	NA	reduced	80	20
En90	7.2.18.17	1.37	0.00386	470.31	Y	N	170	1972	NA	NA	reduced	80	20

Table 2. Continued.

Composition	Sample	Diameter (mm)	Mass (before polish) (g)	Cool Rate (°C/s)	Polished	SEM	Gas Flow	Peak Temp (°C)	% Ar	% O_2	Ox/Red	% CO_2	% CO
En95	7.9.18.1	1.76	0.00762	445.46	Y	N	275	2034	NA	100	oxidized	NA	NA
En95	7.9.18.2	1.41	0.00415	538.88	Y	N	215	2036	NA	100	oxidized	NA	NA
En95	7.9.18.3	1.29	0.00321	628.79	Y	N	255	2170	NA	100	oxidized	NA	NA
En95	7.9.18.4	1.32	0.00351	610.28	Y	N	265	2129	NA	100	oxidized	NA	NA
En95	7.9.18.5	1.10	0.00196	838.33	Y	N	145	2191	NA	100	oxidized	NA	NA
En95	7.9.18.6	1.22	0.00269	695.77	Y	N	152	2096	NA	100	oxidized	NA	NA
En95	7.9.18.7	1.21	0.00259	731.03	Y	N	160	2133	NA	100	oxidized	NA	NA
En95	7.9.18.8	1.11	0.00203	807.34	N	N	150	2186	NA	100	oxidized	NA	NA
En95	12.29.18.6	1.16	0.00250	580.83	N	N	150	1905	NA	100	oxidized	NA	NA
En95	12.29.18.7	1.19	0.00282	536.25	N	N	150	1881	NA	100	oxidized	NA	NA
En95	12.29.18.12	1.17	0.00257	569.73	N	N	155	1906	NA	100	oxidized	NA	NA
En95-half	12.29.18.16	1.21	0.00281	567.67	N	N	174	1965	NA	100	oxidized	NA	NA
En95-half	12.29.18.18	1.33	0.00370	468.11	N	N	190-200	1821	NA	100	oxidized	NA	NA
En95-half	12.29.18.21	1.31	0.00365	525.49	N	N	190	2050	NA	100	oxidized	NA	NA
En95-half	12.29.18.22	1.27	0.00323	535.93	N	N	170	1866	NA	100	oxidized	NA	NA
En90	12.30.18.1	1.33	0.00367	416.93	N	N	150	1950	NA	NA	reduced	80	20
En90	12.30.18.4	1.17	0.00256	473.89	N	N	145	1922	NA	NA	reduced	80	20
En90	12.30.18.6	1.31	0.00351	379.38	N	N	140	1928	NA	NA	reduced	80	20
En90	12.30.18.7	1.16	0.00252	453.98	N	N	140-145	1915	NA	NA	reduced	80	20
En90	12.30.18.9	1.16	0.00235	492.61	N	N	135	1881	NA	NA	reduced	80	20
En90	12.30.18.10	1.27	0.00314	400.66	N	N	135	1943	NA	NA	reduced	80	20
En90	12.30.18.11	1.11	0.00219	494.71	N	N	135-140	1903	NA	NA	reduced	80	20
En90-half	12.30.18.13	1.29	0.00343	410.66	N	N	150	1878	NA	NA	reduced	80	20
En90-half	12.30.18.15	1.31	0.00340	386.72	N	N	145	1867	NA	NA	reduced	80	20
En90-half	12.30.18.18	1.29	0.00335	398.58	N	N	120-140	1874	NA	NA	reduced	80	20
En90-half	12.30.18.21	1.19	0.00254	451.73	N	N	130	1882	NA	NA	reduced	80	20

Table 3. List of all synthetic glasses' SEM analyses.

Composition	**Sample**	**Desired Composition**	**Desired SiO_2 wt%**	**Measured SiO_2 wt%**	**Desired MgO wt%**	**Measured MgO wt%**	**Desired FeO wt%**	**Measured FeO wt%**
Forsterite	7.11.17.15	Yes	42.71	42.73	57.29	57.27	0.00	0.00
Forsterite	8.7.17.14	No	42.71	44.86	57.29	55.14	0.00	0.00
Forsterite	8.4.17.1	No	42.71	53.58	57.29	46.42	0.00	0.00
Forsterite	7.11.17.20	No	42.71	45.32	57.29	54.68	0.00	0.00
Forsterite	8.7.17.21	Yes	42.71	42.88	57.29	57.12	0.00	0.00
Forsterite	8.7.17.20	Yes	42.71	41.24	57.29	58.76	0.00	0.00
Forsterite	7.11.17.18							
Forsterite	8.7.17.16							
Enstatite	7.31.17.9							
Enstatite	7.31.17.6							
Enstatite	7.31.17.5							
Enstatite	7.31.17.4							
Enstatite	7.31.17.3	No	59.85	64.90	40.15	35.10	0.00	0.00
Enstatite	7.31.17.11	Yes	59.85	60.46	40.15	39.54	0.00	0.00
Enstatite	7.31.17.10	Yes	59.85	60.44	40.15	39.56	0.00	0.00
Enstatite	7.31.17.8							
Enstatite	7.11.17.4	Yes	59.85	58.46	40.15	41.54	0.00	0.00
Enstatite	7.11.17.2	No	59.85	64.62	40.15	35.38	0.00	0.00
Enstatite	7.31.17.1							
$MgO_{2.5}SiO_2$	8.14.17.7	No	37.35	46.47	62.65	53.53	0.00	0.00
$MgO_{2.5}SiO_2$	8.14.17.8	No	37.35	49.38	62.65	50.62	0.00	0.00
Enstatite	9.11.17.1							
Enstatite	9.11.17.4							
Enstatite	9.11.17.7							

Table 3. Continued.

Composition	Sample	Desired Composition	Desired SiO_2 wt%	Measured SiO_2 wt%	Desired MgO wt%	Measured MgO wt%	Desired FeO wt%	Measured FeO wt%
Enstatite	9.11.17.8							
Enstatite	9.11.17.3							
Enstatite	9.11.17.5							
Enstatite	9.11.17.6							
Forsterite	10.6.17.13							
Forsterite	10.6.17.20	Yes	42.70	42.31	57.30	57.69	0.00	0.00
Enstatite	11.2.17.1							
Enstatite	11.2.17.2	Yes	59.85	58.74	40.15	41.26	0.00	0.00
Enstatite	11.2.17.3							
Enstatite	11.2.17.4							
Enstatite	11.2.17.5							
Enstatite	11.2.17.6							
En95	11.30.17.1							
En95	11.30.17.2	No	58.70	53.63	37.40	45.73	3.50	0.63
En95	11.30.17.3							
En95	11.30.17.4	No	58.93	54.83	37.55	43.34	3.52	1.82
En95	11.30.17.5							
En95	11.30.17.6							
En95	11.30.17.7							
En95	11.30.17.8							
En90	1.5.18.1							
En90	1.5.18.2							
En90	1.5.18.3							
En90	1.5.18.4	No	57.60	58.27	34.80	40.02	6.90	1.71

Table 3. Continued.

Composition	Sample	Desired Composition	Desired SiO_2 wt%	Measured SiO_2 wt%	Desired MgO wt%	Measured MgO wt%	Desired FeO wt%	Measured FeO wt%
En90	1.5.18.5							
En90	1.5.18.6							
En90	1.5.18.7							
En90	1.5.18.8							
En90	1.5.18.9							
En90	1.5.18.10	No	57.60	58.18	34.80	38.25	6.90	3.57
En90	1.5.18.11							
En95	EN5Fe_O2_10p1mg_60s							
En95	EN5Fe4_1CO2_CO_5p3mg_60s							
En95	EN5Fe4_1CO2_CO_6p0mg_10s							
En95	EN5Fe4_1CO2_CO_6p3mg_60s							
En95	3.6.18.1							
En95	3.6.18.2							
En95	3.6.18.3							
En95	3.6.18.4							
En95	3.6.18.5							

Table 3. Continued.

Composition	Sample	Desired Composition	Desired SiO_2 wt%	Measured SiO_2 wt%	Desired MgO wt%	Measured MgO wt%	Desired FeO wt%	Measured FeO wt%
En95	3.6.18.6							
En95	3.6.18.7							
En95	3.6.18.8							
En95	3.6.18.9							
En95	3.6.18.10							
En95	3.6.18.11							
En95	3.6.18.12							
En95	3.28.18.1	Yes	58.93	57.16	37.55	39.60	3.52	3.24
En95	3.28.18.2							
En95	3.28.18.4							
En95	3.28.18.5	No	58.93	55.07	37.55	40.78	3.52	4.15
En95	3.28.18.6	No	58.93	57.05	37.55	40.19	3.52	2.76
En95	3.28.18.7							
En95	3.28.18.8	No	58.93	52.81	37.55	45.24	3.52	1.95
En95	3.28.18.9							
En95	3.28.18.10							
En95	3.28.18.11	No	58.93	56.56	37.55	41.67	3.52	1.77
En95	3.28.18.12	No	58.93	39.99	37.55	59.98	3.52	0.03
En95	3.28.18.13							
En90	5.16.18.4							
En90	5.16.18.5							
En90	5.16.18.7							
En90	5.16.18.10							
En90	5.16.18.11							

Table 4. SEM multiple spot analysis results for forsterite, enstatite, Mg-enriched enstatite, and Fe-bearing enstatite glasses, using an MRL Block Olivine Standard.

Composition	**Sample**	**Spot**	**MgO %**	**Mean MgO %**	**ΔMgO %**	**SiO_2 %**	**Mean SiO_2 %**	**ΔSiO_2 %**	**FeO %**	**Mean FeO %**	**ΔFeO %**	**MgO wt% stdev**	**SiO_2 wt% stdev**	**Fe_2O_3 wt% stdev**
Forsterite	**TARGET**		**57.30**		0.00	**42.70**		0.00						
Forsterite	7.11.17.15	center	56.24	57.27	**1.06**	43.76	42.73	**1.06**				0.89	0.89	
Forsterite	7.11.17.15	mid	57.78		**0.48**	42.22		**0.48**						
Forsterite	7.11.17.15	edge	57.79		**0.49**	42.21		**0.49**						
Forsterite	7.11.17.20	center	53.97	54.68	**3.33**	46.03	45.32	**3.33**				0.55	0.55	
Forsterite	7.11.17.20	mid	54.54		**2.76**	45.46		**2.76**						
Forsterite	7.11.17.20	edge	55.01		**2.29**	44.99		**2.29**						
Forsterite	7.11.17.20	edge2	55.19		**2.11**	44.81		**2.11**						
Forsterite	8.4.17.1	center	47.67	46.42	**9.63**	52.33	53.58	**9.63**				2.63	2.63	
Forsterite	8.4.17.1	mid	44.08		**13.22**	55.92		**13.22**						
Forsterite	8.4.17.1	edge	44.41		**12.89**	55.59		**12.89**						
Forsterite	8.4.17.1	edge2	49.53		**7.77**	50.47		**7.77**						
Forsterite	8.7.17.14	center	53.88	55.14	**3.42**	46.12	44.86	**3.42**				1.37	1.37	
Forsterite	8.7.17.14	mid	57.10		**0.20**	42.90		**0.20**						
Forsterite	8.7.17.14	edge	54.80		**2.50**	45.20		**2.50**						
Forsterite	8.7.17.14	edge2	54.79		**2.51**	45.21		**2.51**						
Forsterite	8.7.17.20	center	58.76	58.76	**1.46**	41.24	41.24	**1.46**						
Forsterite	8.7.17.21	center	57.12	57.12	**0.18**	42.88	42.88	**0.18**						
Forsterite	10.6.17.20	center	56.96	57.69	0.34	43.04	42.31	0.34				0.67	0.67	
Forsterite	10.6.17.20	edge	58.29		0.99	41.71		0.99						
Forsterite	10.6.17.20	mid	57.82		0.52	42.18		0.52						

Table 4. Continued.

Composition	Sample	Spot	MgO %	Mean MgO %	ΔMgO %	SiO_2 %	Mean SiO_2 %	ΔSiO_2 %	FeO %	Mean FeO %	ΔFeO %	MgO wt% stdev	SiO_2 wt% stdev	Fe_2O_3 wt% stdev
Enstatite	**TARGET**	**En**	**40.31**		0.00	**59.7**		0.00						
Enstatite	7.11.17.4	center	40.63	41.54	**0.32**	59.37	58.46	**0.32**				0.61	0.61	
Enstatite	7.11.17.4	mid	41.92		**1.61**	58.08		**1.61**						
Enstatite	7.11.17.4	edge	41.85		**1.54**	58.15		**1.54**						
Enstatite	7.11.17.4	edge2	41.75		**1.44**	58.25		**1.44**						
Enstatite	7.11.17.2	center	35.59	35.38	**4.72**	64.41	64.62	**4.72**				0.49	0.49	
Enstatite	7.11.17.2	mid	35.92		**4.39**	64.08		**4.39**						
Enstatite	7.11.17.2	edge	35.24		**5.07**	64.76		**5.07**						
Enstatite	7.11.17.2	edge2	34.77		**5.54**	65.23		**5.54**						
Enstatite	7.31.17.10	center	39.43	39.56	**0.88**	60.57	60.44	**0.88**				0.46	0.46	
Enstatite	7.31.17.10	mid	39.32		**0.99**	60.68		**0.99**						
Enstatite	7.31.17.10	edge	40.24		**0.07**	59.76		**0.07**						
Enstatite	7.31.17.10	edge2	39.24		**1.07**	60.76		**1.07**						
Enstatite	7.31.17.11	center	39.00	39.54	**1.31**	61.00	60.46	**1.31**				0.44	0.44	
Enstatite	7.31.17.11	mid	39.38		**0.93**	60.62		**0.93**						
Enstatite	7.31.17.11	edge	39.96		**0.35**	60.04		**0.35**						
Enstatite	7.31.17.11	edge2	39.83		**0.48**	60.17		**0.48**						
Enstatite	7.31.17.3	center	35.10	35.10	**5.21**	64.90	64.90	**5.21**				0.03	0.03	
Enstatite	7.31.17.3	mid	35.11		**5.20**	64.89		**5.20**						
Enstatite	7.31.17.3	edge	35.05		**5.26**	64.95		**5.26**						
Enstatite	7.31.17.3	edge2	35.13		**5.18**	64.87		**5.18**						
Enstatite	11.2.17.2	center	41.27	41.26	0.96	58.73	58.74	0.96				0.05	0.05	
Enstatite	11.2.17.2	edge	41.20		0.89	58.8		0.89						
Enstatite	11.2.17.2	mid	41.30		0.99	58.7		0.99						

Table 4. Continued.

Composition	**Sample**	**Spot**	**MgO %**	**Mean MgO %**	**ΔMgO %**	**SiO_2 %**	**Mean SiO_2 %**	**ΔSiO_2 %**	**FeO %**	**Mean FeO %**	**ΔFeO %**	**MgO wt% stdev**	**SiO_2 wt% stdev**	**Fe_2O_3 wt% stdev**
$(MgO)_{2.5}(SiO_2)$	**TARGET**	**In**	**62.65**		**0.00**	**37.35**		**0.00**						
$(MgO)_{2.5}(SiO_2)$	8.14.17.7	center	53.90	53.53	**8.75**	46.10	46.47	**8.75**				0.36	0.36	
$(MgO)_{2.5}(SiO_2)$	8.14.17.7	mid	53.50		**9.15**	46.50		**9.15**						
$(MgO)_{2.5}(SiO_2)$	8.14.17.7	edge	53.18		**9.47**	46.82		**9.47**						
$(MgO)_{2.5}(SiO_2)$	8.14.17.8	center	47.72	50.62	**14.93**	52.28	49.38	**14.93**				4.10	4.10	
$(MgO)_{2.5}(SiO_2)$	8.14.17.8	edge	53.52		**9.13**	46.48		**9.13**						
En90	**TARGET**	**En90**	**35.00**		0.00	**58.00**		4.65	**6.90**					
En90	1.5.18.4	center	38.00	40.02	3.00	62.00	59.98	0.65	3.42	1.71	3.48	1.80	1.80	1.48
En90	1.5.18.4	edge	40.61		5.61	59.39		3.26	0.87		6.03			
En90	1.5.18.4	mid	41.46		6.46	58.54		4.11	0.84		6.06			
En90	1.5.18.10	center	35.40	37.70	0.40	64.6	62.30	1.95	6.54	4.12	0.36	2.49	2.49	2.60
En90	1.5.18.10	edge	40.00		5.00	60		2.65	1.7		5.20			
En90	1.5.18.10	mid	39.34		4.34	60.66		1.99	2.47		4.43			

Table 4. Continued.

Composition	Sample	Spot	MgO %	Mean MgO %	ΔMgO %	SiO_2 %	Mean SiO_2 %	ΔSiO_2 %	FeO %	Mean FeO %	ΔFeO %	MgO wt% stdev	SiO_2 wt% stdev	Fe_2O_3 wt% stdev
En95	**TARGET**	**En95**	**37.60**		2.71	**58.90**		0.00	**3.50**					
En95	11.30.17.2	center	44.22	45.73	3.91	54.75	53.63	4.15	1.03	0.63	2.47	1.35	1.01	0.35
En95	11.30.17.2	edge	46.17		5.86	53.37		5.53	0.47		3.03			
En95	11.30.17.2	mid	46.81		6.50	52.78		6.12	0.4		3.10			
En95	11.30.17.4	center	41.72	43.34	1.41	54.81	54.83	4.09	3.47	1.82	0.03	1.43	0.45	1.59
En95	11.30.17.4	edge	44.4		4.09	55.29		3.61	0.3		3.20			
En95	11.30.17.4	mid	43.9		3.59	54.4		4.50	1.7		1.80			
En95	3.28.18.1	center	38.28	39.60	2.03	57.09	57.16	1.81	4.63	3.24	1.13	1.17	0.07	1.24
En95	3.28.18.1	edge	40.51		0.20	57.23		1.67	2.26		1.24			
En95	3.28.18.1	mid	40.02		0.29	57.16		1.74	2.82		0.68			
En95	3.28.18.5	midCenter	40.16	40.78	0.15	55.1	55.07	3.80	4.74	4.15	1.24	0.58	0.11	0.62
En95	3.28.18.5	edge	40.87		0.56	54.95		3.95	4.19		0.69			
En95	3.28.18.5	mid	41.32		1.01	55.17		3.73	3.51		0.01			
En95	3.28.18.6	center	39.1	40.19	1.21	57.12	57.05	1.78	3.78	2.76	0.28	1.00	0.14	0.99
En95	3.28.18.6	edge	41.06		0.75	57.13		1.77	1.8		1.70			
En95	3.28.18.6	mid	40.4		0.09	56.89		2.01	2.71		0.79			
En95	3.28.18.8	center	50.55	45.24	10.24	48.04	52.81	10.86	1.41	1.95	2.09	5.16	4.18	1.77
En95	3.28.18.8	edge	40.25		0.06	55.83		3.07	3.92		0.42			
En95	3.28.18.8	mid	44.92		4.61	54.57		4.33	0.51		2.99			
En95	3.28.18.11	center	39.07	41.67	1.24	56.4	56.56	2.50	4.52	1.77	1.02	2.27	0.36	2.38
En95	3.28.18.11	edge	43.26		2.95	56.31		2.59	0.43		3.07			
En95	3.28.18.11	mid	42.67		2.36	56.98		1.92	0.35		3.15			
En95	3.28.18.12	center	68.56	59.98	28.25	31.38	39.99	27.52	0.06	0.03	3.44	6.15	6.18	0.03
En95	3.28.18.12	edge	57.06		16.75	42.94		15.96	0		3.50			
En95	3.28.18.12	edge2	54.38		14.07	45.62		13.28	0		3.50			
En95	3.28.18.12	mid	59.92		19.61	40.03		18.87	0.04		3.46			

Table 5. Account of specific methods used for synthesis of each sample, detailed in section 1.3.

Composition	Sample	Version	Powder Prep Method	Laser Fusing Method	Polishing Method	Intended Formula	SiO_2 mass (mg)	MgO mass (mg)	Fe_2O_3 mass (mg)	batch date
Enstatite	No glasses	1	A	A	A and B	$MgSiO_3$	2994.1	2151.7	0	5/12/2017
Enstatite	7.11.17.2	2	A	B	B and C	$MgSiO_3$	598.51	432.64	0	6/29/2017
Enstatite	7.11.17.4	2	A	B	B and C	$MgSiO_3$	598.51	432.64	0	6/29/2017
Enstatite	7.31.17.1	2	A	B	B	$MgSiO_3$	598.51	432.64	0	6/29/2017
Enstatite	7.31.17.3	2	A	B	B and C	$MgSiO_3$	598.51	432.64	0	6/29/2017
Enstatite	7.31.17.4	2	A	B	B	$MgSiO_3$	598.51	432.64	0	6/29/2017
Enstatite	7.31.17.5	2	A	B	B	$MgSiO_3$	598.51	432.64	0	6/29/2017
Enstatite	7.31.17.6	2	A	B	B	$MgSiO_3$	598.51	432.64	0	6/29/2017
Enstatite	7.31.17.8	2	A	B	B	$MgSiO_3$	598.51	432.64	0	6/29/2017
Enstatite	7.31.17.9	2	A	B	B	$MgSiO_3$	598.51	432.64	0	6/29/2017
Enstatite	7.31.17.10	2	A	B	B and C	$MgSiO_3$	598.51	432.64	0	6/29/2017
Enstatite	7.31.17.11	2	A	B	B and C	$MgSiO_3$	598.51	432.64	0	6/29/2017
Enstatite	9.11.17.1	3	B	B	not polished	$MgSiO_3$	598.55	432.71	0	9/5/2017
Enstatite	9.11.17.4	3	B	B	not polished	$MgSiO_3$	598.55	432.71	0	9/5/2017
Enstatite	9.11.17.7	3	B	B	not polished	$MgSiO_3$	598.55	432.71	0	9/5/2017
Enstatite	9.11.17.8	3	B	B	not polished	$MgSiO_3$	598.55	432.71	0	9/5/2017
Enstatite	9.11.17.3	3	B	B	not polished	$MgSiO_3$	598.55	432.71	0	9/5/2017

Table 5. Continued.

Composition	Sample	Version	Powder Prep Method	Laser Fusing Method	Polishing Method	Intended Formula	SiO_2 mass (mg)	MgO mass (mg)	Fe_2O_3 mass (mg)	batch date
Enstatite	9.11.17.5	3	B	B	not polished	$MgSiO_3$	598.55	432.71	0	9/5/2017
Enstatite	9.11.17.6	3	B	B	not polished	$MgSiO_3$	598.55	432.71	0	9/5/2017
Enstatite	11.2.17.1	3	B	B	not polished	$MgSiO_3$	598.55	432.71	0	9/5/2017
Enstatite	11.2.17.2	3	B	B	E	$MgSiO_3$	598.55	432.71	0	9/5/2017
Enstatite	11.2.17.3	3	B	B	not polished	$MgSiO_3$	598.55	432.71	0	9/5/2017
Enstatite	11.2.17.4	3	B	B	not polished	$MgSiO_3$	598.55	432.71	0	9/5/2017
Enstatite	11.2.17.5	3	B	B	not polished	$MgSiO_3$	598.55	432.71	0	9/5/2017
Enstatite	11.2.17.6	3	B	B	not polished	$MgSiO_3$	598.55	432.71	0	9/5/2017
Forsterite	No glasses	1	A	A	A and B	Mg_2SiO_4	2128.9	3070.8	0	5/12/2017
Forsterite	7.11.17.15	2	A	B	B	Mg_2SiO_4	427.05	617.41	0	6/29/2017
Forsterite	7.11.17.18	2	A	B	not polished	Mg_2SiO_4	427.05	617.41	0	6/29/2017
Forsterite	7.11.17.20	2	A	B	B	Mg_2SiO_4	427.05	617.41	0	6/29/2017
Forsterite	8.4.17.1	2	A	B	not polished	Mg_2SiO_4	427.05	617.41	0	6/29/2017
Forsterite	8.7.17.14	2	A	B	B	Mg_2SiO_4	427.05	617.41	0	6/29/2017
Forsterite	8.7.17.16	2	A	B	not polished	Mg_2SiO_4	427.05	617.41	0	6/29/2017
Forsterite	8.7.17.20	2	A	B	B	Mg_2SiO_4	427.05	617.41	0	6/29/2017

Table 5. Continued.

Composition	Sample	Version	Powder Prep Method	Laser Fusing Method	Polishing Method	Intended Formula	SiO_2 mass (mg)	MgO mass (mg)	Fe_2O_3 mass (mg)	batch date
Forsterite	8.7.17.21	2	A	B	B	Mg_2SiO_4	427.05	617.41	0	6/29/2017
Forsterite	10.6.17.13	3	B	B	D	Mg_2SiO_4	427.66	617.65	0	9/5/2017
Forsterite	10.6.17.20	3	B	B	D	Mg_2SiO_4	427.66	617.65	0	9/5/2017
Enriched MgO Enstatite	8.14.17.7	1	A	B	B	$Mg_{2.5}SiO_3$	182.82	337.56	0	8/11/2017
Enriched MgO Enstatite	8.14.17.8	1	A	B	B	$Mg_{2.5}SiO_3$	182.82	337.56	0	8/11/2017
En95	EN5Fe_O2_10p1 mg_60s	1	A	B	D	$Mg_{0.95}Fe_{0.05}SiO_3$	568.62	411.21	50	6/28/2017
En95	EN5Fe4_1CO2_C O_5p3mg_60s	1	A	B	D	$Mg_{0.95}Fe_{0.05}SiO_3$	568.62	411.21	50	6/28/2017
En95	EN5Fe4_1CO2_C O_6p0mg_10s	1	A	B	D	$Mg_{0.95}Fe_{0.05}SiO_3$	568.62	411.21	50	6/28/2017

Table 5. Continued.

Composition	Sample	Version	Powder Prep Method	Laser Fusing Method	Polishing Method	Intended Formula	SiO_2 mass (mg)	MgO mass (mg)	Fe_2O_3 mass (mg)	batch date
En95	EN5Fe4_1CO2_CO_6p3mg_60s	1	A	B	D	$Mg_{0.95}Fe_{0.05}SiO_3$	568.62	411.21	50	6/28/2017
En95	11.30.17.1	2	B	B	D	$Mg_{0.95}Fe_{0.05}SiO_3$	568.58	411.01	50.00	9/27/2017
En95	11.30.17.2	2	B	B	E	$Mg_{0.95}Fe_{0.05}SiO_3$	568.58	411.01	50.00	9/27/2017
En95	11.30.17.3	2	B	B	E	$Mg_{0.95}Fe_{0.05}SiO_3$	568.58	411.01	50.00	9/27/2017
En95	11.30.17.4	2	B	B	E	$Mg_{0.95}Fe_{0.05}SiO_3$	568.58	411.01	50.00	9/27/2017
En95	11.30.17.5	2	B	B	E	$Mg_{0.95}Fe_{0.05}SiO_3$	568.58	411.01	50.00	9/27/2017
En95	11.30.17.6	2	B	B	E	$Mg_{0.95}Fe_{0.05}SiO_3$	568.58	411.01	50.00	9/27/2017
En95	11.30.17.7	2	B	B	E	$Mg_{0.95}Fe_{0.05}SiO_3$	568.58	411.01	50.00	9/27/2017
En95	11.30.17.8	2	B	B	E	$Mg_{0.95}Fe_{0.05}SiO_3$	568.58	411.01	50.00	9/27/2017
En95	3.6.18.1	2	B	B	E	$Mg_{0.95}Fe_{0.05}SiO_3$	568.58	411.01	50.00	9/27/2017
En95	3.6.18.2	2	B	B	E	$Mg_{0.95}Fe_{0.05}SiO_3$	568.58	411.01	50.00	9/27/2017
En95	3.6.18.3	2	B	B	E	$Mg_{0.95}Fe_{0.05}SiO_3$	568.58	411.01	50.00	9/27/2017
En95	3.6.18.4	2	B	B	E	$Mg_{0.95}Fe_{0.05}SiO_3$	568.58	411.01	50.00	9/27/2017
En95	3.6.18.5	2	B	B	E	$Mg_{0.95}Fe_{0.05}SiO_3$	568.58	411.01	50.00	9/27/2017

Table 5. Continued.

Composition	Sample	Version	Powder Prep Method	Laser Fusing Method	Polishing Method	Intended Formula	SiO_2 mass (mg)	MgO mass (mg)	Fe_2O_3 mass (mg)	batch date
En95	3.6.18.6	2	B	B	E	$Mg_{0.95}Fe_{0.05}SiO_3$	568.58	411.01	50.00	9/27/2017
En95	3.6.18.7	2	B	B	E	$Mg_{0.95}Fe_{0.05}SiO_3$	568.58	411.01	50.00	9/27/2017
En95	3.6.18.8	2	B	B	E	$Mg_{0.95}Fe_{0.05}SiO_3$	568.58	411.01	50.00	9/27/2017
En95	3.6.18.9	2	B	B	E	$Mg_{0.95}Fe_{0.05}SiO_3$	568.58	411.01	50.00	9/27/2017
En95	3.6.18.10	2	B	B	E	$Mg_{0.95}Fe_{0.05}SiO_3$	568.58	411.01	50.00	9/27/2017
En95	3.6.18.11	2	B	B	E	$Mg_{0.95}Fe_{0.05}SiO_3$	568.58	411.01	50.00	9/27/2017
En95	3.6.18.12	2	B	B	E	$Mg_{0.95}Fe_{0.05}SiO_3$	568.58	411.01	50.00	9/27/2017
En95	3.28.18.1	2	B	B	E	$Mg_{0.95}Fe_{0.05}SiO_3$	568.58	411.01	50.00	9/27/2017
En95	3.28.18.2	2	B	B	E	$Mg_{0.95}Fe_{0.05}SiO_3$	568.58	411.01	50.00	9/27/2017
En95	3.28.18.4	2	B	B	E	$Mg_{0.95}Fe_{0.05}SiO_3$	568.58	411.01	50.00	9/27/2017
En95	3.28.18.5	2	B	B	E	$Mg_{0.95}Fe_{0.05}SiO_3$	568.58	411.01	50.00	9/27/2017
En95	3.28.18.6	2	B	B	E	$Mg_{0.95}Fe_{0.05}SiO_3$	568.58	411.01	50.00	9/27/2017
En95	3.28.18.7	2	B	B	E	$Mg_{0.95}Fe_{0.05}SiO_3$	568.58	411.01	50.00	9/27/2017
En95	3.28.18.8	2	B	B	E	$Mg_{0.95}Fe_{0.05}SiO_3$	568.58	411.01	50.00	9/27/2017
En95	3.28.18.9	2	B	B	E	$Mg_{0.95}Fe_{0.05}SiO_3$	568.58	411.01	50.00	9/27/2017
En95	3.28.18.10	2	B	B	E	$Mg_{0.95}Fe_{0.05}SiO_3$	568.58	411.01	50.00	9/27/2017

Table 5. Continued.

Composition	Sample	Version	Powder Prep Method	Laser Fusing Method	Polishing Method	Intended Formula	SiO_2 mass (mg)	MgO mass (mg)	Fe_2O_3 mass (mg)	batch date
En95	3.28.18.11	2	B	B	E	$Mg_{0.95}Fe_{0.05}SiO_3$	568.58	411.01	50.00	9/27/2017
En95	3.28.18.12	2	B	B	E	$Mg_{0.95}Fe_{0.05}SiO_3$	568.58	411.01	50.00	9/27/2017
En95	3.28.18.13	2	B	B	E	$Mg_{0.95}Fe_{0.05}SiO_3$	568.58	411.01	50.00	9/27/2017
En95	5.30.18.1	3	C	B	not polished	$Mg_{0.95}Fe_{0.05}SiO_3$	294.66	202.31	43.5	5/15/2018
En95	5.30.18.2	3	C	B	not polished	$Mg_{0.95}Fe_{0.05}SiO_3$	294.66	202.31	43.5	5/15/2018
En95	5.30.18.10	3	C	B	not polished	$Mg_{0.95}Fe_{0.05}SiO_3$	294.66	202.31	43.5	5/15/2018
En95	5.30.18.11	3	C	B	not polished	$Mg_{0.95}Fe_{0.05}SiO_3$	294.66	202.31	43.5	5/15/2018
En95	5.30.18.12	3	C	B	not polished	$Mg_{0.95}Fe_{0.05}SiO_3$	294.66	202.31	43.5	5/15/2018
En95	5.30.18.13	3	C	B	not polished	$Mg_{0.95}Fe_{0.05}SiO_3$	294.66	202.31	43.5	5/15/2018
En95	5.30.18.14	3	C	B	not polished	$Mg_{0.95}Fe_{0.05}SiO_3$	294.66	202.31	43.5	5/15/2018
En95	6.15.18.3	3	C	B	not polished	$Mg_{0.95}Fe_{0.05}SiO_3$	294.66	202.31	43.5	5/15/2018
En95	6.15.18.5	3	C	B	not polished	$Mg_{0.95}Fe_{0.05}SiO_3$	294.66	202.31	43.5	5/15/2018
En95	6.18.18.1	4	C	B	E	$(Mg_{0.95}Fe_{0.05})(Si_{0.95}Fe_{0.05})O_3$	266.23	192.44	41.4	6/18/2018
En95	6.18.18.2	4	C	B	not polished	$(Mg_{0.95}Fe_{0.05})(Si_{0.95}Fe_{0.05})O_3$	266.23	192.44	41.4	6/18/2018
En95	6.18.18.5	4	C	B	not polished	$(Mg_{0.95}Fe_{0.05})(Si_{0.95}Fe_{0.05})O_3$	266.23	192.44	41.4	6/18/2018
En95	6.18.18.6	4	C	B	not polished	$(Mg_{0.95}Fe_{0.05})(Si_{0.95}Fe_{0.05})O_3$	266.23	192.44	41.4	6/18/2018

Table 5. Continued.

Composition	Sample	Version	Powder Prep Method	Laser Fusing Method	Polishing Method	Intended Formula	SiO_2 mass (mg)	MgO mass (mg)	Fe_2O_3 mass (mg)	batch date
En95	6.18.18.7	4	C	B	not polished	$(Mg_{0.95}Fe_{0.05})(Si_{0.95}Fe_{0.05})O_3$	266.23	192.44	41.4	6/18/2018
En95	6.18.18.8	4	C	B	not polished	$(Mg_{0.95}Fe_{0.05})(Si_{0.95}Fe_{0.05})O_3$	266.23	192.44	41.4	6/18/2018
En95	6.21.18.1	4	C	B	not polished	$(Mg_{0.95}Fe_{0.05})(Si_{0.95}Fe_{0.05})O_3$	266.23	192.44	41.4	6/18/2018
En95	6.21.18.2	4	C	B	not polished	$(Mg_{0.95}Fe_{0.05})(Si_{0.95}Fe_{0.05})O_3$	266.23	192.44	41.4	6/18/2018
En95	6.21.18.3	4	C	B	not polished	$(Mg_{0.95}Fe_{0.05})(Si_{0.95}Fe_{0.05})O_3$	266.23	192.44	41.4	6/18/2018
En95	6.21.18.5	4	C	B	not polished	$(Mg_{0.95}Fe_{0.05})(Si_{0.95}Fe_{0.05})O_3$	266.23	192.44	41.4	6/18/2018
En95	7.2.18.1	4	C	B	E	$(Mg_{0.95}Fe_{0.05})(Si_{0.95}Fe_{0.05})O_3$	266.23	192.44	41.4	6/18/2018
En95	7.2.18.6	4	C	B	E	$(Mg_{0.95}Fe_{0.05})(Si_{0.95}Fe_{0.05})O_3$	266.23	192.44	41.4	6/18/2018
En95	7.2.18.7	4	C	B	E	$(Mg_{0.95}Fe_{0.05})(Si_{0.95}Fe_{0.05})O_3$	266.23	192.44	41.4	6/18/2018
En95	7.9.18.1	4	C	B	E	$(Mg_{0.95}Fe_{0.05})(Si_{0.95}Fe_{0.05})O_3$	266.23	192.44	41.4	6/18/2018
En95	7.9.18.2	4	C	B	E	$(Mg_{0.95}Fe_{0.05})(Si_{0.95}Fe_{0.05})O_3$	266.23	192.44	41.4	6/18/2018
En95	7.9.18.3	4	C	B	E	$(Mg_{0.95}Fe_{0.05})(Si_{0.95}Fe_{0.05})O_3$	266.23	192.44	41.4	6/18/2018
En95	7.9.18.4	4	C	B	E	$(Mg_{0.95}Fe_{0.05})(Si_{0.95}Fe_{0.05})O_3$	266.23	192.44	41.4	6/18/2018
En95	7.9.18.5	4	C	B	E	$(Mg_{0.95}Fe_{0.05})(Si_{0.95}Fe_{0.05})O_3$	266.23	192.44	41.4	6/18/2018
En95	7.9.18.6	4	C	B	E	$(Mg_{0.95}Fe_{0.05})(Si_{0.95}Fe_{0.05})O_3$	266.23	192.44	41.4	6/18/2018
En95	7.9.18.7	4	C	B	E	$(Mg_{0.95}Fe_{0.05})(Si_{0.95}Fe_{0.05})O_3$	266.23	192.44	41.4	6/18/2018

Table 5. Continued.

Composition	Sample	Version	Powder Prep Method	Laser Fusing Method	Polishing Method	Intended Formula	SiO_2 mass (mg)	MgO mass (mg)	Fe_2O_3 mass (mg)	batch date
En95	7.9.18.8	4	C	B	not polished	$(Mg_{0.95}Fe_{0.05})(Si_{0.95}Fe_{0.05})O_3$	266.23	192.44	41.4	6/18/2018
En90	1.5.18.1	1	B	B	E	$Mg_{0.9}Fe_{0.1}SiO_3$	287.96	187.21	42.5	1/3/2018
En90	1.5.18.2	1	B	B	not polished	$Mg_{0.9}Fe_{0.1}SiO_3$	287.96	187.21	42.5	1/3/2018
En90	1.5.18.3	1	B	B	not polished	$Mg_{0.9}Fe_{0.1}SiO_3$	287.96	187.21	42.5	1/3/2018
En90	1.5.18.4	1	B	B	E	$Mg_{0.9}Fe_{0.1}SiO_3$	287.96	187.21	42.5	1/3/2018
En90	1.5.18.5	1	B	B	not polished	$Mg_{0.9}Fe_{0.1}SiO_3$	287.96	187.21	42.5	1/3/2018
En90	1.5.18.6	1	B	B	not polished	$Mg_{0.9}Fe_{0.1}SiO_3$	287.96	187.21	42.5	1/3/2018
En90	1.5.18.7	1	B	B	not polished	$Mg_{0.9}Fe_{0.1}SiO_3$	287.96	187.21	42.5	1/3/2018
En90	1.5.18.8	1	B	B	not polished	$Mg_{0.9}Fe_{0.1}SiO_3$	287.96	187.21	42.5	1/3/2018
En90	1.5.18.9	1	B	B	E	$Mg_{0.9}Fe_{0.1}SiO_3$	287.96	187.21	42.5	1/3/2018
En90	1.5.18.10	1	B	B	E	$Mg_{0.9}Fe_{0.1}SiO_3$	287.96	187.21	42.5	1/3/2018
En90	1.5.18.11	1	B	B	not polished	$Mg_{0.9}Fe_{0.1}SiO_3$	287.96	187.21	42.5	1/3/2018
En90	5.16.18.4	2	C	B	not polished	$Mg_{0.9}Fe_{0.1}SiO_3$	290.18	188.81	85.6	5/15/2018
En90	5.16.18.5	2	C	B	not polished	$Mg_{0.9}Fe_{0.1}SiO_3$	290.18	188.81	85.6	5/15/2018
En90	5.16.18.7	2	C	B	not polished	$Mg_{0.9}Fe_{0.1}SiO_3$	290.18	188.81	85.6	5/15/2018
En90	5.16.18.10	2	C	B	not polished	$Mg_{0.9}Fe_{0.1}SiO_3$	290.18	188.81	85.6	5/15/2018

Table 5. Continued.

Composition	Sample	Version	Powder Prep Method	Laser Fusing Method	Polishing Method	Intended Formula	SiO_2 mass (mg)	MgO mass (mg)	Fe_2O_3 mass (mg)	batch date
En90	5.16.18.11	2	C	B	not polished	$Mg_{0.9}Fe_{0.1}SiO_3$	290.18	188.81	85.6	5/15/2018
En90	5.18.18.2	2	C	B	not polished	$Mg_{0.9}Fe_{0.1}SiO_3$	290.18	188.81	85.6	5/15/2018
En90	5.18.18.5	2	C	B	not polished	$Mg_{0.9}Fe_{0.1}SiO_3$	290.18	188.81	85.6	5/15/2018
En90	5.21.18.1	2	C	B	not polished	$Mg_{0.9}Fe_{0.1}SiO_3$	290.18	188.81	85.6	5/15/2018
En90	5.21.18.2	2	C	B	not polished	$Mg_{0.9}Fe_{0.1}SiO_3$	290.18	188.81	85.6	5/15/2018
En90	5.21.18.3	2	C	B	not polished	$Mg_{0.9}Fe_{0.1}SiO_3$	290.18	188.81	85.6	5/15/2018
En90	5.21.18.7	2	C	B	not polished	$Mg_{0.9}Fe_{0.1}SiO_3$	290.18	188.81	85.6	5/15/2018
En90	5.21.18.10	2	C	B	not polished	$Mg_{0.9}Fe_{0.1}SiO_3$	290.18	188.81	85.6	5/15/2018
En90	6.11.18.1	2	C	B	not polished	$Mg_{0.9}Fe_{0.1}SiO_3$	290.18	188.81	85.6	5/15/2018
En90	6.11.18.2	2	C	B	not polished	$Mg_{0.9}Fe_{0.1}SiO_3$	290.18	188.81	85.6	5/15/2018
En90	6.11.18.6	2	C	B	not polished	$Mg_{0.9}Fe_{0.1}SiO_3$	290.18	188.81	85.6	5/15/2018
En90	6.11.18.7	2	C	B	not polished	$Mg_{0.9}Fe_{0.1}SiO_3$	290.18	188.81	85.6	5/15/2018
En90	6.11.18.9	2	C	B	not polished	$Mg_{0.9}Fe_{0.1}SiO_3$	290.18	188.81	85.6	5/15/2018
En90	6.22.18.1	3	C	B	not polished	$Mg_{0.9}Fe_{0.1}SiO_3$	278.07	180.91	41.1	6/18/2018
En90	6.22.18.2	3	C	B	not polished	$Mg_{0.9}Fe_{0.1}SiO_3$	278.07	180.91	41.1	6/18/2018
En90	6.22.18.3	3	C	B	not polished	$Mg_{0.9}Fe_{0.1}SiO_3$	278.07	180.91	41.1	6/18/2018

Table 5. Continued.

Composition	Sample	Version	Powder Prep Method	Laser Fusing Method	Polishing Method	Intended Formula	SiO_2 mass (mg)	MgO mass (mg)	Fe_2O_3 mass (mg)	batch date
En90	6.22.18.4	3	C	B	not polished	$Mg_{0.9}Fe_{0.1}SiO_3$	278.07	180.91	41.1	6/18/2018
En90	6.22.18.5	3	C	B	not polished	$Mg_{0.9}Fe_{0.1}SiO_3$	278.07	180.91	41.1	6/18/2018
En90	6.22.18.6	3	C	B	not polished	$Mg_{0.9}Fe_{0.1}SiO_3$	278.07	180.91	41.1	6/18/2018
En90	6.22.18.7	3	C	B	not polished	$Mg_{0.9}Fe_{0.1}SiO_3$	278.07	180.91	41.1	6/18/2018
En90	6.22.18.8	3	C	B	not polished	$Mg_{0.9}Fe_{0.1}SiO_3$	278.07	180.91	41.1	6/18/2018
En90	7.2.18.8	3	C	B	E	$Mg_{0.9}Fe_{0.1}SiO_3$	278.07	180.91	41.1	6/18/2018
En90	7.2.18.13	3	C	B	E	$Mg_{0.9}Fe_{0.1}SiO_3$	278.07	180.91	41.1	6/18/2018
En90	7.2.18.14	3	C	B	E	$Mg_{0.9}Fe_{0.1}SiO_3$	278.07	180.91	41.1	6/18/2018
En90	7.2.18.15	3	C	B	E	$Mg_{0.9}Fe_{0.1}SiO_3$	278.07	180.91	41.1	6/18/2018
En90	7.2.18.16	3	C	B	E	$Mg_{0.9}Fe_{0.1}SiO_3$	278.07	180.91	41.1	6/18/2018
En90	7.2.18.17	3	C	B	E	$Mg_{0.9}Fe_{0.1}SiO_3$	278.07	180.91	41.1	6/18/2018
Fe-57 En95	12.29.18.6.1	1	C	B	E	$(Mg_{0.95}Fe_{0.05})(Si_{0.95}Fe_{0.05})O_3$	132.94	96.13	20.9	12/20/2018
Fe-57 En95	12.29.18.7.1	1	C	B	E	$(Mg_{0.95}Fe_{0.05})(Si_{0.95}Fe_{0.05})O_3$	132.94	96.13	20.9	12/20/2018
Fe-57 En95	12.29.18.12.1	1	C	B	E	$(Mg_{0.95}Fe_{0.05})(Si_{0.95}Fe_{0.05})O_3$	132.94	96.13	20.9	12/20/2018
Fe-57 En95-half	12.29.18.16.1	1	C	B	E	$(Mg_{0.95}Fe_{0.05})(Si_{0.95}Fe_{0.05})O_3$	133.52	96.51	20	12/20/2018

Table 5. Continued.

Composition	Sample	Version	Powder Prep Method	Laser Fusing Method	Polishing Method	Intended Formula	SiO_2 mass (mg)	MgO mass (mg)	Fe_2O_3 mass (mg)	batch date
Fe-57 En95-half	12.29.18.18.1	1	C	B	E	$(Mg_{0.95}Fe_{0.05})(Si_{0.95}Fe_{0.05})O_3$	133.52	96.51	20	12/20/2018
Fe-57 En95-half	12.29.18.21.1	1	C	B	E	$(Mg_{0.95}Fe_{0.05})(Si_{0.95}Fe_{0.05})O_3$	133.52	96.51	20	12/20/2018
Fe-57 En95-half	12.29.18.22.1	1	C	B	E	$(Mg_{0.95}Fe_{0.05})(Si_{0.95}Fe_{0.05})O_3$	133.52	96.51	20	12/20/2018
Fe-57 En90	12.30.18.1.1	1	C	B	not polished	$Mg_{0.9}Fe_{0.1}SiO_3$	138.87	90.34	20.8	12/20/2018
Fe-57 En90	12.30.18.4.1	1	C	B	not polished	$Mg_{0.9}Fe_{0.1}SiO_3$	138.87	90.34	20.8	12/20/2018
Fe-57 En90	12.30.18.6.1	1	C	B	not polished	$Mg_{0.9}Fe_{0.1}SiO_3$	138.87	90.34	20.8	12/20/2018
Fe-57 En90	12.30.18.7.1	1	C	B	not polished	$Mg_{0.9}Fe_{0.1}SiO_3$	138.87	90.34	20.8	12/20/2018
Fe-57 En90	12.30.18.9.1	1	C	B	not polished	$Mg_{0.9}Fe_{0.1}SiO_3$	138.87	90.34	20.8	12/20/2018
Fe-57 En90	12.30.18.10.1	1	C	B	not polished	$Mg_{0.9}Fe_{0.1}SiO_3$	138.87	90.34	20.8	12/20/2018
Fe-57 En90	12.30.18.11.1	1	C	B	not polished	$Mg_{0.9}Fe_{0.1}SiO_3$	138.87	90.34	20.8	12/20/2018
Fe-57 En90-half	12.30.18.13.1	1	C	B	not polished	$Mg_{0.9}Fe_{0.1}SiO_3$	139.45	90.72	19.8	12/20/2018
Fe-57 En90-half	12.30.18.15.1	1	C	B	not polished	$Mg_{0.9}Fe_{0.1}SiO_3$	139.45	90.72	19.8	12/20/2018
Fe-57 En90-half	12.30.18.18.1	1	C	B	not polished	Mg0.9Fe0.1SiO3	139.45	90.72	19.8	12/20/2018
Fe-57 En90-half	12.30.18.21.1	1	C	B	not polished	Mg0.9Fe0.1SiO3	139.45	90.72	19.8	12/20/2018

Table 6. EMPA analysis results for Fe-bearing En90 and En95 glasses (weight % and cation proportions).

Sample Information			**Concentrations (in wt. %)**					**Cation Proportions**			
Sample Name	Number	Line	O	Mg	Si	Fe	Total	O	Mg	Fe	Si
6.21.18.2	9	84	47.504	21.0748	26.7212	5.72153	101.022	2.969111	0.867097	0.102453	0.951423
6.21.18.2	9	85	47.1236	21.0838	26.9283	5.77553	100.911	2.945335	0.867468	0.10342	0.958797
6.21.18.2	9	86	47.0916	21.034	26.9121	5.7271	100.765	2.943335	0.865419	0.102553	0.95822
6.21.18.2	9	87	47.2772	21.0861	26.7079	5.77106	100.842	2.954936	0.867562	0.10334	0.95095
6.21.18.2	9	88	47.3692	21.1204	26.981	5.70714	101.178	2.960686	0.868973	0.102196	0.960674
6.21.18.2	9	89	47.3103	21.0302	26.9893	5.72895	101.059	2.957005	0.865262	0.102586	0.960969
6.21.18.2	9	90	47.056	21.0239	26.8647	5.77612	100.721	2.94111	0.865003	0.103431	0.956533
6.21.18.2	9	91	47.0466	21.0149	26.8842	5.72287	100.669	2.940523	0.864633	0.102477	0.957227
6.21.18.2	9	92	47.1831	21.0855	26.9284	5.75313	100.95	2.949054	0.867538	0.103019	0.958801
6.21.18.2	9	93	47.144	21.0603	26.9215	5.6952	100.821	2.94661	0.866501	0.101982	0.958555
6.21.18.2	9	94	47.0861	20.9621	26.6884	5.72091	100.458	2.942992	0.86246	0.102442	0.950255
6.21.18.2	9	95	47.2781	21.0622	26.9966	5.78292	101.12	2.954992	0.866579	0.103553	0.961229
6.21.18.2	9	96	46.9757	21.1116	26.8048	5.75963	100.652	2.936091	0.868611	0.103136	0.9544
6.21.18.2	9	97	47.3568	21.1729	26.9541	5.72278	101.207	2.959911	0.871134	0.102476	0.959716
6.21.18.2	9	98	47.0469	21.0845	26.7566	5.64963	100.538	2.940542	0.867496	0.101166	0.952684
6.21.18.2	9	99	47.0911	21.0136	26.9679	5.7005	100.773	2.943304	0.864579	0.102077	0.960207
6.21.18.2	9	100	47.2639	21.0336	26.8434	5.64887	100.79	2.954105	0.865402	0.101152	0.955774
6.21.18.2	9	101	47.1091	21.0451	27.1018	5.67636	100.932	2.944429	0.865875	0.101645	0.964975
6.21.18.2	9	102	47.0932	21.0126	26.8345	5.71822	100.659	2.943435	0.864538	0.102394	0.955457
6.21.18.2	9	103	47.1979	21.0595	26.8197	5.76917	100.846	2.949979	0.866468	0.103307	0.95493
6.21.18.2	9	104	47.079	21.1932	26.3756	5.6882	100.336	2.942548	0.871969	0.101857	0.939118
6.21.18.2	9	105	47.0866	21.0636	26.8407	5.64705	100.638	2.943023	0.866636	0.10112	0.955678
6.21.18.2	9	106	46.9143	20.9806	26.6505	5.69119	100.237	2.932254	0.863222	0.10191	0.948906
6.21.18.2	9	107	47.0099	21.1164	26.4307	5.68406	100.241	2.938229	0.868809	0.101783	0.94108
6.21.18.2	9	108	46.9225	20.9193	26.5857	5.75107	100.179	2.932766	0.860699	0.102982	0.946599
6.21.18.2	9	109	47.0621	21.2236	26.7555	5.74514	100.786	2.941492	0.87322	0.102876	0.952645

Table 6. Continued.

Sample Information			**Concentrations (in wt. %)**					**Cation Proportions**			
Sample Name	Number	Line	O	Mg	Si	Fe	Total	O	Mg	Fe	Si
6.21.18.2	9	110	47.1234	21.1373	26.7755	5.72442	100.761	2.945323	0.869669	0.102505	0.953357
6.21.18.2	9	111	46.8754	20.8964	26.523	5.67308	99.9678	2.929822	0.859757	0.101586	0.944366
6.21.18.2	9	112	47.0817	21.0994	26.6856	5.63893	100.506	2.942717	0.868109	0.100974	0.950156
6.21.18.2	9	113	47.0828	21.1018	26.6402	5.70235	100.527	2.942785	0.868208	0.10211	0.948539
6.21.18.2	9	114	46.9999	21.0234	26.6653	5.75816	100.447	2.937604	0.864983	0.103109	0.949433
6.21.18.2	9	115	47.0101	20.923	26.6307	5.77925	100.343	2.938241	0.860852	0.103487	0.948201
6.21.18.2	9	116	47.0026	21.1309	26.5213	5.68095	100.336	2.937773	0.869405	0.101727	0.944306
6.21.18.2	9	117	47.0185	21.0714	26.4663	5.71818	100.274	2.938766	0.866957	0.102393	0.942347
6.21.18.2	9	118	47.1399	20.9509	26.5435	5.69661	100.331	2.946354	0.862	0.102007	0.945096
6.21.18.2	9	119	47.0053	21.113	26.4496	5.71306	100.281	2.937941	0.868669	0.102302	0.941753
6.21.18.2	9	120	47.0765	20.9456	26.5359	5.72363	100.282	2.942392	0.861782	0.102491	0.944826
6.21.18.2	9	121	46.9799	21.1253	26.7112	5.72694	100.543	2.936354	0.869175	0.10255	0.951067
6.21.18.2	9	122	46.8557	20.9175	26.688	5.73361	100.195	2.928591	0.860625	0.10267	0.950241
6.21.18.2	9	123	46.7555	21.0284	26.7471	5.76737	100.298	2.922328	0.865188	0.103274	0.952346
6.21.18.2	9	124	47.1665	20.9658	26.4989	5.76863	100.4	2.948017	0.862613	0.103297	0.943508
6.21.18.2	9	125	47.2203	21.0815	26.4646	5.7374	100.504	2.951379	0.867373	0.102738	0.942287
6.21.18.2	9	126	46.9053	20.9774	26.4158	5.69485	99.9934	2.931691	0.86309	0.101976	0.940549
6.21.18.2	9	127	46.7779	20.9741	26.3884	5.70021	99.8406	2.923728	0.862954	0.102072	0.939574
6.21.18.2	9	128	46.8014	20.9162	26.2728	5.70112	99.6915	2.925197	0.860572	0.102088	0.935458
6.21.18.2	9	129	46.7825	21.0565	26.3097	5.71953	99.8682	2.924016	0.866344	0.102418	0.936772
6.21.18.2	9	130	47.025	20.9847	26.5844	5.6593	100.253	2.939173	0.86339	0.101339	0.946552
6.21.18.2	9	131	46.869	21.0718	26.3682	5.75051	100.06	2.929422	0.866974	0.102972	0.938855
6.21.18.3	11	137	47.7306	20.9747	26.4579	5.58388	100.747	2.983274	0.862979	0.099989	0.942048
6.21.18.3	11	138	47.7051	21.0843	26.6204	5.79141	101.201	2.981681	0.867488	0.103705	0.947834
6.21.18.3	11	139	47.393	21.0812	26.6614	5.74029	100.876	2.962174	0.867361	0.102789	0.949294

Table 6. Continued.

Sample Information			**Concentrations (in wt. %)**					**Cation Proportions**			
Sample Name	Number	Line	O	Mg	Si	Fe	Total	O	Mg	Fe	Si
6.21.18.3	11	140	47.5441	21.1305	26.9101	5.77353	101.358	2.971618	0.869389	0.103385	0.958149
6.21.18.3	11	141	47.5504	21.1779	26.5996	5.693	101.021	2.972011	0.871339	0.101943	0.947094
6.21.18.3	11	142	47.4119	21.0487	26.6157	5.74484	100.821	2.963355	0.866023	0.102871	0.947667
6.21.18.3	11	143	47.5116	21.1171	26.5623	5.76717	100.958	2.969586	0.868838	0.103271	0.945766
6.21.18.3	11	144	47.6029	21.151	26.6317	5.69697	101.083	2.975293	0.870232	0.102014	0.948237
6.21.18.3	11	145	47.4089	21.1232	26.2767	5.64677	100.456	2.963167	0.869089	0.101115	0.935597
6.21.18.3	11	146	47.3934	21.1321	26.6645	5.72955	100.92	2.962199	0.869455	0.102597	0.949404
6.21.18.3	11	147	47.6984	21.1362	26.439	5.77386	101.047	2.981262	0.869624	0.103391	0.941375
6.21.18.3	11	148	47.6555	21.0751	26.7	5.71221	101.143	2.97858	0.86711	0.102287	0.950668
6.21.18.3	11	149	47.5561	21.2468	26.5736	5.76574	101.142	2.972368	0.874174	0.103245	0.946168
6.21.18.3	11	150	47.2267	21.1146	26.3642	5.74692	100.452	2.951779	0.868735	0.102908	0.938712
6.21.18.3	11	151	47.4917	21.2233	26.4675	5.74376	100.926	2.968343	0.873207	0.102852	0.94239
6.21.18.3	11	152	47.5458	21.0413	26.6152	5.77558	100.978	2.971724	0.865719	0.103421	0.947649
6.21.18.3	11	153	47.2785	20.99	26.4607	5.68056	100.41	2.955017	0.863608	0.10172	0.942148
6.21.18.3	11	154	47.4658	21.0561	26.509	5.80982	100.841	2.966724	0.866328	0.104034	0.943868
6.21.18.3	11	155	47.4315	21.121	26.3744	5.71407	100.641	2.96458	0.868998	0.10232	0.939075
6.21.18.3	11	156	47.4201	21.1293	26.5998	5.73269	100.882	2.963867	0.86934	0.102653	0.947101
6.21.18.3	11	157	47.295	20.9722	26.2371	5.74972	100.254	2.956048	0.862876	0.102958	0.934187
6.21.18.3	11	158	47.2609	21.1065	26.4412	5.77138	100.58	2.953917	0.868402	0.103346	0.941454
6.21.18.3	11	159	47.549	21.1071	26.3534	5.74412	100.754	2.971924	0.868426	0.102858	0.938328
6.21.18.3	11	160	47.3245	20.9613	26.2074	5.75514	100.248	2.957892	0.862427	0.103055	0.933129
6.21.18.3	11	161	47.5002	21.093	26.8644	5.73629	101.194	2.968874	0.867846	0.102718	0.956522
6.21.18.3	11	162	47.4892	21.0539	26.5236	5.71986	100.786	2.968186	0.866237	0.102424	0.944388
6.21.18.3	11	163	47.6756	21.0476	26.6704	5.66388	101.057	2.979837	0.865978	0.101421	0.949615
6.21.18.3	11	164	47.5228	20.9068	26.5057	5.73479	100.67	2.970286	0.860185	0.102691	0.94375

Table 6. Continued.

Sample Information			**Concentrations (in wt. %)**					**Cation Proportions**			
Sample Name	Number	Line	O	Mg	Si	Fe	Total	O	Mg	Fe	Si
6.21.18.3	11	165	47.6154	21.139	26.6265	5.74916	101.13	2.976074	0.869739	0.102948	0.948051
6.21.18.3	11	166	47.5518	21.242	26.5538	5.74626	101.094	2.972099	0.873977	0.102896	0.945463
6.21.18.3	11	167	47.4277	21.0074	26.8022	5.77685	101.014	2.964342	0.864324	0.103444	0.954307
6.21.18.3	11	168	47.495	21.1033	26.8132	5.79187	101.203	2.968549	0.86827	0.103713	0.954699
6.21.18.3	11	169	47.4648	20.9721	26.8273	5.74296	101.007	2.966661	0.862872	0.102837	0.955201
6.21.18.3	11	170	47.3903	20.9759	26.832	5.69337	100.892	2.962005	0.863028	0.101949	0.955368
6.21.18.3	11	171	47.5139	20.9267	26.867	5.65477	100.962	2.96973	0.861004	0.101258	0.956615
6.21.18.3	11	172	47.4603	20.8969	26.7653	5.74617	100.869	2.96638	0.859778	0.102895	0.952994
6.21.18.3	11	173	47.3737	21.1081	26.6771	5.7769	100.936	2.960967	0.868467	0.103445	0.949853
6.21.18.3	11	174	47.2781	21.0359	26.5569	5.76327	100.634	2.954992	0.865497	0.103201	0.945573
6.21.18.3	11	175	47.4454	20.9428	26.5189	5.78033	100.687	2.965449	0.861666	0.103506	0.94422
6.21.18.3	11	176	47.4399	20.9656	26.4314	5.73854	100.575	2.965105	0.862604	0.102758	0.941105
6.21.18.3	11	177	47.3982	20.9352	26.4778	5.78057	100.592	2.962499	0.861354	0.103511	0.942757
6.21.18.3	11	178	47.4285	20.9119	26.5779	5.6727	100.591	2.964392	0.860395	0.101579	0.946321
6.21.18.3	11	179	47.4617	20.9215	26.6894	5.69735	100.77	2.966467	0.86079	0.10202	0.950291
6.21.18.3	11	180	47.3592	20.9414	26.3805	5.66074	100.342	2.960061	0.861609	0.101365	0.939293
6.21.18.3	11	181	47.4385	20.8919	26.6741	5.77689	100.781	2.965017	0.859572	0.103445	0.949746
6.21.18.3	11	182	47.6949	21.0489	26.5648	5.75566	101.064	2.981043	0.866032	0.103065	0.945855
6.21.18.3	11	183	47.5448	21.0753	26.6484	5.75496	101.024	2.971661	0.867118	0.103052	0.948831
6.21.18.3	11	184	47.5053	21.0654	26.4601	5.75601	100.787	2.969193	0.866711	0.103071	0.942127
6.21.18.3	11	185	47.3562	20.8617	26.4753	5.74418	100.437	2.959873	0.85833	0.102859	0.942668
6.21.18.3	11	186	47.3545	20.9456	26.4727	5.7431	100.516	2.959767	0.861782	0.10284	0.942575
6.21.18.3	11	187	37.0626	18.6402	24.1333	5.06951	84.9057	2.316499	0.766929	0.090778	0.85928
6.21.18.3	11	188	47.4013	20.96	26.4448	5.70344	100.509	2.962692	0.862374	0.10213	0.941582
6.21.18.3	11	189	47.6312	20.9775	26.6234	5.73187	100.964	2.977062	0.863094	0.102639	0.947941

Table 6. Continued.

Sample Information			**Concentrations (in wt. %)**					**Cation Proportions**			
Sample Name	Number	Line	O	Mg	Si	Fe	Total	O	Mg	Fe	Si
6.21.18.3	11	190	47.3108	20.9316	26.3751	5.77023	100.388	2.957036	0.861206	0.103326	0.9391
6.21.18.3	11	191	47.9277	21.1462	26.3696	5.7394	101.183	2.995594	0.870035	0.102773	0.938904
6.21.18.3	11	192	47.4215	21.0061	26.4355	5.74913	100.612	2.963955	0.864271	0.102948	0.941251
6.21.18.3	11	193	47.3852	21.0789	26.7366	5.74523	100.946	2.961686	0.867266	0.102878	0.951972
6.21.18.3	11	194	45.9013	20.7917	26.5062	5.72351	98.9227	2.868939	0.855449	0.102489	0.943768
6.21.18.3	11	195	47.4427	20.9196	26.6517	5.72085	100.735	2.96528	0.860712	0.102441	0.948949
6.21.18.3	11	196	47.4278	20.9823	26.6576	5.77399	100.842	2.964349	0.863292	0.103393	0.949159
6.21.18.3	11	197	47.2553	21.0418	26.6268	5.75452	100.678	2.953567	0.86574	0.103044	0.948062
6.21.18.3	11	198	47.3444	20.9613	26.4168	5.76631	100.489	2.959136	0.862427	0.103255	0.940585
6.21.18.3	11	199	47.4216	20.9667	26.538	5.78429	100.711	2.963961	0.86265	0.103577	0.9449
6.21.18.3	11	200	47.3263	20.977	26.5201	5.73606	100.559	2.958005	0.863073	0.102714	0.944263
6.21.18.3	11	201	47.3657	21.0194	26.6353	5.72795	100.748	2.960467	0.864818	0.102568	0.948365
6.21.18.3	11	202	47.5268	21.139	26.7165	5.70029	101.083	2.970536	0.869739	0.102073	0.951256
6.21.18.3	11	203	47.3182	20.9443	26.6487	5.72883	100.64	2.957498	0.861728	0.102584	0.948842
6.21.18.3	11	204	47.4468	20.9457	26.7062	5.7443	100.843	2.965536	0.861786	0.102861	0.950889
6.21.18.3	11	205	47.683	20.9878	26.8035	5.7812	101.256	2.980299	0.863518	0.103522	0.954354
6.21.18.3	11	206	47.3977	20.9518	26.6695	5.74769	100.767	2.962467	0.862037	0.102922	0.949583
6.21.18.3	11	207	47.5035	21.0883	26.6481	5.72546	100.965	2.96908	0.867653	0.102524	0.948821
6.21.18.3	11	208	47.5381	20.9136	26.9033	5.66534	101.02	2.971243	0.860465	0.101447	0.957907
6.21.18.5	18	328	47.0762	21.4249	26.7656	5.70123	100.968	2.942373	0.881502	0.10209	0.953004
6.21.18.5	18	329	47.0064	21.374	26.8404	5.7419	100.963	2.93801	0.879408	0.102818	0.955668
6.21.18.5	18	330	46.9249	21.4386	26.8151	5.74393	100.923	2.932916	0.882065	0.102855	0.954767
6.21.18.5	18	331	47.0293	21.4105	26.612	5.80335	100.855	2.939441	0.880909	0.103919	0.947535
6.21.18.5	18	332	46.6301	21.4109	26.1979	5.75619	99.9951	2.914491	0.880926	0.103074	0.932791
6.21.18.5	18	333	46.9885	21.1704	26.8459	5.66151	100.666	2.936891	0.871031	0.101379	0.955863

Table 6. Continued.

Sample Information			**Concentrations (in wt. %)**					**Cation Proportions**			
Sample Name	Number	Line	O	Mg	Si	Fe	Total	O	Mg	Fe	Si
6.21.18.5	18	334	46.9037	21.4346	26.8703	5.74146	100.95	2.931591	0.881901	0.10281	0.956732
6.21.18.5	18	335	46.8196	21.2654	26.6388	5.74096	100.465	2.926335	0.874939	0.102801	0.948489
6.21.18.5	18	336	46.9172	21.439	26.7538	5.79771	100.908	2.932435	0.882082	0.103818	0.952584
6.21.18.5	18	337	46.9873	21.2854	26.5881	5.82873	100.69	2.936816	0.875762	0.104373	0.946684
6.21.18.5	18	338	46.9119	21.3824	26.6596	5.74736	100.701	2.932104	0.879753	0.102916	0.94923
6.21.18.5	18	339	46.9322	21.2424	26.7136	5.77967	100.668	2.933373	0.873993	0.103495	0.951153
6.21.18.5	18	340	46.7643	21.3409	26.6331	5.73055	100.469	2.922878	0.878046	0.102615	0.948286
6.21.18.5	18	341	46.8355	21.2994	26.916	5.76338	100.814	2.927329	0.876338	0.103203	0.958359
6.21.18.5	18	342	46.7875	21.3062	26.327	5.73807	100.159	2.924328	0.876618	0.10275	0.937388
6.21.18.5	18	343	47.162	21.3917	26.8267	5.78617	101.167	2.947736	0.880136	0.103611	0.95518
6.21.18.5	18	344	46.8845	21.2718	26.7932	5.66938	100.619	2.930391	0.875203	0.10152	0.953987
6.21.18.5	18	345	47.0858	21.462	26.6589	5.72762	100.934	2.942973	0.883028	0.102563	0.949205
6.21.18.5	18	346	46.8147	21.351	26.8379	5.79424	100.798	2.926028	0.878461	0.103755	0.955579
6.21.18.5	18	347	47.0253	21.2909	26.7037	5.7716	100.792	2.939191	0.875988	0.10335	0.9508
6.21.18.5	18	348	46.7774	21.3894	26.4569	5.73154	100.355	2.923697	0.880041	0.102633	0.942013
6.21.18.5	18	349	46.7049	21.1792	26.6591	5.69748	100.241	2.919166	0.871393	0.102023	0.949212
6.21.18.5	18	350	46.9545	21.2588	26.847	5.66097	100.721	2.934766	0.874668	0.101369	0.955903
6.21.18.5	18	351	46.755	21.3126	26.8962	5.75925	100.723	2.922297	0.876881	0.103129	0.957654
6.21.18.5	18	352	46.8826	21.4171	26.6623	5.79194	100.754	2.930272	0.881181	0.103714	0.949326
6.21.18.5	18	353	46.8696	21.3705	26.5095	5.75325	100.503	2.92946	0.879264	0.103021	0.943886
6.21.18.5	18	354	46.7628	21.3567	26.6161	5.70477	100.44	2.922785	0.878696	0.102153	0.947681
6.21.18.5	18	355	47.022	21.3418	26.5254	5.68948	100.579	2.938985	0.878083	0.10188	0.944452
6.21.18.5	18	356	46.8574	21.4502	26.5346	5.78561	100.628	2.928697	0.882543	0.103601	0.944779
6.21.18.5	18	357	46.8651	21.2116	26.281	5.77089	100.129	2.929179	0.872726	0.103337	0.93575
6.21.18.5	18	358	46.8746	21.3481	26.6683	5.75328	100.644	2.929772	0.878342	0.103022	0.94954

Table 6. Continued.

Sample Information			**Concentrations (in wt. %)**					**Cation Proportions**			
Sample Name	Number	Line	O	Mg	Si	Fe	Total	O	Mg	Fe	Si
6.21.18.5	18	359	46.9675	21.3943	26.7063	5.73754	100.806	2.935579	0.880243	0.10274	0.950893
6.21.18.5	18	360	46.8312	21.2631	26.3429	5.75328	100.191	2.92706	0.874845	0.103022	0.937954
6.21.18.5	18	361	46.761	21.2158	26.3576	5.73389	100.068	2.922672	0.872899	0.102675	0.938477
6.21.18.5	18	362	46.8547	21.3346	26.5832	5.77666	100.549	2.928529	0.877786	0.103441	0.94651
6.21.18.5	18	363	46.6786	21.31	26.389	5.75926	100.137	2.917522	0.876774	0.103129	0.939595
6.21.18.5	18	364	46.891	21.3506	26.7581	5.71605	100.716	2.930797	0.878445	0.102355	0.952737
6.21.18.5	18	365	46.928	21.2437	26.4849	5.71275	100.369	2.93311	0.874046	0.102296	0.94301
6.21.18.5	18	366	46.6945	21.2736	26.4185	5.76166	100.148	2.918516	0.875277	0.103172	0.940646
6.21.18.5	18	367	46.8456	21.2007	26.4997	5.80363	100.35	2.92796	0.872277	0.103924	0.943537
6.21.18.5	18	368	46.8833	21.3636	26.6151	5.75052	100.613	2.930316	0.87898	0.102973	0.947646
6.21.18.5	18	369	46.9492	21.4591	26.4641	5.75579	100.628	2.934435	0.882909	0.103067	0.942269
6.22.18.3	16	274	46.606	22.5564	25.4309	5.89188	100.485	2.912984	0.928056	0.105504	0.905481
6.22.18.3	16	275	46.5917	22.4971	25.766	5.86395	100.719	2.91209	0.925616	0.105004	0.917413
6.22.18.3	16	276	46.7889	22.5694	26.0378	5.82296	101.219	2.924416	0.928591	0.10427	0.92709
6.22.18.3	16	277	46.7448	22.414	25.9562	5.82118	100.936	2.92166	0.922197	0.104238	0.924185
6.22.18.3	16	278	46.7279	22.3777	25.9605	5.77615	100.842	2.920603	0.920704	0.103432	0.924338
6.22.18.3	16	279	46.9629	22.4747	26.009	5.79498	101.242	2.935291	0.924695	0.103769	0.926065
6.22.18.3	16	280	46.7262	22.6048	25.9031	5.86778	101.102	2.920497	0.930047	0.105072	0.922294
6.22.18.3	16	281	46.5979	22.5711	25.825	5.85271	100.847	2.912478	0.928661	0.104802	0.919514
6.22.18.3	16	282	46.641	22.4308	25.7631	5.83857	100.673	2.915172	0.922888	0.104549	0.91731
6.22.18.3	16	283	46.7941	22.4994	26.0454	5.78879	101.128	2.924741	0.925711	0.103658	0.927361
6.22.18.3	16	284	46.6039	22.4606	25.7889	5.81435	100.668	2.912853	0.924114	0.104116	0.918228
6.22.18.3	16	285	46.8619	22.572	26.0158	5.79858	101.248	2.928979	0.928698	0.103833	0.926307
6.22.18.3	16	286	46.9612	22.6196	25.8854	5.85295	101.319	2.935185	0.930656	0.104807	0.921664

Table 6. Continued.

Sample Information			**Concentrations (in wt. %)**					**Cation Proportions**			
Sample Name	Number	Line	O	Mg	Si	Fe	Total	O	Mg	Fe	Si
6.22.18.3	16	287	46.8206	22.6127	25.6109	5.87971	100.924	2.926397	0.930372	0.105286	0.91189
6.22.18.3	16	288	46.5973	22.5629	25.6988	5.93992	100.799	2.91244	0.928323	0.106364	0.91502
6.22.18.3	16	289	46.723	22.4711	26.0061	5.79265	100.993	2.920297	0.924546	0.103727	0.925962
6.22.18.3	16	290	46.8428	22.6043	26.0348	5.84236	101.324	2.927785	0.930027	0.104617	0.926984
6.22.18.3	16	291	46.5999	22.5305	25.8876	5.83424	100.852	2.912603	0.92699	0.104472	0.921743
6.22.18.3	16	292	46.7946	22.5349	25.9787	5.84995	101.158	2.924772	0.927171	0.104753	0.924986
6.22.18.3	16	293	46.8026	22.5568	25.8925	5.81348	101.065	2.925272	0.928072	0.1041	0.921917
6.22.18.3	16	294	46.654	22.7215	25.798	5.89958	101.073	2.915984	0.934849	0.105642	0.918552
6.22.18.3	16	295	46.5552	22.5833	25.8814	5.91673	100.937	2.909809	0.929163	0.105949	0.921522
6.22.18.3	16	296	46.7919	22.5189	25.763	5.75823	100.832	2.924603	0.926513	0.103111	0.917306
6.22.18.3	16	297	46.5631	22.6097	25.8858	5.92513	100.984	2.910303	0.930249	0.106099	0.921678
6.22.18.3	16	298	46.4596	22.7338	25.8534	5.86124	100.908	2.903834	0.935355	0.104955	0.920525
6.22.18.3	16	299	46.6267	22.4907	25.8055	5.88245	100.805	2.914278	0.925353	0.105335	0.918819
6.22.18.3	16	300	46.6769	22.4218	25.9438	5.94647	100.989	2.917416	0.922518	0.106481	0.923744
6.22.18.3	16	301	46.8735	22.5101	26.1488	5.81796	101.35	2.929704	0.926151	0.10418	0.931043
6.22.18.3	16	302	46.7201	22.5111	25.9771	5.7978	101.006	2.920116	0.926192	0.103819	0.924929
6.22.18.3	16	303	46.6094	22.4435	25.7626	5.89527	100.711	2.913197	0.923411	0.105565	0.917292
6.22.18.3	16	304	46.6289	22.6793	25.6649	5.95129	100.924	2.914416	0.933113	0.106568	0.913813
6.22.18.3	16	305	46.8827	22.6323	25.7905	5.92376	101.229	2.930279	0.931179	0.106075	0.918285
6.22.18.3	16	306	46.8444	22.4184	25.7156	5.91413	100.893	2.927885	0.922378	0.105902	0.915618
6.22.18.3	16	307	46.6905	22.419	26.1065	5.89318	101.109	2.918266	0.922403	0.105527	0.929537
6.22.18.3	16	308	46.8084	22.5457	25.8642	5.93339	101.152	2.925635	0.927616	0.106247	0.920909
6.22.18.3	16	309	46.6442	22.551	25.6998	5.92521	100.82	2.915372	0.927834	0.106101	0.915056
6.22.18.3	16	310	46.7609	22.5681	25.7937	5.91659	101.039	2.922666	0.928537	0.105946	0.918399
6.22.18.3	16	311	46.5866	22.5832	25.7287	5.86869	100.767	2.911772	0.929159	0.105089	0.916085
6.22.18.3	16	312	46.604	22.5856	25.7455	5.86672	100.802	2.912859	0.929257	0.105053	0.916683

Table 6. Continued.

Sample Information			**Concentrations (in wt. %)**					**Cation Proportions**			
Sample Name	Number	Line	O	Mg	Si	Fe	Total	O	Mg	Fe	Si
6.22.18.3	16	313	46.709	22.6144	25.709	5.89702	100.93	2.919422	0.930442	0.105596	0.915383
6.22.18.3	16	314	46.6178	22.647	25.7304	5.93514	100.93	2.913722	0.931784	0.106279	0.916145
6.22.18.3	16	315	46.5106	22.5141	25.5675	5.90053	100.493	2.907022	0.926316	0.105659	0.910345
6.22.18.3	16	316	46.1515	22.4948	25.5437	5.88366	100.074	2.884577	0.925521	0.105357	0.909498
6.22.18.3	16	317	46.5778	22.5794	25.7368	5.90586	100.8	2.911222	0.929002	0.105754	0.916373
6.22.18.3	16	318	46.3293	22.531	25.698	5.84124	100.4	2.89569	0.927011	0.104597	0.914992
6.22.18.3	16	319	46.5477	22.404	25.8645	5.78995	100.606	2.90934	0.921786	0.103679	0.92092
6.22.18.3	16	320	46.6336	22.5704	25.692	5.80045	100.697	2.914709	0.928632	0.103867	0.914778
6.22.18.3	16	321	46.749	22.392	25.8363	5.8271	100.804	2.921922	0.921292	0.104344	0.919916
6.22.18.3	16	322	46.6988	22.4119	25.9517	5.79554	100.858	2.918784	0.922111	0.103779	0.924025
6.22.18.1	29	285	46.3421	22.2165	25.3898	5.81827	99.7667	2.89649	0.914071	0.104186	0.904018
6.22.18.1	29	286	46.1576	22.3013	25.3084	5.8568	99.6241	2.884958	0.91756	0.104876	0.90112
6.22.18.1	29	287	46.2082	22.3566	25.3269	5.82241	99.7142	2.888121	0.919835	0.10426	0.901778
6.22.18.1	29	288	46.2006	22.2969	25.3686	5.86154	99.7277	2.887646	0.917379	0.104961	0.903263
6.22.18.1	29	289	46.2206	22.2893	25.3662	5.86068	99.7369	2.888896	0.917066	0.104945	0.903178
6.22.18.1	29	290	46.1059	22.2333	25.2413	5.85184	99.4324	2.881727	0.914762	0.104787	0.898731
6.22.18.1	29	291	46.1456	22.1542	25.2177	5.8532	99.3707	2.884208	0.911508	0.104811	0.89789
6.22.18.1	29	292	46.4451	22.3148	25.4786	5.79403	100.033	2.902928	0.918116	0.103752	0.90718
6.22.18.1	29	293	46.3862	22.2574	25.4691	5.88043	99.9931	2.899246	0.915754	0.105299	0.906842
6.22.18.1	29	294	46.275	22.2269	25.5218	5.87183	99.8956	2.892296	0.914499	0.105145	0.908718
6.22.18.1	29	295	46.3075	22.3676	25.3196	5.85769	99.8524	2.894327	0.920288	0.104892	0.901519
6.22.18.1	29	296	46.4027	22.3146	25.4127	5.85551	99.9855	2.900278	0.918107	0.104853	0.904833
6.22.18.1	29	297	46.3045	22.2358	25.6189	5.7883	99.9475	2.89414	0.914865	0.103649	0.912175
6.22.18.1	29	298	46.024	22.1974	25.3355	5.81531	99.3723	2.876608	0.913285	0.104133	0.902085

Table 6. Continued.

Sample Information			**Concentrations (in wt. %)**					**Cation Proportions**			
Sample Name	Number	Line	O	Mg	Si	Fe	Total	O	Mg	Fe	Si
6.22.18.1	29	299	46.3754	22.2553	25.505	5.83023	99.966	2.898571	0.915668	0.1044	0.90812
6.22.18.1	29	300	46.3718	22.2462	25.4825	5.80164	99.9022	2.898346	0.915293	0.103888	0.907319
6.22.18.1	29	301	46.3702	22.546	25.6532	5.87515	100.445	2.898246	0.927628	0.105204	0.913397
6.22.18.1	29	302	46.2748	22.5346	25.5555	5.89046	100.255	2.892283	0.927159	0.105478	0.909918
6.22.18.1	29	303	46.3301	22.3173	25.6552	5.81028	100.113	2.89574	0.918218	0.104043	0.913468
6.22.18.1	29	304	46.1802	22.1796	25.5288	5.77376	99.6623	2.886371	0.912553	0.103389	0.908967
6.22.18.1	29	305	46.1779	22.0732	25.4381	5.7867	99.4759	2.886227	0.908175	0.10362	0.905738
6.22.18.1	29	306	46.2388	22.1651	25.6639	5.85268	99.9205	2.890033	0.911956	0.104802	0.913778
6.22.18.1	29	307	46.2701	22.3713	25.7338	5.84265	100.218	2.89199	0.92044	0.104622	0.916266
6.22.18.1	29	308	46.2302	22.3459	25.7646	5.88372	100.224	2.889496	0.919395	0.105358	0.917363
6.22.18.1	29	309	46.436	22.0954	25.7345	5.78054	100.046	2.902359	0.909089	0.10351	0.916291
6.22.18.1	29	310	46.1922	22.2021	25.7087	5.78291	99.886	2.887121	0.913479	0.103553	0.915373
6.22.18.1	29	311	46.1422	22.3323	25.7487	5.85886	100.082	2.883996	0.918836	0.104913	0.916797
6.22.18.1	29	312	46.4086	22.2364	25.6377	5.81153	100.094	2.900646	0.91489	0.104065	0.912845
6.22.18.1	29	313	46.3312	22.3097	25.7019	5.83636	100.179	2.895809	0.917906	0.10451	0.915131
6.22.18.1	29	314	46.2699	22.2483	25.5509	5.89184	99.961	2.891977	0.91538	0.105503	0.909754
6.22.18.1	29	315	46.2769	22.2189	25.7978	5.78531	100.079	2.892415	0.91417	0.103596	0.918545
6.22.18.1	29	316	46.1438	22.1484	25.8369	5.76913	99.8982	2.884096	0.911269	0.103306	0.919937
6.22.18.1	29	317	46.2526	22.1517	25.7756	5.79162	99.9715	2.890896	0.911405	0.103709	0.917755
6.22.18.1	29	318	46.1631	22.3676	25.8182	5.81752	100.167	2.885302	0.920288	0.104172	0.919272
6.22.18.1	29	319	46.4236	22.2149	25.5128	5.89172	100.043	2.901584	0.914005	0.105501	0.908398

Table 6. Continued.

Sample Information			**Concentrations (in wt. %)**					**Cation Proportions**			
Sample Name	Number	Line	O	Mg	Si	Fe	Total	O	Mg	Fe	Si
6.22.18.1	29	320	46.2756	22.5111	25.6124	5.86314	100.262	2.892333	0.926192	0.104989	0.911944
6.22.18.1	29	321	46.2405	22.2213	25.5444	5.80252	99.8087	2.89014	0.914269	0.103904	0.909523
6.22.18.1	29	322	45.9795	22.2095	25.6759	5.77259	99.6374	2.873827	0.913783	0.103368	0.914205
6.22.18.1	29	323	46.3065	22.1596	25.861	5.81539	100.143	2.894265	0.91173	0.104134	0.920795
6.22.18.1	29	324	46.1684	22.2208	25.8223	5.85674	100.068	2.885633	0.914248	0.104875	0.919417
6.22.18.1	29	325	46.075	22.2604	25.7545	5.89195	99.9819	2.879795	0.915877	0.105505	0.917003
6.22.18.1	29	326	46.2063	22.2978	25.9986	5.883	100.386	2.888002	0.917416	0.105345	0.925695
6.22.18.2	28	249	45.9014	22.3754	25.5965	5.90135	99.7747	2.868945	0.920609	0.105673	0.911378
6.22.18.2	28	250	45.9135	22.345	25.6739	5.89912	99.8315	2.869701	0.919358	0.105634	0.914134
6.22.18.2	28	251	45.7209	22.374	25.4335	5.88607	99.4144	2.857663	0.920551	0.1054	0.905574
6.22.18.2	28	252	45.7456	22.277	25.5553	5.88707	99.465	2.859207	0.91656	0.105418	0.909911
6.22.18.2	28	253	46.0304	22.465	25.7693	5.8768	100.142	2.877008	0.924295	0.105234	0.91753
6.22.18.2	28	254	45.8968	22.2982	25.7167	5.77517	99.6868	2.868658	0.917433	0.103414	0.915658
6.22.18.2	28	255	45.8192	22.2522	25.5394	5.90877	99.5195	2.863807	0.91554	0.105806	0.909345
6.22.18.2	28	256	45.727	22.277	25.5699	5.88603	99.4599	2.858045	0.91656	0.105399	0.910431
6.22.18.2	28	257	45.838	22.2775	25.6784	5.88785	99.6817	2.864982	0.916581	0.105432	0.914294
6.22.18.2	28	258	45.8162	22.2595	25.6671	5.906	99.6488	2.86362	0.91584	0.105757	0.913892
6.22.18.2	28	259	45.7741	22.4791	25.795	5.89832	99.9465	2.860989	0.924876	0.105619	0.918445
6.22.18.2	28	260	45.879	22.4206	25.736	5.86263	99.8982	2.867545	0.922469	0.10498	0.916345
6.22.18.2	28	261	45.7572	22.413	25.4124	5.95203	99.5346	2.859932	0.922156	0.106581	0.904823
6.22.18.2	28	262	45.8506	22.3971	25.5058	5.93511	99.6886	2.86577	0.921502	0.106278	0.908148
6.22.18.2	28	263	45.9799	22.2639	25.6521	5.87889	99.7748	2.873852	0.916021	0.105271	0.913357
6.22.18.2	28	264	45.85	22.4364	25.677	5.80992	99.7733	2.865732	0.923119	0.104036	0.914244
6.22.18.2	28	265	45.9737	22.4312	25.5188	5.81841	99.7421	2.873464	0.922905	0.104188	0.908611

Table 6. Continued.

Sample Information			**Concentrations (in wt. %)**					**Cation Proportions**			
Sample Name	Number	Line	O	Mg	Si	Fe	Total	O	Mg	Fe	Si
6.22.18.2	28	266	45.9978	22.3783	25.8288	5.86878	100.074	2.87497	0.920728	0.10509	0.919649
6.22.18.2	28	267	45.7713	22.2948	25.3951	5.89961	99.3608	2.860814	0.917293	0.105642	0.904207
6.22.18.2	28	268	45.7064	22.3505	25.5574	5.83776	99.452	2.856757	0.919584	0.104535	0.909986
6.22.18.2	28	269	45.7662	22.2236	25.6931	5.75195	99.4348	2.860495	0.914363	0.102998	0.914817
6.22.18.2	28	270	45.9497	22.4716	25.7956	5.74703	99.964	2.871964	0.924567	0.10291	0.918467
6.22.18.2	28	271	45.9149	22.3417	25.7324	5.83601	99.8249	2.869789	0.919222	0.104503	0.916217
6.22.18.2	28	272	45.9233	22.2604	25.7482	5.84937	99.7812	2.870314	0.915877	0.104743	0.916779
6.22.18.2	28	273	45.784	22.175	25.6468	5.8189	99.4247	2.861607	0.912364	0.104197	0.913169
6.22.18.2	28	274	45.8323	22.3081	25.6062	5.75728	99.5038	2.864626	0.91784	0.103094	0.911723
6.22.18.2	28	275	45.7654	22.3567	25.69	5.7226	99.5347	2.860445	0.91984	0.102473	0.914707
6.22.18.2	28	276	46.0113	22.312	25.7822	5.72836	99.8339	2.875814	0.918	0.102576	0.91799
6.22.18.2	28	277	45.8106	22.4081	25.7029	5.8699	99.7914	2.86327	0.921954	0.10511	0.915166
6.22.18.2	28	278	45.8099	22.2806	25.6682	5.90889	99.6676	2.863226	0.916708	0.105808	0.913931
6.22.18.2	28	279	45.7186	22.2405	25.4617	5.8265	99.2473	2.85752	0.915059	0.104333	0.906578
6.22.18.2	28	280	45.8008	22.4854	25.475	5.87838	99.6396	2.862657	0.925135	0.105262	0.907052
6.22.18.2	28	281	45.7405	22.4192	25.6158	5.74443	99.52	2.858888	0.922411	0.102864	0.912065
6.22.18.2	28	282	45.9762	22.5074	25.6868	5.78228	99.9526	2.87362	0.92604	0.103541	0.914593
6.22.18.2	28	283	46.069	22.2483	25.5133	5.94176	99.7723	2.87942	0.91538	0.106397	0.908415
6.22.18.2	28	284	45.8695	22.3825	25.4847	5.89588	99.6325	2.866951	0.920901	0.105576	0.907397
6.22.18.4	23	131	46.0541	22.1597	25.54	5.78653	99.5404	2.878489	0.911734	0.103617	0.909366
6.22.18.4	23	132	45.8491	22.2687	25.5585	5.82566	99.5019	2.865676	0.916219	0.104318	0.910025
6.22.18.4	23	133	45.7616	22.3286	25.3627	5.84902	99.3019	2.860207	0.918683	0.104736	0.903053
6.22.18.4	23	134	45.9872	22.269	25.5205	5.87767	99.6544	2.874308	0.916231	0.105249	0.908672
6.22.18.4	23	135	45.9347	22.3981	25.3318	5.89648	99.5611	2.871026	0.921543	0.105586	0.901953
6.22.18.4	23	136	46.1062	22.2966	25.4999	5.91192	99.8145	2.881746	0.917367	0.105863	0.907938

Table 6. Continued.

Sample Information			Concentrations (in wt. %)					Cation Proportions			
Sample Name	Number	Line	O	Mg	Si	Fe	Total	O	Mg	Fe	Si
6.22.18.4	23	137	45.5169	22.3194	25.4972	5.88946	99.223	2.844913	0.918305	0.105461	0.907842
6.22.18.4	23	138	45.7281	22.2685	25.4034	5.83701	99.237	2.858113	0.916211	0.104521	0.904502
6.22.18.4	23	139	45.9267	22.3139	25.6016	5.87941	99.7216	2.870526	0.918079	0.105281	0.911559
6.22.18.4	23	140	45.7977	22.3476	25.6479	5.88389	99.6772	2.862464	0.919465	0.105361	0.913208
6.22.18.4	23	141	46.0046	22.2479	25.6722	5.84084	99.7655	2.875395	0.915363	0.10459	0.914073
6.22.18.4	23	142	45.9026	22.2102	25.6204	5.87297	99.6061	2.86902	0.913812	0.105165	0.912229
6.22.18.4	23	143	45.7815	22.248	25.5368	5.90884	99.4751	2.861451	0.915367	0.105808	0.909252
6.22.18.4	23	144	45.7187	22.1449	25.5015	5.86869	99.2337	2.857526	0.911125	0.105089	0.907995
6.22.18.4	23	145	45.8986	22.3893	25.8337	5.8207	99.9422	2.86877	0.921181	0.104229	0.919823
6.22.18.4	23	146	45.7854	22.3107	25.6697	5.8899	99.6556	2.861695	0.917947	0.105468	0.913984
6.22.18.4	23	147	45.9574	22.2181	25.7084	5.86981	99.7537	2.872445	0.914137	0.105109	0.915362
6.22.18.4	23	148	45.605	22.0808	25.7677	5.89807	99.3516	2.850419	0.908488	0.105615	0.917473
6.22.18.4	23	149	45.7437	22.1746	25.6429	5.87588	99.4371	2.859088	0.912347	0.105217	0.91303
6.22.18.4	23	150	46.1234	22.3117	25.8848	5.89898	100.219	2.882821	0.917988	0.105631	0.921643
6.22.18.4	23	151	45.828	22.1836	25.7303	5.88871	99.6306	2.864357	0.912718	0.105447	0.916142
6.22.18.4	23	152	45.8639	22.2492	25.6964	5.84521	99.6547	2.866601	0.915417	0.104668	0.914935
6.22.18.4	23	153	45.8489	22.2473	25.7504	5.91091	99.7575	2.865664	0.915338	0.105845	0.916857
6.22.18.4	23	154	46.0684	22.3226	25.6918	5.85301	99.9358	2.879383	0.918437	0.104808	0.914771
6.22.18.4	23	155	45.587	22.2925	25.8394	5.74406	99.463	2.849294	0.917198	0.102857	0.920026
6.22.18.4	23	156	45.7417	22.1681	25.7221	5.86778	99.4996	2.858963	0.91208	0.105072	0.91585
6.22.18.4	23	157	45.8221	22.205	25.6661	5.86836	99.5616	2.863989	0.913598	0.105083	0.913856
6.22.18.4	23	158	45.9512	22.1412	25.6672	5.83014	99.5897	2.872058	0.910973	0.104398	0.913895
6.22.18.4	23	159	45.7581	22.1406	25.7288	5.90445	99.532	2.859988	0.910948	0.105729	0.916088

Table 6. Continued.

Sample Information			Concentrations (in wt. %)					Cation Proportions			
Sample Name	Number	Line	O	Mg	Si	Fe	Total	O	Mg	Fe	Si
6.22.18.4	23	160	45.7851	22.0887	25.8223	5.89875	99.5949	2.861676	0.908813	0.105627	0.919417
6.22.18.4	23	161	45.8492	22.0404	25.8675	5.72565	99.4828	2.865682	0.906826	0.102527	0.921027
6.22.18.4	23	162	45.8147	22.2564	25.7995	5.83332	99.704	2.863526	0.915713	0.104455	0.918606
6.22.18.4	23	163	45.7443	22.15	25.567	5.85248	99.3138	2.859126	0.911335	0.104798	0.910327
6.22.18.4	23	164	45.7735	22.2183	25.7639	5.82576	99.5815	2.860951	0.914145	0.10432	0.917338
6.22.18.4	23	165	45.7098	22.1816	25.21	5.83677	98.9381	2.85697	0.912635	0.104517	0.897616
6.22.18.4	23	166	45.8794	22.1979	25.4063	5.90503	99.3886	2.86757	0.913306	0.105739	0.904606
6.22.18.4	23	167	45.6129	22.0072	25.6723	5.66033	98.9528	2.850913	0.90546	0.101358	0.914077
6.22.18.4	23	168	45.4649	22.3173	25.3608	5.80559	98.9485	2.841663	0.918218	0.103959	0.902986
6.22.18.4	23	169	45.6921	22.3169	25.1218	5.87567	99.0065	2.855863	0.918202	0.105214	0.894476
6.22.18.4	23	170	45.7925	22.2322	25.2963	5.83957	99.1605	2.862139	0.914717	0.104567	0.900689
6.22.18.4	23	171	45.7594	22.3748	25.3169	5.93104	99.3821	2.86007	0.920584	0.106205	0.901422
6.22.18.4	23	172	45.8959	22.4328	25.4333	5.91236	99.6743	2.868601	0.922971	0.105871	0.905567
6.22.18.5	25	178	46.4229	22.2237	25.4538	5.89435	99.9948	2.90154	0.914367	0.105548	0.906297
6.22.18.5	25	179	46.3529	22.4389	25.7318	5.87576	100.399	2.897165	0.923222	0.105215	0.916195
6.22.18.5	25	180	46.2707	22.3742	25.3382	5.83499	99.8181	2.892027	0.92056	0.104485	0.902181
6.22.18.5	25	181	46.3649	22.4782	25.6037	5.86983	100.317	2.897915	0.924839	0.105109	0.911634
6.22.18.5	25	182	46.5261	22.4594	25.753	5.83585	100.574	2.90799	0.924065	0.104501	0.91695
6.22.18.5	25	183	46.4758	22.4564	25.5917	5.83521	100.359	2.904846	0.923942	0.104489	0.911207
6.22.18.5	25	184	46.317	22.4273	25.5463	5.88381	100.175	2.894921	0.922744	0.105359	0.90959
6.22.18.5	25	185	46.4272	22.4059	25.5006	5.92418	100.258	2.901809	0.921864	0.106082	0.907963
6.22.18.5	25	186	46.4588	22.3913	25.6123	5.8468	100.309	2.903784	0.921263	0.104697	0.91194
6.22.18.5	25	187	46.1446	22.4801	25.5587	5.84784	100.031	2.884146	0.924917	0.104715	0.910032

Table 6. Continued.

Sample Information			Concentrations (in wt. %)					Cation Proportions			
Sample Name	Number	Line	O	Mg	Si	Fe	Total	O	Mg	Fe	Si
6.22.18.5	25	188	46.2335	22.3064	25.4584	5.86048	99.8587	2.889702	0.91777	0.104942	0.906461
6.22.18.5	25	189	46.5363	22.3007	25.5136	5.86804	100.219	2.908628	0.917535	0.105077	0.908426
6.22.18.5	25	190	46.1479	22.2642	25.505	5.80729	99.7244	2.884352	0.916034	0.103989	0.90812
6.22.18.5	25	191	46.2235	22.2859	25.5454	5.83312	99.8879	2.889077	0.916927	0.104452	0.909558
6.22.18.5	25	192	46.3312	22.4023	25.7162	5.85471	100.305	2.895809	0.921716	0.104838	0.91564
6.22.18.5	25	193	46.4467	22.4461	25.5136	5.80687	100.213	2.903028	0.923518	0.103982	0.908426
6.22.18.5	25	194	46.3032	22.4415	25.4492	5.83455	100.029	2.894059	0.923329	0.104477	0.906133
6.22.18.5	25	195	46.4195	22.5344	25.6931	5.8254	100.473	2.901328	0.927151	0.104313	0.914817
6.22.18.5	25	196	46.3293	22.4076	25.6977	5.82293	100.258	2.89569	0.921934	0.104269	0.914981
6.22.18.5	25	197	46.1383	22.3688	25.444	5.82982	99.7809	2.883752	0.920337	0.104393	0.905948
6.22.18.5	25	198	46.3441	22.3982	25.4837	5.86034	100.086	2.896615	0.921547	0.104939	0.907361
6.22.18.5	25	199	46.4018	22.3964	25.5541	5.8479	100.2	2.900221	0.921473	0.104716	0.909868
6.22.18.5	25	200	46.3867	22.3976	25.489	5.91861	100.192	2.899277	0.921522	0.105983	0.90755
6.22.18.5	25	201	46.5591	22.273	25.7456	5.8666	100.444	2.910053	0.916396	0.105051	0.916687
6.22.18.5	25	202	46.1889	22.4092	25.9321	5.82107	100.351	2.886915	0.922	0.104236	0.923327
6.22.18.5	25	203	46.3278	22.3906	25.8953	5.85912	100.473	2.895596	0.921234	0.104917	0.922017
6.22.18.5	25	204	46.3899	22.331	25.9292	5.82744	100.478	2.899477	0.918782	0.10435	0.923224
6.22.18.5	25	205	46.2377	22.2583	25.8693	5.88292	100.248	2.889965	0.915791	0.105343	0.921091
6.22.18.5	25	206	46.4845	22.361	25.7334	5.90768	100.487	2.90539	0.920016	0.105787	0.916252
6.22.18.5	25	207	46.5729	22.4876	25.9044	5.88411	100.849	2.910915	0.925225	0.105365	0.922341
6.22.18.5	25	208	46.2024	22.2735	25.8098	5.86048	100.146	2.887758	0.916416	0.104942	0.918972
6.22.18.5	25	209	46.2238	22.3543	25.711	5.79835	100.088	2.889096	0.919741	0.103829	0.915455
6.22.18.5	25	210	46.569	22.3247	25.7709	5.85212	100.517	2.910672	0.918523	0.104792	0.917587
6.22.18.5	25	211	46.43	22.3614	25.6925	5.91522	100.399	2.901984	0.920033	0.105922	0.914796

Table 6. Continued.

Sample Information			**Concentrations (in wt. %)**					**Cation Proportions**			
Sample Name	Number	Line	O	Mg	Si	Fe	Total	O	Mg	Fe	Si
6.22.18.5	25	212	46.3621	22.3364	25.7044	5.85285	100.256	2.89774	0.919004	0.104805	0.91522
6.22.18.5	25	213	46.4823	22.3966	25.6316	5.83091	100.342	2.905253	0.921481	0.104412	0.912628
6.22.18.6	6	38	45.9802	22.1713	25.4027	5.82499	99.3791	2.87387	0.912211	0.104306	0.904477
6.22.18.6	6	39	46.2948	22.1049	25.3285	5.87862	99.6068	2.893534	0.90948	0.105266	0.901835
6.22.18.6	6	40	45.9293	22.0414	25.3969	5.85369	99.2213	2.870689	0.906867	0.10482	0.904271
6.22.18.6	6	41	46.1035	22.1064	25.1733	5.87977	99.263	2.881577	0.909541	0.105287	0.896309
6.22.18.6	6	42	46.0535	22.2625	25.4331	5.86106	99.6101	2.878452	0.915964	0.104952	0.90556
6.22.18.6	6	43	45.9811	22.1376	25.2796	5.87345	99.2717	2.873927	0.910825	0.105174	0.900094
6.22.18.6	6	44	45.8402	22.1089	25.4096	5.80937	99.168	2.86512	0.909644	0.104026	0.904723
6.22.18.6	6	45	45.9611	22.2559	25.2248	5.83744	99.2792	2.872676	0.915692	0.104529	0.898143
6.22.18.6	6	46	46.2694	22.0072	25.5273	5.82879	99.6326	2.891946	0.90546	0.104374	0.908914
6.22.18.6	6	47	46.0004	22.0776	25.4458	5.86299	99.3867	2.875133	0.908356	0.104987	0.906012
6.22.18.6	6	48	46.0129	22.2643	25.467	5.78275	99.527	2.875914	0.916038	0.10355	0.906767
6.22.18.6	6	49	46.1524	22.1189	25.6388	5.85322	99.7633	2.884633	0.910056	0.104812	0.912884
6.22.18.6	6	50	45.8877	21.9701	25.3008	5.82003	98.9786	2.868089	0.903933	0.104217	0.900849
6.22.18.6	6	51	46.1489	21.9956	25.4073	5.84951	99.4013	2.884414	0.904983	0.104745	0.904641
6.22.18.6	6	52	45.9046	22.1135	25.3853	5.89604	99.2995	2.869145	0.909833	0.105578	0.903858
6.22.18.6	6	53	46.0731	22.1488	25.3449	5.87069	99.4374	2.879677	0.911286	0.105124	0.902419
6.22.18.6	6	54	46.0509	22.2187	25.4698	5.89989	99.6392	2.878289	0.914162	0.105647	0.906867
6.22.18.6	6	55	45.8489	22.136	25.3525	5.83588	99.1732	2.865664	0.910759	0.104501	0.90269
6.22.18.6	6	56	45.8435	22.0917	25.324	5.90425	99.1634	2.865326	0.908936	0.105725	0.901675
6.22.18.6	6	57	45.8096	22.1302	25.2662	5.87805	99.0841	2.863207	0.91052	0.105256	0.899617
6.22.18.6	6	58	45.9866	22.1153	25.3425	5.89057	99.335	2.87427	0.909907	0.10548	0.902334

Table 6. Continued.

Sample Information			**Concentrations (in wt. %)**					**Cation Proportions**			
Sample Name	Number	Line	O	Mg	Si	Fe	Total	O	Mg	Fe	Si
6.22.18.6	6	59	45.8464	22.1859	25.3172	5.84319	99.1927	2.865507	0.912812	0.104632	0.901433
6.22.18.6	6	60	45.9358	22.1062	25.3874	5.90733	99.3367	2.871095	0.909533	0.105781	0.903933
6.22.18.6	6	61	45.9595	22.1784	25.3346	5.84564	99.3182	2.872576	0.912504	0.104676	0.902053
6.22.18.6	6	62	45.8861	22.2039	25.3093	5.9065	99.3058	2.867989	0.913553	0.105766	0.901152
6.22.18.6	6	63	45.9552	22.138	25.3324	5.83651	99.2621	2.872308	0.910841	0.104512	0.901974
6.22.18.6	6	64	45.8807	22.1181	25.2799	5.82325	99.102	2.867651	0.910023	0.104275	0.900105
6.22.18.6	6	65	45.9591	22.0441	25.58	5.90773	99.4909	2.872551	0.906978	0.105788	0.91079
6.22.18.6	6	66	45.8328	22.2899	25.5815	5.8704	99.5746	2.864657	0.917091	0.105119	0.910844
6.22.18.6	6	67	45.864	22.1795	25.5037	5.87771	99.4249	2.866607	0.912549	0.10525	0.908074
6.22.18.6	6	68	45.9642	22.1262	25.5212	5.87577	99.4874	2.87287	0.910356	0.105215	0.908697
6.22.18.6	6	69	45.9394	22.0889	25.6222	5.84728	99.4977	2.87132	0.908821	0.104705	0.912293
6.22.18.6	6	70	46.0096	22.0744	25.7514	5.90104	99.7364	2.875708	0.908225	0.105668	0.916893
6.22.18.6	6	71	45.7695	22.1137	25.5229	5.8935	99.2997	2.860701	0.909842	0.105533	0.908757
6.22.18.6	6	72	46.0953	22.0411	25.4879	5.9034	99.5277	2.881064	0.906855	0.10571	0.907511
6.22.18.6	6	73	46.0225	22.0644	25.4921	5.86216	99.4411	2.876514	0.907813	0.104972	0.907661

Table 7. EMPA analysis results for Fe-bearing En90 and En95 glasses (atoms per formula unit and Fe charge balance).

		APFU (3 Oxygens)					**Charge Balance (3 Oxygens)**					
Sample Name	Line	Mg	Fe	Si	O	Cations	(Mg+Fe)/Si	Fe/ (total cations)	Fe Charge	Fe^{2+}	Fe^{3+}	Fe^{3+}/ (total Fe)
6.21.18.2	84	0.876118	0.103519	0.961321	3	1.940959	1.0191	0.0533	0.4025	-0.0919	0.1954	1.8880
6.21.18.2	85	0.883568	0.10534	0.976592	3	1.9655	1.0126	0.0536	0.3265	-0.0105	0.1158	1.0995
6.21.18.2	86	0.88208	0.104528	0.976668	3	1.963275	1.0102	0.0532	0.3292	-0.0156	0.1201	1.1491
6.21.18.2	87	0.880793	0.104916	0.965452	3	1.951162	1.0210	0.0538	0.3766	-0.0619	0.1668	1.5896
6.21.18.2	88	0.880512	0.103553	0.97343	3	1.957495	1.0109	0.0529	0.3453	-0.0346	0.1381	1.3341
6.21.18.2	89	0.877843	0.104078	0.974942	3	1.956863	1.0072	0.0532	0.3445	-0.0323	0.1364	1.3105
6.21.18.2	90	0.882323	0.105502	0.975685	3	1.96351	1.0124	0.0537	0.3326	-0.0161	0.1216	1.1527
6.21.18.2	91	0.882122	0.10455	0.976589	3	1.96326	1.0103	0.0533	0.3294	-0.0158	0.1203	1.1507
6.21.18.2	92	0.882524	0.104799	0.975364	3	1.962688	1.0123	0.0534	0.3335	-0.0191	0.1239	1.1822
6.21.18.2	93	0.882201	0.10383	0.975923	3	1.961954	1.0104	0.0529	0.3319	-0.0204	0.1242	1.1966
6.21.18.2	94	0.879167	0.104427	0.968663	3	1.952257	1.0154	0.0535	0.3670	-0.0537	0.1582	1.5146
6.21.18.2	95	0.879778	0.10513	0.97587	3	1.960778	1.0093	0.0536	0.3370	-0.0216	0.1267	1.2052
6.21.18.2	96	0.887518	0.105381	0.975174	3	1.968073	1.0182	0.0535	0.3243	-0.0081	0.1135	1.0771
6.21.18.2	97	0.882932	0.103864	0.972714	3	1.95951	1.0145	0.0530	0.3433	-0.0317	0.1356	1.3051
6.21.18.2	98	0.885037	0.103212	0.971947	3	1.960196	1.0168	0.0527	0.3421	-0.0325	0.1357	1.3149
6.21.18.2	99	0.881233	0.104043	0.978703	3	1.96398	1.0067	0.0530	0.3227	-0.0106	0.1146	1.1018
6.21.18.2	100	0.878847	0.102724	0.970623	3	1.952195	1.0113	0.0526	0.3598	-0.0516	0.1544	1.5027
6.21.18.2	101	0.882217	0.103563	0.983187	3	1.968967	1.0026	0.0526	0.3028	0.0079	0.0957	0.9240
6.21.18.2	102	0.881152	0.104362	0.973819	3	1.959333	1.0120	0.0533	0.3424	-0.0293	0.1337	1.2811
6.21.18.2	103	0.88116	0.105058	0.971123	3	1.957341	1.0155	0.0537	0.3532	-0.0380	0.1431	1.3619
6.21.18.2	104	0.888994	0.103845	0.957454	3	1.950293	1.0370	0.0532	0.3922	-0.0807	0.1845	1.7767
6.21.18.2	105	0.883415	0.103077	0.97418	3	1.960672	1.0126	0.0526	0.3364	-0.0272	0.1303	1.2640
6.21.18.2	106	0.883165	0.104265	0.970829	3	1.958259	1.0171	0.0532	0.3504	-0.0376	0.1418	1.3602
6.21.18.2	107	0.887074	0.103922	0.960864	3	1.951861	1.0314	0.0532	0.3824	-0.0706	0.1745	1.6796
6.21.18.2	108	0.880431	0.105343	0.9683	3	1.954074	1.0180	0.0539	0.3659	-0.0499	0.1553	1.4738
6.21.18.2	109	0.890588	0.104923	0.971593	3	1.967104	1.0246	0.0533	0.3324	-0.0177	0.1226	1.1685

Table 7. Continued.

		APFU (3 Oxygens)					Charge Balance (3 Oxygens)					
Sample Name	Line	Mg	Fe	Si	O	Cations	(Mg+Fe)/Si	Fe/ (total cations)	Fe Charge	Fe^{2+}	Fe^{3+}	Fe^{3+}/(total Fe)
6.21.18.2	110	0.885813	0.104408	0.971055	3	1.961276	1.0197	0.0532	0.3442	-0.0309	0.1353	1.2962
6.21.18.2	111	0.880351	0.104019	0.966987	3	1.951357	1.0180	0.0533	0.3714	-0.0593	0.1633	1.5700
6.21.18.2	112	0.885008	0.10294	0.968652	3	1.9566	1.0199	0.0526	0.3554	-0.0466	0.1495	1.4523
6.21.18.2	113	0.885088	0.104095	0.966981	3	1.956165	1.0230	0.0532	0.3619	-0.0496	0.1537	1.4766
6.21.18.2	114	0.883355	0.105299	0.969599	3	1.958254	1.0197	0.0538	0.3549	-0.0390	0.1443	1.3703
6.21.18.2	115	0.878946	0.105662	0.968131	3	1.952739	1.0170	0.0541	0.3696	-0.0526	0.1583	1.4978
6.21.18.2	116	0.887821	0.103882	0.964308	3	1.956011	1.0284	0.0531	0.3671	-0.0555	0.1594	1.5341
6.21.18.2	117	0.885022	0.104527	0.961983	3	1.951531	1.0287	0.0536	0.3820	-0.0684	0.1730	1.6548
6.21.18.2	118	0.877694	0.103865	0.962304	3	1.943863	1.0200	0.0534	0.3954	-0.0838	0.1877	1.8068
6.21.18.2	119	0.887018	0.104463	0.961646	3	1.953126	1.0310	0.0535	0.3794	-0.0660	0.1705	1.6317
6.21.18.2	120	0.878654	0.104498	0.963324	3	1.946476	1.0206	0.0537	0.3894	-0.0759	0.1804	1.7263
6.21.18.2	121	0.888015	0.104773	0.971682	3	1.96447	1.0217	0.0533	0.3372	-0.0229	0.1277	1.2188
6.21.18.2	122	0.88161	0.105173	0.973411	3	1.960195	1.0137	0.0537	0.3431	-0.0276	0.1328	1.2626
6.21.18.2	123	0.888184	0.106019	0.977658	3	1.971861	1.0169	0.0538	0.3130	0.0051	0.1010	0.9523
6.21.18.2	124	0.877823	0.105118	0.960145	3	1.943087	1.0237	0.0541	0.4038	-0.0884	0.1935	1.8411
6.21.18.2	125	0.881662	0.10443	0.95781	3	1.943902	1.0295	0.0537	0.4054	-0.0921	0.1966	1.8824
6.21.18.2	126	0.8832	0.104352	0.962464	3	1.950016	1.0261	0.0535	0.3837	-0.0707	0.1750	1.6774
6.21.18.2	127	0.885466	0.104734	0.964085	3	1.954285	1.0271	0.0536	0.3727	-0.0585	0.1633	1.5588
6.21.18.2	128	0.882578	0.104699	0.959379	3	1.946656	1.0291	0.0538	0.3973	-0.0832	0.1879	1.7950
6.21.18.2	129	0.888857	0.105079	0.961115	3	1.955051	1.0341	0.0537	0.3778	-0.0626	0.1677	1.5956
6.21.18.2	130	0.881258	0.103436	0.966142	3	1.950837	1.0192	0.0530	0.3729	-0.0626	0.1660	1.6053
6.21.18.2	131	0.887862	0.105453	0.961474	3	1.954789	1.0331	0.0539	0.3784	-0.0620	0.1675	1.5881
6.21.18.3	137	0.867817	0.100549	0.94733	3	1.915696	1.0222	0.0525	0.4750	-0.1734	0.2739	2.7245
6.21.18.3	138	0.872818	0.104342	0.953658	3	1.930818	1.0246	0.0540	0.4397	-0.1267	0.2310	2.2143
6.21.18.3	139	0.878437	0.104102	0.961416	3	1.943955	1.0220	0.0536	0.3975	-0.0852	0.1893	1.8180

Table 7. Continued.

		APFU (3 Oxygens)					Charge Balance (3 Oxygens)					
Sample Name	Line	Mg	Fe	Si	O	Cations	(Mg+Fe)/Si	Fe/ (total cations)	Fe Charge	Fe^{2+}	Fe^{3+}	Fe^{3+}/(total Fe)
6.21.18.3	140	0.877693	0.104372	0.967301	3	1.949365	1.0153	0.0535	0.3754	-0.0623	0.1667	1.5969
6.21.18.3	141	0.879545	0.102903	0.956013	3	1.93846	1.0277	0.0531	0.4169	-0.1082	0.2111	2.0510
6.21.18.3	142	0.876733	0.104143	0.959386	3	1.940262	1.0224	0.0537	0.4090	-0.0966	0.2007	1.9272
6.21.18.3	143	0.877736	0.104328	0.955452	3	1.937516	1.0279	0.0538	0.4227	-0.1097	0.2141	2.0518
6.21.18.3	144	0.877459	0.102861	0.956111	3	1.936431	1.0253	0.0531	0.4206	-0.1121	0.2149	2.0894
6.21.18.3	145	0.879892	0.102372	0.947226	3	1.929489	1.0370	0.0531	0.4513	-0.1442	0.2466	2.4086
6.21.18.3	146	0.88055	0.103906	0.96152	3	1.945977	1.0239	0.0534	0.3928	-0.0811	0.1850	1.7805
6.21.18.3	147	0.875089	0.10404	0.947292	3	1.926422	1.0336	0.0540	0.4607	-0.1485	0.2526	2.4276
6.21.18.3	148	0.873345	0.103022	0.957505	3	1.933872	1.0197	0.0533	0.4233	-0.1142	0.2172	2.1087
6.21.18.3	149	0.882301	0.104205	0.954964	3	1.94147	1.0330	0.0537	0.4155	-0.1029	0.2071	1.9877
6.21.18.3	150	0.882927	0.104589	0.954047	3	1.941563	1.0351	0.0539	0.4180	-0.1042	0.2088	1.9962
6.21.18.3	151	0.88252	0.103948	0.952441	3	1.938909	1.0357	0.0536	0.4252	-0.1134	0.2173	2.0905
6.21.18.3	152	0.873956	0.104405	0.956666	3	1.935028	1.0227	0.0540	0.4254	-0.1122	0.2166	2.0747
6.21.18.3	153	0.876755	0.103268	0.95649	3	1.936513	1.0246	0.0533	0.4205	-0.1107	0.2140	2.0722
6.21.18.3	154	0.876045	0.105201	0.954455	3	1.935701	1.0281	0.0543	0.4301	-0.1145	0.2197	2.0883
6.21.18.3	155	0.879381	0.103542	0.950295	3	1.933218	1.0343	0.0536	0.4401	-0.1294	0.2330	2.2500
6.21.18.3	156	0.879938	0.103905	0.958647	3	1.94249	1.0263	0.0535	0.4055	-0.0938	0.1977	1.9030
6.21.18.3	157	0.875706	0.104489	0.948077	3	1.928271	1.0339	0.0542	0.4563	-0.1428	0.2473	2.3668
6.21.18.3	158	0.881949	0.104958	0.956141	3	1.943049	1.0322	0.0540	0.4115	-0.0967	0.2016	1.9210
6.21.18.3	159	0.87663	0.10383	0.947192	3	1.927652	1.0351	0.0539	0.4580	-0.1465	0.2503	2.4108
6.21.18.3	160	0.874705	0.104522	0.946413	3	1.92564	1.0347	0.0543	0.4649	-0.1514	0.2559	2.4482
6.21.18.3	161	0.876945	0.103795	0.96655	3	1.94729	1.0147	0.0533	0.3799	-0.0685	0.1723	1.6602
6.21.18.3	162	0.875522	0.103521	0.95451	3	1.933553	1.0257	0.0535	0.4309	-0.1204	0.2239	2.1626
6.21.18.3	163	0.871838	0.102107	0.95604	3	1.929986	1.0187	0.0529	0.4322	-0.1258	0.2279	2.2324
6.21.18.3	164	0.86879	0.103718	0.953191	3	1.9257	1.0203	0.0539	0.4497	-0.1385	0.2422	2.3354

Table 7. Continued.

		APFU (3 Oxygens)					Charge Balance (3 Oxygens)					
Sample Name	Line	Mg	Fe	Si	O	Cations	(Mg+Fe)/Si	Fe/ (total cations)	Fe Charge	Fe^{2+}	Fe^{3+}	Fe^{3+}/(total Fe)
6.21.18.3	165	0.876731	0.103776	0.955673	3	1.93618	1.0260	0.0536	0.4238	-0.1125	0.2163	2.0842
6.21.18.3	166	0.882181	0.103862	0.954339	3	1.940382	1.0332	0.0535	0.4183	-0.1067	0.2106	2.0273
6.21.18.3	167	0.874721	0.104688	0.965787	3	1.945196	1.0141	0.0538	0.3874	-0.0733	0.1780	1.7006
6.21.18.3	168	0.877469	0.104812	0.964814	3	1.947095	1.0181	0.0538	0.3858	-0.0714	0.1762	1.6809
6.21.18.3	169	0.872569	0.103993	0.965935	3	1.942497	1.0110	0.0535	0.3911	-0.0791	0.1831	1.7610
6.21.18.3	170	0.874099	0.103257	0.967623	3	1.944979	1.0101	0.0531	0.3813	-0.0715	0.1748	1.6928
6.21.18.3	171	0.86978	0.10229	0.966365	3	1.938435	1.0059	0.0528	0.3950	-0.0881	0.1904	1.8614
6.21.18.3	172	0.869522	0.104061	0.963794	3	1.937378	1.0102	0.0537	0.4058	-0.0936	0.1977	1.8994
6.21.18.3	173	0.879916	0.104809	0.962374	3	1.947099	1.0232	0.0538	0.3907	-0.0762	0.1811	1.7275
6.21.18.3	174	0.878679	0.104773	0.959976	3	1.943428	1.0245	0.0539	0.4027	-0.0884	0.1932	1.8439
6.21.18.3	175	0.871706	0.104712	0.955222	3	1.93164	1.0222	0.0542	0.4357	-0.1216	0.2263	2.1609
6.21.18.3	176	0.872756	0.103967	0.95218	3	1.928904	1.0258	0.0539	0.4458	-0.1339	0.2378	2.2876
6.21.18.3	177	0.872257	0.104821	0.954691	3	1.931769	1.0234	0.0543	0.4367	-0.1223	0.2271	2.1664
6.21.18.3	178	0.87073	0.102799	0.957688	3	1.931217	1.0165	0.0532	0.4278	-0.1194	0.2222	2.1614
6.21.18.3	179	0.87052	0.103174	0.961033	3	1.934727	1.0132	0.0533	0.4148	-0.1053	0.2085	2.0207
6.21.18.3	180	0.873234	0.102733	0.951966	3	1.927933	1.0252	0.0533	0.4457	-0.1375	0.2402	2.3381
6.21.18.3	181	0.869714	0.104665	0.960952	3	1.935331	1.0140	0.0541	0.4168	-0.1028	0.2074	1.9819
6.21.18.3	182	0.871539	0.10372	0.951869	3	1.927128	1.0246	0.0538	0.4494	-0.1383	0.2420	2.3332
6.21.18.3	183	0.875387	0.104035	0.95788	3	1.937301	1.0225	0.0537	0.4177	-0.1056	0.2096	2.0151
6.21.18.3	184	0.875703	0.10414	0.951902	3	1.931746	1.0294	0.0539	0.4410	-0.1286	0.2327	2.2345
6.21.18.3	185	0.869966	0.104254	0.955448	3	1.929667	1.0196	0.0540	0.4383	-0.1255	0.2298	2.2040
6.21.18.3	186	0.873496	0.104238	0.955388	3	1.933122	1.0234	0.0539	0.4315	-0.1187	0.2230	2.1392
6.21.18.3	187	0.993217	0.117563	1.112817	3	2.223596	0.9982	0.0529	-0.4377	0.7904	-0.6728	-5.7231
6.21.18.3	188	0.873233	0.103416	0.953439	3	1.930088	1.0243	0.0536	0.4398	-0.1295	0.2329	2.2525
6.21.18.3	189	0.869744	0.103429	0.955245	3	1.928419	1.0188	0.0536	0.4395	-0.1292	0.2327	2.2496

Table 7. Continued.

		APFU (3 Oxygens)					Charge Balance (3 Oxygens)					
Sample Name	Line	Mg	Fe	Si	O	Cations	(Mg+Fe)/Si	Fe/ (total cations)	Fe Charge	Fe^{2+}	Fe^{3+}	Fe^{3+}/(total Fe)
6.21.18.3	190	0.873718	0.104827	0.952745	3	1.93129	1.0271	0.0543	0.4416	-0.1271	0.2319	2.2125
6.21.18.3	191	0.871315	0.102925	0.940286	3	1.914525	1.0361	0.0538	0.4962	-0.1875	0.2904	2.8213
6.21.18.3	192	0.874781	0.1042	0.952698	3	1.931678	1.0276	0.0539	0.4396	-0.1270	0.2312	2.2193
6.21.18.3	193	0.878485	0.104209	0.964287	3	1.946981	1.0191	0.0535	0.3859	-0.0733	0.1775	1.7030
6.21.18.3	194	0.894529	0.107171	0.986882	3	1.988582	1.0150	0.0539	0.2634	0.0581	0.0491	0.4579
6.21.18.3	195	0.87079	0.103641	0.96006	3	1.93449	1.0150	0.0536	0.4182	-0.1073	0.2109	2.0349
6.21.18.3	196	0.873674	0.104636	0.960574	3	1.938884	1.0185	0.0540	0.4104	-0.0964	0.2011	1.9217
6.21.18.3	197	0.87935	0.104664	0.962967	3	1.946981	1.0219	0.0538	0.3894	-0.0754	0.1801	1.7208
6.21.18.3	198	0.874337	0.104681	0.953574	3	1.932592	1.0267	0.0542	0.4370	-0.1230	0.2277	2.1749
6.21.18.3	199	0.873139	0.104837	0.956389	3	1.934365	1.0226	0.0542	0.4282	-0.1137	0.2185	2.0841
6.21.18.3	200	0.875327	0.104172	0.957669	3	1.937167	1.0228	0.0538	0.4187	-0.1062	0.2103	2.0190
6.21.18.3	201	0.876366	0.103938	0.961029	3	1.941333	1.0201	0.0535	0.4032	-0.0913	0.1953	1.8788
6.21.18.3	202	0.878365	0.103086	0.960691	3	1.942142	1.0216	0.0531	0.4005	-0.0912	0.1943	1.8852
6.21.18.3	203	0.874112	0.104058	0.962478	3	1.940648	1.0163	0.0536	0.4019	-0.0897	0.1937	1.8619
6.21.18.3	204	0.871801	0.104057	0.96194	3	1.937797	1.0145	0.0537	0.4086	-0.0965	0.2005	1.9271
6.21.18.3	205	0.869226	0.104206	0.960662	3	1.934094	1.0133	0.0539	0.4189	-0.1063	0.2105	2.0199
6.21.18.3	206	0.872958	0.104226	0.961613	3	1.938797	1.0162	0.0538	0.4076	-0.0950	0.1992	1.9110
6.21.18.3	207	0.876688	0.103592	0.958702	3	1.938982	1.0225	0.0534	0.4118	-0.1010	0.2046	1.9754
6.21.18.3	208	0.868793	0.102429	0.967178	3	1.9384	1.0042	0.0528	0.3937	-0.0864	0.1888	1.8436
6.21.18.5	328	0.898766	0.104089	0.971669	3	1.974525	1.0321	0.0527	0.3158	-0.0035	0.1076	1.0338
6.21.18.5	329	0.897962	0.104988	0.975831	3	1.978781	1.0278	0.0531	0.3007	0.0142	0.0908	0.8646
6.21.18.5	330	0.902241	0.105207	0.976605	3	1.984053	1.0316	0.0530	0.2891	0.0265	0.0787	0.7479
6.21.18.5	331	0.899058	0.10606	0.967056	3	1.972174	1.0394	0.0538	0.3337	-0.0155	0.1215	1.1460
6.21.18.5	332	0.906772	0.106098	0.960158	3	1.973028	1.0549	0.0538	0.3458	-0.0275	0.1336	1.2595
6.21.18.5	333	0.889748	0.103557	0.976403	3	1.969708	1.0173	0.0526	0.3149	-0.0042	0.1078	1.0408

Table 7. Continued.

		APFU (3 Oxygens)					Charge Balance (3 Oxygens)					
Sample Name	Line	Mg	Fe	Si	O	Cations	(Mg+Fe)/Si	Fe/ (total cations)	Fe Charge	Fe^{2+}	Fe^{3+}	Fe^{3+}/(total Fe)
6.21.18.5	334	0.90248	0.105209	0.979058	3	1.986747	1.0292	0.0530	0.2788	0.0368	0.0684	0.6500
6.21.18.5	335	0.896964	0.105389	0.972366	3	1.97472	1.0308	0.0534	0.3166	-0.0004	0.1058	1.0042
6.21.18.5	336	0.902406	0.10621	0.974532	3	1.983147	1.0350	0.0536	0.2971	0.0216	0.0846	0.7969
6.21.18.5	337	0.894604	0.106619	0.967052	3	1.968274	1.0353	0.0542	0.3426	-0.0227	0.1293	1.2132
6.21.18.5	338	0.900125	0.105299	0.971211	3	1.976635	1.0352	0.0533	0.3149	0.0010	0.1043	0.9906
6.21.18.5	339	0.893845	0.105845	0.972757	3	1.972447	1.0277	0.0537	0.3213	-0.0037	0.1096	1.0354
6.21.18.5	340	0.901213	0.105323	0.973308	3	1.979843	1.0341	0.0532	0.3043	0.0116	0.0937	0.8896
6.21.18.5	341	0.898093	0.105765	0.982151	3	1.986009	1.0221	0.0533	0.2752	0.0421	0.0637	0.6021
6.21.18.5	342	0.899302	0.105408	0.961644	3	1.966354	1.0448	0.0536	0.3548	-0.0386	0.1440	1.3661
6.21.18.5	343	0.895741	0.105448	0.972115	3	1.973304	1.0299	0.0534	0.3201	-0.0037	0.1092	1.0352
6.21.18.5	344	0.895992	0.103931	0.976648	3	1.976572	1.0238	0.0526	0.3014	0.0104	0.0936	0.9002
6.21.18.5	345	0.900139	0.10455	0.967598	3	1.972287	1.0383	0.0530	0.3293	-0.0157	0.1202	1.1500
6.21.18.5	346	0.900669	0.106378	0.979736	3	1.986784	1.0279	0.0535	0.2797	0.0394	0.0670	0.6295
6.21.18.5	347	0.894112	0.105488	0.970471	3	1.970071	1.0300	0.0535	0.3299	-0.0134	0.1189	1.1273
6.21.18.5	348	0.903009	0.105311	0.966598	3	1.974917	1.0432	0.0533	0.3276	-0.0117	0.1170	1.1107
6.21.18.5	349	0.895522	0.104848	0.975497	3	1.975867	1.0255	0.0531	0.3070	0.0076	0.0973	0.9277
6.21.18.5	350	0.89411	0.103622	0.97715	3	1.974882	1.0211	0.0525	0.3032	0.0077	0.0959	0.9258
6.21.18.5	351	0.900197	0.105871	0.983118	3	1.989186	1.0233	0.0532	0.2671	0.0505	0.0554	0.5232
6.21.18.5	352	0.902149	0.106182	0.971916	3	1.980247	1.0375	0.0536	0.3080	0.0105	0.0957	0.9010
6.21.18.5	353	0.900436	0.105502	0.966614	3	1.972552	1.0407	0.0535	0.3327	-0.0162	0.1217	1.1532
6.21.18.5	354	0.90191	0.104852	0.972717	3	1.979479	1.0350	0.0530	0.3053	0.0092	0.0956	0.9118
6.21.18.5	355	0.896312	0.103995	0.964059	3	1.964366	1.0376	0.0529	0.3511	-0.0392	0.1432	1.3765
6.21.18.5	356	0.904029	0.106123	0.967781	3	1.977934	1.0438	0.0537	0.3208	-0.0024	0.1086	1.0231
6.21.18.5	357	0.893826	0.105836	0.958374	3	1.958037	1.0431	0.0541	0.3789	-0.0613	0.1672	1.5796
6.21.18.5	358	0.899396	0.105491	0.972301	3	1.977188	1.0335	0.0534	0.3120	0.0045	0.1010	0.9576

Table 7. Continued.

		APFU (3 Oxygens)					Charge Balance (3 Oxygens)					
Sample Name	Line	Mg	Fe	Si	O	Cations	(Mg+Fe)/Si	Fe/ (total cations)	Fe Charge	Fe^{2+}	Fe^{3+}	Fe^{3+}/(total Fe)
6.21.18.5	359	0.89956	0.104995	0.97176	3	1.976315	1.0337	0.0531	0.3138	0.0011	0.1039	0.9891
6.21.18.5	360	0.896645	0.105589	0.961327	3	1.963561	1.0426	0.0538	0.3614	-0.0446	0.1502	1.4227
6.21.18.5	361	0.895994	0.105391	0.963307	3	1.964692	1.0395	0.0536	0.3548	-0.0386	0.1440	1.3663
6.21.18.5	362	0.899209	0.105965	0.96961	3	1.974784	1.0367	0.0537	0.3231	-0.0052	0.1112	1.0495
6.21.18.5	363	0.901561	0.106045	0.966157	3	1.973763	1.0429	0.0537	0.3322	-0.0141	0.1202	1.1331
6.21.18.5	364	0.899187	0.104772	0.975233	3	1.979192	1.0295	0.0529	0.3007	0.0136	0.0911	0.8700
6.21.18.5	365	0.893979	0.104629	0.964515	3	1.963124	1.0353	0.0533	0.3540	-0.0401	0.1447	1.3832
6.21.18.5	366	0.899714	0.106053	0.966908	3	1.972675	1.0402	0.0538	0.3329	-0.0148	0.1208	1.1394
6.21.18.5	367	0.893739	0.106481	0.966752	3	1.966971	1.0346	0.0541	0.3455	-0.0261	0.1326	1.2449
6.21.18.5	368	0.899882	0.105421	0.970181	3	1.975484	1.0362	0.0534	0.3195	-0.0032	0.1087	1.0308
6.21.18.5	369	0.902636	0.10537	0.963323	3	1.971328	1.0464	0.0535	0.3414	-0.0253	0.1307	1.2404
6.22.18.3	274	0.955779	0.108655	0.93253	3	1.996964	1.1414	0.0544	0.3583	-0.0324	0.1410	1.2978
6.22.18.3	275	0.953558	0.108174	0.945108	3	2.00684	1.1234	0.0539	0.3125	0.0121	0.0961	0.8884
6.22.18.3	276	0.952591	0.106965	0.951052	3	2.010608	1.1141	0.0532	0.2906	0.0303	0.0767	0.7169
6.22.18.3	277	0.946925	0.107033	0.948966	3	2.002923	1.1106	0.0534	0.3103	0.0108	0.0962	0.8990
6.22.18.3	278	0.945733	0.106243	0.949466	3	2.001443	1.1080	0.0531	0.3107	0.0081	0.0982	0.9241
6.22.18.3	279	0.945079	0.106056	0.94648	3	1.997616	1.1106	0.0531	0.3239	-0.0058	0.1118	1.0542
6.22.18.3	280	0.955365	0.107933	0.947402	3	2.0107	1.1223	0.0537	0.2997	0.0241	0.0838	0.7764
6.22.18.3	281	0.956568	0.107952	0.947146	3	2.011665	1.1239	0.0537	0.2983	0.0256	0.0824	0.7631
6.22.18.3	282	0.949743	0.107592	0.944002	3	2.001337	1.1201	0.0538	0.3245	-0.0017	0.1093	1.0161
6.22.18.3	283	0.949531	0.106325	0.951224	3	2.00708	1.1100	0.0530	0.2960	0.0229	0.0834	0.7843
6.22.18.3	284	0.951762	0.107231	0.9457	3	2.004693	1.1198	0.0535	0.3137	0.0080	0.0992	0.9253
6.22.18.3	285	0.951217	0.106351	0.948768	3	2.006336	1.1147	0.0530	0.3025	0.0166	0.0898	0.8443
6.22.18.3	286	0.951207	0.107121	0.942016	3	2.000345	1.1235	0.0536	0.3295	-0.0082	0.1153	1.0761

Table 7. Continued.

		APFU (3 Oxygens)					Charge Balance (3 Oxygens)					
Sample Name	Line	Mg	Fe	Si	O	Cations	(Mg+Fe)/ Si	Fe/ (total cations)	Fe Charge	Fe^{2+}	Fe^{3+}	Fe^{3+}/ (total Fe)
6.22.18.3	287	0.953772	0.107934	0.934826	3	1.996532	1.1357	0.0541	0.3532	-0.0294	0.1373	1.2719
6.22.18.3	288	0.956232	0.109562	0.942529	3	2.008324	1.1308	0.0546	0.3174	0.0113	0.0983	0.8972
6.22.18.3	289	0.94978	0.106558	0.951234	3	2.007572	1.1105	0.0531	0.2955	0.0242	0.0824	0.7732
6.22.18.3	290	0.952966	0.107198	0.949848	3	2.010012	1.1161	0.0533	0.2947	0.0269	0.0803	0.7489
6.22.18.3	291	0.954806	0.107607	0.949401	3	2.011813	1.1190	0.0535	0.2928	0.0300	0.0776	0.7209
6.22.18.3	292	0.951019	0.107447	0.948778	3	2.007244	1.1156	0.0535	0.3029	0.0195	0.0880	0.8186
6.22.18.3	293	0.951781	0.106759	0.945468	3	2.004008	1.1196	0.0533	0.3146	0.0057	0.1010	0.9465
6.22.18.3	294	0.961784	0.108686	0.945018	3	2.015487	1.1328	0.0539	0.2964	0.0297	0.0790	0.7268
6.22.18.3	295	0.957963	0.109233	0.950085	3	2.01728	1.1233	0.0541	0.2837	0.0440	0.0653	0.5975
6.22.18.3	296	0.950399	0.105769	0.940954	3	1.997122	1.1224	0.0530	0.3354	-0.0181	0.1238	1.1709
6.22.18.3	297	0.95892	0.109369	0.950085	3	2.018374	1.1244	0.0542	0.2818	0.0463	0.0631	0.5768
6.22.18.3	298	0.966331	0.108431	0.95101	3	2.025772	1.1301	0.0535	0.2633	0.0620	0.0464	0.4283
6.22.18.3	299	0.952572	0.108433	0.945846	3	2.006851	1.1218	0.0540	0.3115	0.0138	0.0946	0.8725
6.22.18.3	300	0.948632	0.109496	0.949892	3	2.00802	1.1139	0.0545	0.3032	0.0253	0.0842	0.7688
6.22.18.3	301	0.948373	0.10668	0.953382	3	2.008436	1.1066	0.0531	0.2897	0.0303	0.0764	0.7158
6.22.18.3	302	0.95153	0.106659	0.950232	3	2.008421	1.1136	0.0531	0.2960	0.0240	0.0827	0.7753
6.22.18.3	303	0.950925	0.10871	0.944624	3	2.004259	1.1218	0.0542	0.3197	0.0065	0.1022	0.9404
6.22.18.3	304	0.960514	0.109697	0.940648	3	2.01086	1.1377	0.0546	0.3164	0.0127	0.0970	0.8841
6.22.18.3	305	0.953335	0.108599	0.940134	3	2.002068	1.1296	0.0542	0.3328	-0.0070	0.1156	1.0644
6.22.18.3	306	0.945097	0.108511	0.93817	3	1.991778	1.1230	0.0545	0.3571	-0.0316	0.1401	1.2911
6.22.18.3	307	0.948237	0.108483	0.955571	3	2.012291	1.1059	0.0539	0.2812	0.0442	0.0643	0.5925
6.22.18.3	308	0.951194	0.108948	0.944318	3	2.00446	1.1227	0.0544	0.3203	0.0065	0.1024	0.9403
6.22.18.3	309	0.954767	0.109181	0.941618	3	2.005566	1.1299	0.0544	0.3240	0.0035	0.1056	0.9675
6.22.18.3	310	0.953107	0.10875	0.9427	3	2.004556	1.1264	0.0543	0.3230	0.0033	0.1055	0.9700
6.22.18.3	311	0.957313	0.108273	0.943843	3	2.009428	1.1290	0.0539	0.3100	0.0148	0.0935	0.8632
6.22.18.3	312	0.957057	0.108196	0.944106	3	2.009359	1.1283	0.0538	0.3095	0.0151	0.0931	0.8602

Table 7. Continued.

		APFU (3 Oxygens)					Charge Balance (3 Oxygens)					
Sample Name	Line	Mg	Fe	Si	O	Cations	(Mg+Fe)/Si	Fe/ (total cations)	Fe Charge	Fe^{2+}	Fe^{3+}	Fe^{3+}/ (total Fe)
6.22.18.3	313	0.956123	0.10851	0.940649	3	2.005282	1.1318	0.0541	0.3252	0.0004	0.1081	0.9966
6.22.18.3	314	0.959375	0.109426	0.943273	3	2.012073	1.1331	0.0544	0.3082	0.0201	0.0893	0.8161
6.22.18.3	315	0.955943	0.109038	0.939462	3	2.004443	1.1336	0.0544	0.3303	-0.0032	0.1122	1.0289
6.22.18.3	316	0.962555	0.109572	0.94589	3	2.018018	1.1335	0.0543	0.2913	0.0374	0.0722	0.6588
6.22.18.3	317	0.957332	0.108979	0.944318	3	2.01063	1.1292	0.0542	0.3081	0.0189	0.0901	0.8268
6.22.18.3	318	0.960404	0.108365	0.947952	3	2.016721	1.1275	0.0537	0.2874	0.0377	0.0707	0.6520
6.22.18.3	319	0.95051	0.106909	0.949617	3	2.007037	1.1135	0.0533	0.3005	0.0202	0.0867	0.8109
6.22.18.3	320	0.955806	0.106906	0.941546	3	2.004258	1.1287	0.0533	0.3222	-0.0015	0.1084	1.0139
6.22.18.3	321	0.94591	0.107132	0.944497	3	1.99754	1.1149	0.0536	0.3302	-0.0088	0.1159	1.0821
6.22.18.3	322	0.947769	0.106666	0.949736	3	2.004171	1.1102	0.0532	0.3055	0.0145	0.0922	0.8642
6.22.18.1	285	0.946737	0.107909	0.936324	3	1.99097	1.1264	0.0542	0.3612	-0.0375	0.1454	1.3475
6.22.18.1	286	0.954149	0.109058	0.937053	3	2.00026	1.1346	0.0545	0.3435	-0.0163	0.1254	1.1496
6.22.18.1	287	0.955468	0.108299	0.936711	3	2.000478	1.1356	0.0541	0.3422	-0.0173	0.1256	1.1600
6.22.18.1	288	0.953073	0.109044	0.938408	3	2.000525	1.1318	0.0545	0.3402	-0.0131	0.1221	1.1200
6.22.18.1	289	0.952336	0.108981	0.937913	3	1.99923	1.1316	0.0545	0.3437	-0.0167	0.1257	1.1535
6.22.18.1	290	0.952307	0.109088	0.935617	3	1.997011	1.1344	0.0546	0.3529	-0.0257	0.1347	1.2352
6.22.18.1	291	0.948102	0.109019	0.933938	3	1.991059	1.1319	0.0548	0.3680	-0.0410	0.1500	1.3760
6.22.18.1	292	0.948817	0.107221	0.937515	3	1.993554	1.1264	0.0538	0.3523	-0.0306	0.1379	1.2858
6.22.18.1	293	0.947578	0.108958	0.938356	3	1.994892	1.1259	0.0546	0.3514	-0.0245	0.1335	1.2253
6.22.18.1	294	0.948553	0.10906	0.942557	3	2.000171	1.1221	0.0545	0.3327	-0.0055	0.1145	1.0503
6.22.18.1	295	0.953888	0.108721	0.934433	3	1.997043	1.1372	0.0544	0.3545	-0.0283	0.1370	1.2605
6.22.18.1	296	0.949675	0.108458	0.935945	3	1.994078	1.1306	0.0544	0.3569	-0.0315	0.1400	1.2904
6.22.18.1	297	0.948329	0.10744	0.94554	3	2.001309	1.1166	0.0537	0.3212	0.0011	0.1063	0.9894
6.22.18.1	298	0.952461	0.1086	0.94078	3	2.00184	1.1279	0.0542	0.3320	-0.0062	0.1148	1.0567

Table 7. Continued.

-		APFU (3 Oxygens)					Charge Balance (3 Oxygens)					
Sample Name	Line	Mg	Fe	Si	O	Cations	(Mg+Fe)/Si	Fe/ (total cations)	Fe Charge	Fe^{2+}	Fe^{3+}	Fe^{3+}/ (total Fe)
6.22.18.1	299	0.947709	0.108053	0.939897	3	1.99566	1.1233	0.0541	0.3450	-0.0208	0.1289	1.1928
6.22.18.1	300	0.947395	0.107532	0.939141	3	1.994068	1.1233	0.0539	0.3486	-0.0260	0.1336	1.2423
6.22.18.1	301	0.960196	0.108898	0.945465	3	2.014559	1.1308	0.0541	0.2977	0.0289	0.0800	0.7342
6.22.18.1	302	0.961689	0.109407	0.943806	3	2.014901	1.1349	0.0543	0.3014	0.0268	0.0826	0.7548
6.22.18.1	303	0.951279	0.107789	0.946357	3	2.005424	1.1191	0.0537	0.3120	0.0114	0.0964	0.8947
6.22.18.1	304	0.948478	0.107459	0.944751	3	2.000688	1.1177	0.0537	0.3240	-0.0017	0.1091	1.0155
6.22.18.1	305	0.943975	0.107705	0.941441	3	1.993121	1.1171	0.0540	0.3463	-0.0232	0.1309	1.2151
6.22.18.1	306	0.946657	0.10879	0.948547	3	2.003993	1.1127	0.0543	0.3125	0.0139	0.0949	0.8725
6.22.18.1	307	0.954817	0.10853	0.950487	3	2.013834	1.1187	0.0539	0.2884	0.0372	0.0714	0.6575
6.22.18.1	308	0.954556	0.109387	0.952446	3	2.016389	1.1171	0.0542	0.2811	0.0471	0.0623	0.5698
6.22.18.1	309	0.939672	0.106992	0.947117	3	1.993782	1.1051	0.0537	0.3322	-0.0112	0.1182	1.1048
6.22.18.1	310	0.949193	0.107601	0.951161	3	2.007956	1.1111	0.0536	0.2970	0.0258	0.0818	0.7599
6.22.18.1	311	0.955794	0.109133	0.953674	3	2.018601	1.1167	0.0541	0.2737	0.0537	0.0555	0.5081
6.22.18.1	312	0.946227	0.10763	0.944112	3	1.997968	1.1162	0.0539	0.3311	-0.0082	0.1158	1.0763
6.22.18.1	313	0.950932	0.10827	0.948057	3	2.007259	1.1172	0.0539	0.3059	0.0189	0.0894	0.8254
6.22.18.1	314	0.949571	0.109444	0.943736	3	2.002751	1.1222	0.0546	0.3259	0.0024	0.1070	0.9779
6.22.18.1	315	0.948173	0.107449	0.952711	3	2.008333	1.1080	0.0535	0.2928	0.0295	0.0779	0.7251
6.22.18.1	316	0.947891	0.107457	0.956907	3	2.012256	1.1029	0.0534	0.2766	0.0458	0.0617	0.5739
6.22.18.1	317	0.945802	0.107623	0.952391	3	2.005816	1.1061	0.0537	0.2988	0.0240	0.0836	0.7767
6.22.18.1	318	0.956872	0.108313	0.955815	3	2.021	1.1144	0.0536	0.2630	0.0619	0.0464	0.4281
6.22.18.1	319	0.945007	0.109079	0.939209	3	1.993295	1.1223	0.0547	0.3532	-0.0259	0.1350	1.2376

Table 7. Continued.

-		APFU (3 Oxygens)					Charge Balance (3 Oxygens)					
Sample Name	Line	Mg	Fe	Si	O	Cations	(Mg+Fe)/Si	Fe/ (total cations)	Fe Charge	Fe^{2+}	Fe^{3+}	Fe^{3+}/ (total Fe)
6.22.18.1	320	0.960669	0.108897	0.945891	3	2.015458	1.1308	0.0540	0.2951	0.0316	0.0773	0.7099
6.22.18.1	321	0.949022	0.107853	0.944096	3	2.000971	1.1195	0.0539	0.3256	-0.0020	0.1099	1.0187
6.22.18.1	322	0.953902	0.107906	0.954342	3	2.016151	1.1126	0.0535	0.2748	0.0489	0.0590	0.5469
6.22.18.1	323	0.945038	0.107938	0.954435	3	2.007411	1.1032	0.0538	0.2922	0.0316	0.0763	0.7070
6.22.18.1	324	0.950483	0.109031	0.955857	3	2.015371	1.1084	0.0541	0.2756	0.0515	0.0575	0.5278
6.22.18.1	325	0.954107	0.109909	0.95528	3	2.019295	1.1138	0.0544	0.2707	0.0591	0.0508	0.4627
6.22.18.1	326	0.952994	0.10943	0.961594	3	2.024018	1.1049	0.0541	0.2476	0.0807	0.0288	0.2630
6.22.18.2	249	0.962663	0.110501	0.95301	3	2.026173	1.1261	0.0545	0.2626	0.0689	0.0416	0.3768
6.22.18.2	250	0.961102	0.11043	0.95564	3	2.027171	1.1213	0.0545	0.2552	0.0761	0.0344	0.3113
6.22.18.2	251	0.966403	0.11065	0.95068	3	2.027732	1.1329	0.0546	0.2645	0.0675	0.0432	0.3902
6.22.18.2	252	0.961694	0.110609	0.954717	3	2.027019	1.1232	0.0546	0.2577	0.0741	0.0365	0.3303
6.22.18.2	253	0.963809	0.109733	0.956755	3	2.030296	1.1221	0.0540	0.2454	0.0838	0.0259	0.2360
6.22.18.2	254	0.959438	0.108149	0.957581	3	2.025168	1.1149	0.0534	0.2508	0.0736	0.0345	0.3190
6.22.18.2	255	0.95908	0.110838	0.95259	3	2.022508	1.1232	0.0548	0.2715	0.0610	0.0498	0.4493
6.22.18.2	256	0.962085	0.110634	0.955651	3	2.028369	1.1225	0.0545	0.2532	0.0787	0.0320	0.2889
6.22.18.2	257	0.959777	0.1104	0.957382	3	2.027559	1.1178	0.0544	0.2509	0.0803	0.0301	0.2728
6.22.18.2	258	0.959457	0.110793	0.957416	3	2.027666	1.1179	0.0546	0.2514	0.0810	0.0298	0.2693
6.22.18.2	259	0.969814	0.110751	0.963071	3	2.043636	1.1220	0.0542	0.2081	0.1242	-0.0134	-0.1211
6.22.18.2	260	0.965078	0.109829	0.958672	3	2.033579	1.1212	0.0540	0.2352	0.0943	0.0155	0.1411
6.22.18.2	261	0.967319	0.111801	0.949137	3	2.028257	1.1369	0.0551	0.2688	0.0666	0.0452	0.4044
6.22.18.2	262	0.964664	0.111256	0.950685	3	2.026605	1.1317	0.0549	0.2679	0.0658	0.0454	0.4082
6.22.18.2	263	0.95623	0.109892	0.953449	3	2.019572	1.1182	0.0544	0.2737	0.0559	0.0540	0.4910
6.22.18.2	264	0.966369	0.108911	0.957079	3	2.032359	1.1235	0.0536	0.2389	0.0878	0.0211	0.1940
6.22.18.2	265	0.963546	0.108776	0.948623	3	2.020945	1.1304	0.0538	0.2784	0.0479	0.0609	0.5595

Table 7. Continued.

		APFU (3 Oxygens)					Charge Balance (3 Oxygens)					
Sample Name	Line	Mg	Fe	Si	O	Cations	(Mg+Fe)/Si	Fe/ (total cations)	Fe Charge	Fe^{2+}	Fe^{3+}	Fe^{3+}/ (total Fe)
6.22.18.2	266	0.96077	0.109661	0.959644	3	2.030074	1.1154	0.0540	0.2399	0.0891	0.0206	0.1875
6.22.18.2	267	0.961922	0.110782	0.948199	3	2.020903	1.1313	0.0548	0.2834	0.0490	0.0618	0.5578
6.22.18.2	268	0.965694	0.109776	0.955614	3	2.031084	1.1254	0.0540	0.2462	0.0832	0.0266	0.2423
6.22.18.2	269	0.958956	0.108021	0.959433	3	2.02641	1.1121	0.0533	0.2444	0.0797	0.0283	0.2621
6.22.18.2	270	0.965785	0.107498	0.959413	3	2.032697	1.1187	0.0529	0.2308	0.0917	0.0158	0.1468
6.22.18.2	271	0.96093	0.109245	0.957788	3	2.027964	1.1173	0.0539	0.2470	0.0807	0.0285	0.2609
6.22.18.2	272	0.957258	0.109475	0.958201	3	2.024934	1.1133	0.0541	0.2527	0.0757	0.0337	0.3081
6.22.18.2	273	0.956487	0.109236	0.957331	3	2.023055	1.1132	0.0540	0.2577	0.0700	0.0392	0.3591
6.22.18.2	274	0.961214	0.107966	0.954808	3	2.023988	1.1198	0.0533	0.2583	0.0656	0.0424	0.3928
6.22.18.2	275	0.964717	0.107472	0.959334	3	2.031522	1.1176	0.0529	0.2332	0.0892	0.0183	0.1702
6.22.18.2	276	0.957642	0.107005	0.957631	3	2.022279	1.1118	0.0529	0.2542	0.0668	0.0402	0.3755
6.22.18.2	277	0.965981	0.11013	0.958868	3	2.034978	1.1223	0.0541	0.2326	0.0978	0.0123	0.1117
6.22.18.2	278	0.960499	0.110863	0.957588	3	2.02895	1.1188	0.0546	0.2486	0.0839	0.0269	0.2429
6.22.18.2	279	0.960685	0.109535	0.951782	3	2.022002	1.1244	0.0542	0.2715	0.0571	0.0524	0.4787
6.22.18.2	280	0.96952	0.110312	0.95057	3	2.030402	1.1360	0.0543	0.2587	0.0723	0.0381	0.3450
6.22.18.2	281	0.96794	0.107941	0.957083	3	2.032964	1.1241	0.0531	0.2358	0.0880	0.0199	0.1844
6.22.18.2	282	0.966766	0.108095	0.954816	3	2.029678	1.1257	0.0533	0.2472	0.0771	0.0310	0.2869
6.22.18.2	283	0.953712	0.110853	0.946456	3	2.011021	1.1248	0.0551	0.3067	0.0258	0.0850	0.7672
6.22.18.2	284	0.963638	0.110475	0.949507	3	2.02362	1.1312	0.0546	0.2747	0.0567	0.0537	0.4865
6.22.18.4	131	0.950222	0.107991	0.947753	3	2.005967	1.1165	0.0538	0.3085	0.0154	0.0926	0.8571
6.22.18.4	132	0.959165	0.109208	0.952681	3	2.021054	1.1214	0.0540	0.2709	0.0567	0.0525	0.4810
6.22.18.4	133	0.963584	0.109855	0.94719	3	2.020629	1.1333	0.0544	0.2841	0.0455	0.0644	0.5859
6.22.18.4	134	0.956298	0.109852	0.948408	3	2.014557	1.1241	0.0545	0.2938	0.0358	0.0741	0.6743
6.22.18.4	135	0.962941	0.110329	0.942471	3	2.015741	1.1388	0.0547	0.3042	0.0268	0.0836	0.7575
6.22.18.4	136	0.955012	0.110207	0.945196	3	2.010415	1.1270	0.0548	0.3092	0.0214	0.0888	0.8056

Table 7. Continued.

		APFU (3 Oxygens)					Charge Balance (3 Oxygens)					
Sample Name	Line	Mg	Fe	Si	O	Cations	(Mg+Fe)/Si	Fe/ (total cations)	Fe Charge	Fe^{2+}	Fe^{3+}	Fe^{3+}/ (total Fe)
6.22.18.4	137	0.968365	0.11121	0.957332	3	2.036907	1.1277	0.0546	0.2339	0.0997	0.0115	0.1036
6.22.18.4	138	0.961695	0.10971	0.949405	3	2.02081	1.1285	0.0543	0.2790	0.0501	0.0596	0.5430
6.22.18.4	139	0.959488	0.110029	0.952675	3	2.022192	1.1226	0.0544	0.2703	0.0598	0.0503	0.4568
6.22.18.4	140	0.963644	0.110423	0.957086	3	2.031153	1.1222	0.0544	0.2444	0.0869	0.0235	0.2130
6.22.18.4	141	0.95503	0.109122	0.953684	3	2.017837	1.1158	0.0541	0.2752	0.0522	0.0570	0.5220
6.22.18.4	142	0.95553	0.109966	0.953875	3	2.019372	1.1170	0.0545	0.2734	0.0565	0.0535	0.4866
6.22.18.4	143	0.959688	0.110931	0.953277	3	2.023896	1.1231	0.0548	0.2675	0.0653	0.0457	0.4115
6.22.18.4	144	0.956553	0.110328	0.953267	3	2.020149	1.1192	0.0546	0.2738	0.0572	0.0532	0.4819
6.22.18.4	145	0.96332	0.108997	0.9619	3	2.034217	1.1148	0.0536	0.2258	0.1012	0.0078	0.0713
6.22.18.4	146	0.962311	0.110566	0.958157	3	2.031034	1.1197	0.0544	0.2428	0.0889	0.0216	0.1955
6.22.18.4	147	0.95473	0.109776	0.95601	3	2.020517	1.1135	0.0543	0.2665	0.0628	0.0469	0.4277
6.22.18.4	148	0.956162	0.111157	0.965619	3	2.032939	1.1053	0.0547	0.2252	0.1083	0.0029	0.0259
6.22.18.4	149	0.957313	0.110403	0.958029	3	2.025745	1.1145	0.0545	0.2533	0.0780	0.0325	0.2939
6.22.18.4	150	0.955302	0.109925	0.959105	3	2.024332	1.1106	0.0543	0.2530	0.0768	0.0331	0.3013
6.22.18.4	151	0.95594	0.110441	0.959526	3	2.025906	1.1114	0.0545	0.2500	0.0813	0.0291	0.2638
6.22.18.4	152	0.958016	0.109539	0.957512	3	2.025067	1.1149	0.0541	0.2539	0.0747	0.0348	0.3181
6.22.18.4	153	0.958248	0.110806	0.959838	3	2.028892	1.1138	0.0546	0.2442	0.0883	0.0225	0.2034
6.22.18.4	154	0.95691	0.109198	0.953091	3	2.019199	1.1186	0.0541	0.2738	0.0538	0.0554	0.5075
6.22.18.4	155	0.965711	0.108297	0.968689	3	2.042697	1.1087	0.0530	0.1938	0.1311	-0.0228	-0.2103
6.22.18.4	156	0.957074	0.110256	0.96103	3	2.02836	1.1106	0.0544	0.2417	0.0890	0.0212	0.1925
6.22.18.4	157	0.956985	0.110073	0.957255	3	2.024313	1.1147	0.0544	0.2570	0.0732	0.0369	0.3349
6.22.18.4	158	0.951554	0.109049	0.954607	3	2.01521	1.1110	0.0541	0.2785	0.0487	0.0604	0.5536
6.22.18.4	159	0.955544	0.110905	0.960936	3	2.027385	1.1098	0.0547	0.2452	0.0875	0.0234	0.2106

Table 7. Continued.

		APFU (3 Oxygens)					Charge Balance (3 Oxygens)					
Sample Name	Line	Mg	Fe	Si	O	Cations	(Mg+Fe)/Si	Fe/ (total cations)	Fe Charge	Fe^{2+}	Fe^{3+}	Fe^{3+}/ (total Fe)
6.22.18.4	160	0.952742	0.110733	0.963859	3	2.027334	1.1034	0.0546	0.2391	0.0931	0.0176	0.1591
6.22.18.4	161	0.94933	0.107333	0.964196	3	2.020859	1.0959	0.0531	0.2446	0.0774	0.0299	0.2785
6.22.18.4	162	0.959355	0.109434	0.962386	3	2.031175	1.1106	0.0539	0.2317	0.0966	0.0129	0.1177
6.22.18.4	163	0.956238	0.109962	0.955181	3	2.021381	1.1162	0.0544	0.2668	0.0631	0.0469	0.4263
6.22.18.4	164	0.958575	0.10939	0.961923	3	2.029888	1.1102	0.0539	0.2352	0.0930	0.0164	0.1497
6.22.18.4	165	0.958325	0.10975	0.942554	3	2.010629	1.1332	0.0546	0.3131	0.0161	0.0936	0.8532
6.22.18.4	166	0.955484	0.110623	0.946382	3	2.012489	1.1265	0.0550	0.3035	0.0284	0.0823	0.7436
6.22.18.4	167	0.95281	0.106658	0.961878	3	2.021346	1.1015	0.0528	0.2469	0.0731	0.0336	0.3146
6.22.18.4	168	0.969382	0.109751	0.9533	3	2.032433	1.1320	0.0540	0.2480	0.0812	0.0285	0.2600
6.22.18.4	169	0.964544	0.110524	0.93962	3	2.014688	1.1442	0.0549	0.3124	0.0191	0.0914	0.8268
6.22.18.4	170	0.958777	0.109604	0.944073	3	2.012453	1.1317	0.0545	0.3062	0.0227	0.0869	0.7933
6.22.18.4	171	0.965624	0.111401	0.945525	3	2.02255	1.1391	0.0551	0.2867	0.0476	0.0638	0.5731
6.22.18.4	172	0.965248	0.11072	0.947047	3	2.023015	1.1361	0.0547	0.2813	0.0508	0.0599	0.5408
6.22.18.5	178	0.945395	0.10913	0.937051	3	1.991576	1.1254	0.0548	0.3610	-0.0336	0.1427	1.3080
6.22.18.5	179	0.955991	0.10895	0.948716	3	2.013657	1.1225	0.0541	0.2932	0.0337	0.0753	0.6907
6.22.18.5	180	0.954928	0.108386	0.935863	3	1.999178	1.1362	0.0542	0.3467	-0.0215	0.1299	1.1987
6.22.18.5	181	0.957418	0.108812	0.943748	3	2.009978	1.1298	0.0541	0.3102	0.0163	0.0925	0.8505
6.22.18.5	182	0.953303	0.107807	0.945963	3	2.007072	1.1217	0.0537	0.3095	0.0139	0.0939	0.8713
6.22.18.5	183	0.954207	0.107912	0.941055	3	2.003174	1.1286	0.0539	0.3274	-0.0036	0.1115	1.0336
6.22.18.5	184	0.956238	0.109184	0.942606	3	2.008028	1.1303	0.0544	0.3171	0.0105	0.0987	0.9043
6.22.18.5	185	0.953058	0.109672	0.938687	3	2.001416	1.1321	0.0548	0.3391	-0.0101	0.1198	1.0923
6.22.18.5	186	0.951789	0.108166	0.942157	3	2.002112	1.1250	0.0540	0.3278	-0.0033	0.1115	1.0305
6.22.18.5	187	0.96207	0.108922	0.946587	3	2.017579	1.1314	0.0540	0.2895	0.0373	0.0717	0.6580

Table 7. Continued.

		APFU (3 Oxygens)					Charge Balance (3 Oxygens)					
Sample Name	Line	Mg	Fe	Si	O	Cations	(Mg+Fe)/Si	Fe/ (total cations)	Fe Charge	Fe^{2+}	Fe^{3+}	Fe^{3+}/ (total Fe)
6.22.18.5	188	0.952801	0.108947	0.94106	3	2.002807	1.1282	0.0544	0.3302	-0.0033	0.1123	1.0305
6.22.18.5	189	0.946359	0.108378	0.936964	3	1.991701	1.1257	0.0544	0.3594	-0.0343	0.1427	1.3164
6.22.18.5	190	0.952762	0.108159	0.944531	3	2.005452	1.1232	0.0539	0.3164	0.0081	0.1000	0.9249
6.22.18.5	191	0.952131	0.108462	0.94448	3	2.005073	1.1229	0.0541	0.3178	0.0076	0.1009	0.9302
6.22.18.5	192	0.954879	0.10861	0.948585	3	2.012074	1.1211	0.0540	0.2959	0.0299	0.0787	0.7245
6.22.18.5	193	0.954367	0.107455	0.938771	3	2.000593	1.1311	0.0537	0.3362	-0.0138	0.1213	1.1286
6.22.18.5	194	0.957128	0.108302	0.939303	3	2.004734	1.1343	0.0540	0.3285	-0.0036	0.1119	1.0335
6.22.18.5	195	0.958683	0.107861	0.94593	3	2.012473	1.1275	0.0536	0.2989	0.0247	0.0832	0.7713
6.22.18.5	196	0.955144	0.108025	0.947941	3	2.01111	1.1216	0.0537	0.2979	0.0261	0.0819	0.7581
6.22.18.5	197	0.957437	0.108601	0.942468	3	2.008506	1.1311	0.0541	0.3153	0.0105	0.0981	0.9029
6.22.18.5	198	0.954439	0.108685	0.939747	3	2.00287	1.1313	0.0543	0.3321	-0.0061	0.1148	1.0560
6.22.18.5	199	0.953175	0.108319	0.941171	3	2.002665	1.1278	0.0541	0.3290	-0.0040	0.1123	1.0370
6.22.18.5	200	0.953537	0.109664	0.939079	3	2.00228	1.1322	0.0548	0.3366	-0.0076	0.1173	1.0695
6.22.18.5	201	0.944721	0.108298	0.945021	3	1.99804	1.1143	0.0542	0.3305	-0.0056	0.1139	1.0515
6.22.18.5	202	0.958116	0.108319	0.959495	3	2.02593	1.1115	0.0535	0.2458	0.0792	0.0291	0.2691
6.22.18.5	203	0.95445	0.1087	0.955261	3	2.018412	1.1129	0.0539	0.2701	0.0560	0.0527	0.4844
6.22.18.5	204	0.950636	0.107968	0.955231	3	2.013834	1.1082	0.0536	0.2778	0.0461	0.0619	0.5730
6.22.18.5	205	0.95066	0.109354	0.956161	3	2.016176	1.1086	0.0542	0.2740	0.0540	0.0553	0.5059
6.22.18.5	206	0.949975	0.109232	0.946089	3	2.005296	1.1196	0.0545	0.3157	0.0120	0.0972	0.8901
6.22.18.5	207	0.953541	0.108589	0.950568	3	2.012697	1.1174	0.0540	0.2906	0.0351	0.0735	0.6766
6.22.18.5	208	0.952036	0.10902	0.954691	3	2.015747	1.1114	0.0541	0.2772	0.0499	0.0591	0.5423
6.22.18.5	209	0.955047	0.107815	0.950596	3	2.013458	1.1181	0.0535	0.2875	0.0359	0.0719	0.6668
6.22.18.5	210	0.946712	0.108008	0.945748	3	2.000468	1.1152	0.0540	0.3236	0.0004	0.1076	0.9959
6.22.18.5	211	0.951108	0.109499	0.945694	3	2.006301	1.1215	0.0546	0.3150	0.0135	0.0960	0.8768

Table 7. Continued.

		APFU (3 Oxygens)					Charge Balance (3 Oxygens)					
Sample Name	Line	Mg	Fe	Si	O	Cations	(Mg+Fe)/Si	Fe/ (total cations)	Fe Charge	Fe^{2+}	Fe^{3+}	Fe^{3+}/ (total Fe)
6.22.18.5	212	0.951436	0.108504	0.947517	3	2.007456	1.1186	0.0541	0.3071	0.0185	0.0901	0.8299
6.22.18.5	213	0.951533	0.107817	0.94239	3	2.001741	1.1241	0.0539	0.3274	-0.0039	0.1117	1.0364
6.22.18.6	38	0.952247	0.108884	0.944174	3	2.005304	1.1239	0.0543	0.3188	0.0078	0.1010	0.9280
6.22.18.6	39	0.942943	0.10914	0.935018	3	1.987101	1.1252	0.0549	0.3740	-0.0466	0.1558	1.4272
6.22.18.6	40	0.947717	0.109542	0.945004	3	2.002263	1.1188	0.0547	0.3245	0.0041	0.1055	0.9628
6.22.18.6	41	0.94692	0.109614	0.933145	3	1.989679	1.1322	0.0551	0.3736	-0.0447	0.1544	1.4081
6.22.18.6	42	0.954642	0.109384	0.943799	3	2.007825	1.1274	0.0545	0.3155	0.0126	0.0968	0.8845
6.22.18.6	43	0.950781	0.109788	0.93958	3	2.000148	1.1288	0.0549	0.3401	-0.0108	0.1205	1.0980
6.22.18.6	44	0.952467	0.108924	0.947314	3	2.008705	1.1204	0.0542	0.3058	0.0210	0.0880	0.8076
6.22.18.6	45	0.956278	0.109162	0.937951	3	2.003391	1.1359	0.0545	0.3356	-0.0082	0.1173	1.0747
6.22.18.6	46	0.939291	0.108274	0.942874	3	1.990439	1.1110	0.0544	0.3499	-0.0251	0.1334	1.2318
6.22.18.6	47	0.947806	0.109546	0.94536	3	2.002713	1.1185	0.0547	0.3229	0.0057	0.1039	0.9480
6.22.18.6	48	0.955562	0.108018	0.945891	3	2.00947	1.1244	0.0538	0.3053	0.0187	0.0893	0.8265
6.22.18.6	49	0.946452	0.109003	0.949393	3	2.004849	1.1117	0.0544	0.3095	0.0175	0.0915	0.8396
6.22.18.6	50	0.945508	0.109011	0.942282	3	1.9968	1.1191	0.0546	0.3399	-0.0128	0.1218	1.1177
6.22.18.6	51	0.941247	0.108943	0.940892	3	1.991082	1.1162	0.0547	0.3539	-0.0271	0.1361	1.2488
6.22.18.6	52	0.951329	0.110394	0.945081	3	2.006803	1.1234	0.0550	0.3170	0.0142	0.0962	0.8717
6.22.18.6	53	0.949363	0.109517	0.940126	3	1.999005	1.1263	0.0548	0.3408	-0.0122	0.1217	1.1116
6.22.18.6	54	0.952818	0.110115	0.945214	3	2.008147	1.1245	0.0548	0.3135	0.0168	0.0933	0.8471
6.22.18.6	55	0.953454	0.1094	0.945006	3	2.00786	1.1247	0.0545	0.3131	0.0151	0.0943	0.8617
6.22.18.6	56	0.951658	0.110695	0.944055	3	2.006407	1.1253	0.0552	0.3205	0.0116	0.0991	0.8950
6.22.18.6	57	0.954022	0.110285	0.942597	3	2.006904	1.1291	0.0550	0.3216	0.0093	0.1010	0.9158
6.22.18.6	58	0.94971	0.110094	0.941805	3	2.001609	1.1253	0.0550	0.3334	-0.0031	0.1132	1.0280

Table 7. Continued.

		APFU (3 Oxygens)					Charge Balance (3 Oxygens)					
Sample Name	Line	Mg	Fe	Si	O	Cations	(Mg+Fe)/Si	Fe/ (total cations)	Fe Charge	Fe^{2+}	Fe^{3+}	Fe^{3+}/ (total Fe)
6.22.18.6	59	0.955655	0.109543	0.943742	3	2.00894	1.1287	0.0545	0.3137	0.0149	0.0946	0.8639
6.22.18.6	60	0.950369	0.11053	0.944517	3	2.005415	1.1232	0.0551	0.3212	0.0104	0.1001	0.9060
6.22.18.6	61	0.952981	0.109319	0.942066	3	2.004367	1.1276	0.0545	0.3258	0.0022	0.1071	0.9800
6.22.18.6	62	0.955603	0.110634	0.942631	3	2.008868	1.1311	0.0551	0.3183	0.0136	0.0970	0.8768
6.22.18.6	63	0.951334	0.109159	0.942073	3	2.002565	1.1257	0.0545	0.3290	-0.0016	0.1107	1.0143
6.22.18.6	64	0.952022	0.109087	0.941647	3	2.002757	1.1269	0.0545	0.3294	-0.0021	0.1112	1.0193
6.22.18.6	65	0.947219	0.110481	0.9512	3	2.0089	1.1120	0.0550	0.3008	0.0307	0.0798	0.7223
6.22.18.6	66	0.96042	0.110086	0.953877	3	2.024382	1.1223	0.0544	0.2637	0.0666	0.0435	0.3950
6.22.18.6	67	0.955013	0.110148	0.950329	3	2.01549	1.1208	0.0547	0.2887	0.0418	0.0684	0.6206
6.22.18.6	68	0.950641	0.109871	0.948908	3	2.00942	1.1176	0.0547	0.3031	0.0265	0.0833	0.7586
6.22.18.6	69	0.949551	0.109398	0.953178	3	2.012126	1.1110	0.0544	0.2882	0.0400	0.0694	0.6343
6.22.18.6	70	0.947479	0.110235	0.956522	3	2.014237	1.1058	0.0547	0.2790	0.0518	0.0585	0.5305
6.22.18.6	71	0.954145	0.110672	0.953008	3	2.017825	1.1173	0.0548	0.2797	0.0523	0.0583	0.5271
6.22.18.6	72	0.944291	0.110074	0.944975	3	1.99934	1.1158	0.0551	0.3315	-0.0013	0.1114	1.0118
6.22.18.6	73	0.946785	0.109478	0.946625	3	2.002888	1.1158	0.0547	0.3199	0.0085	0.1010	0.9223

Table 8. LaserPlot example csv output file.

Sample Name	Date	Gas A	Gas A %	Gas B	Gas B %	Gas Flow (CC/min)	Heating Duration (s)	Holding Duration (s)
Sample_data	5/26/2017	Ar*	15	O2*	85	375	12.363	4.175

Table 8. Continued - Additional columns to the right of those above.

Mean Hold Temp (°C)	Peak Temp (°C)	Deriv. Cool Rate (°C/s)	Reg. Cool Rate(°C/s)	Deriv. Heat Rate (°C/s)	Reg. Heat Rate (°C/s)	Additional Notes
1874.299	1881.278	312.682	312.2881	101.6368	100.4061	

Figures

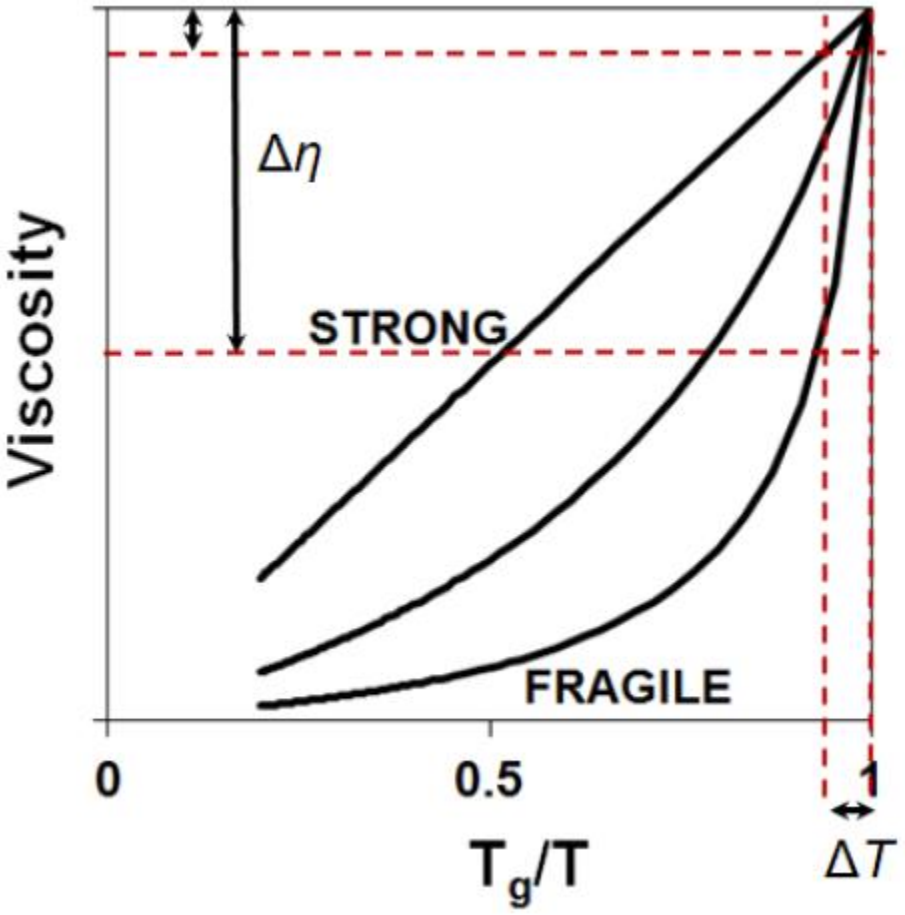

Fig. 1. Graph of glass-forming melt strengths, with respect to viscosity and temperature changes (Lucas et al., 2017 – modelled after Angell, 1991).

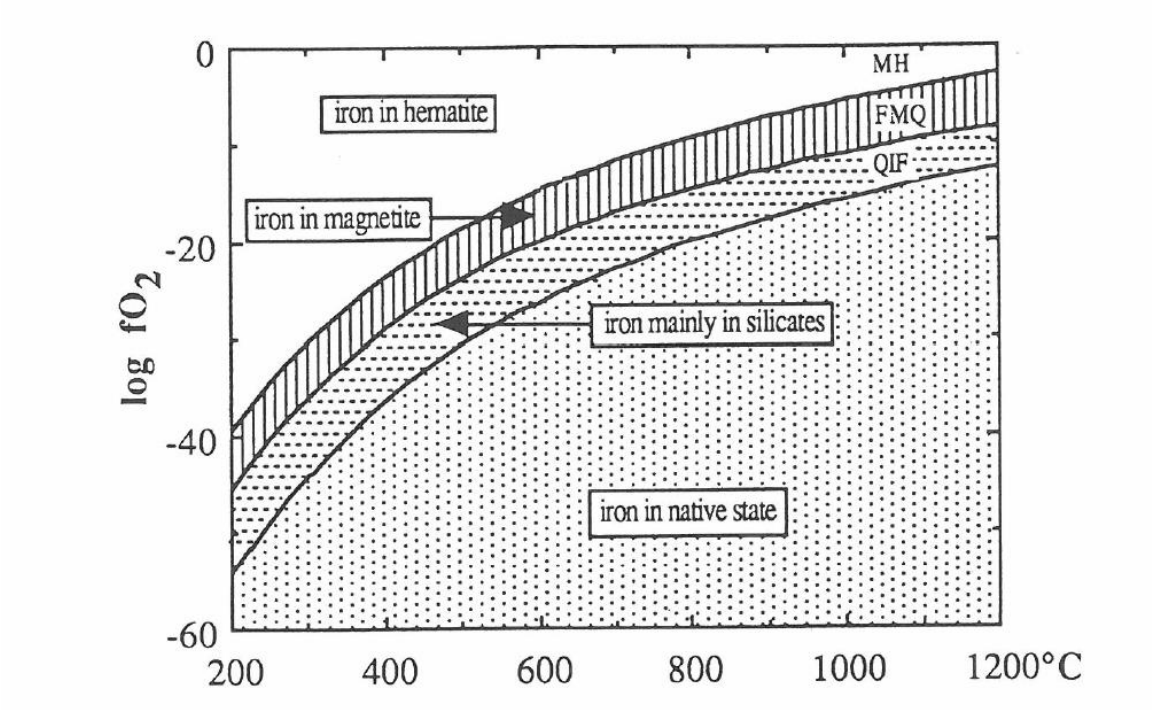

Fig. 2. Log f_{O2} vs temperature buffers depicting the stable iron oxidation states in the Fe-Si-O system (Frost, 1991).

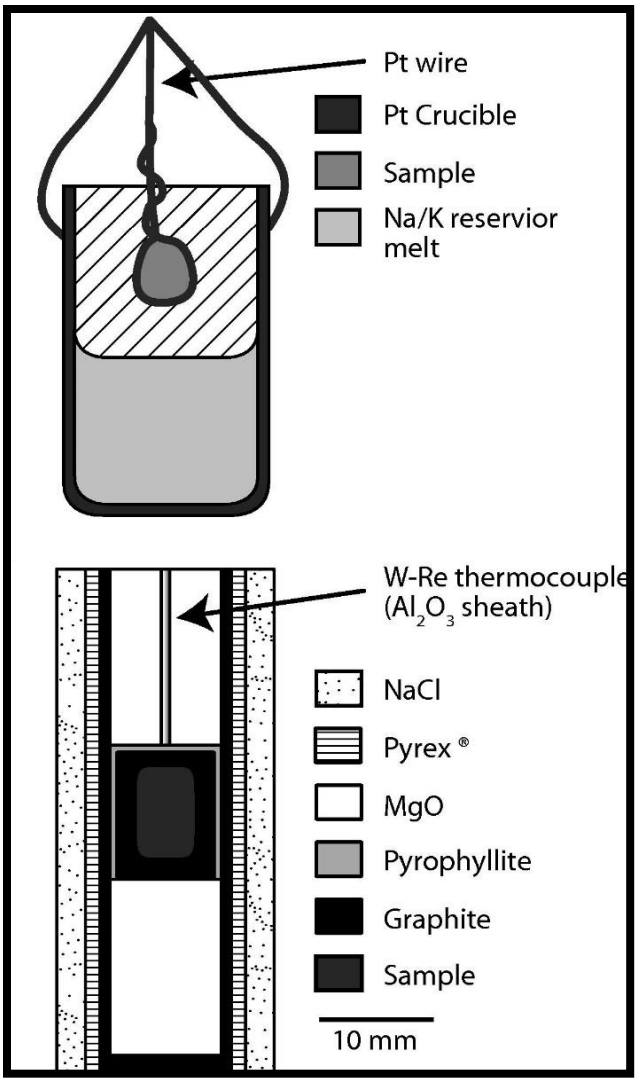

Fig. 3. Vertical-tube gas mixing furnace diagram showing platinum wire loop and platinum and graphite crucibles used in glass synthesis experiments (Smythe and Brenan, 2015).

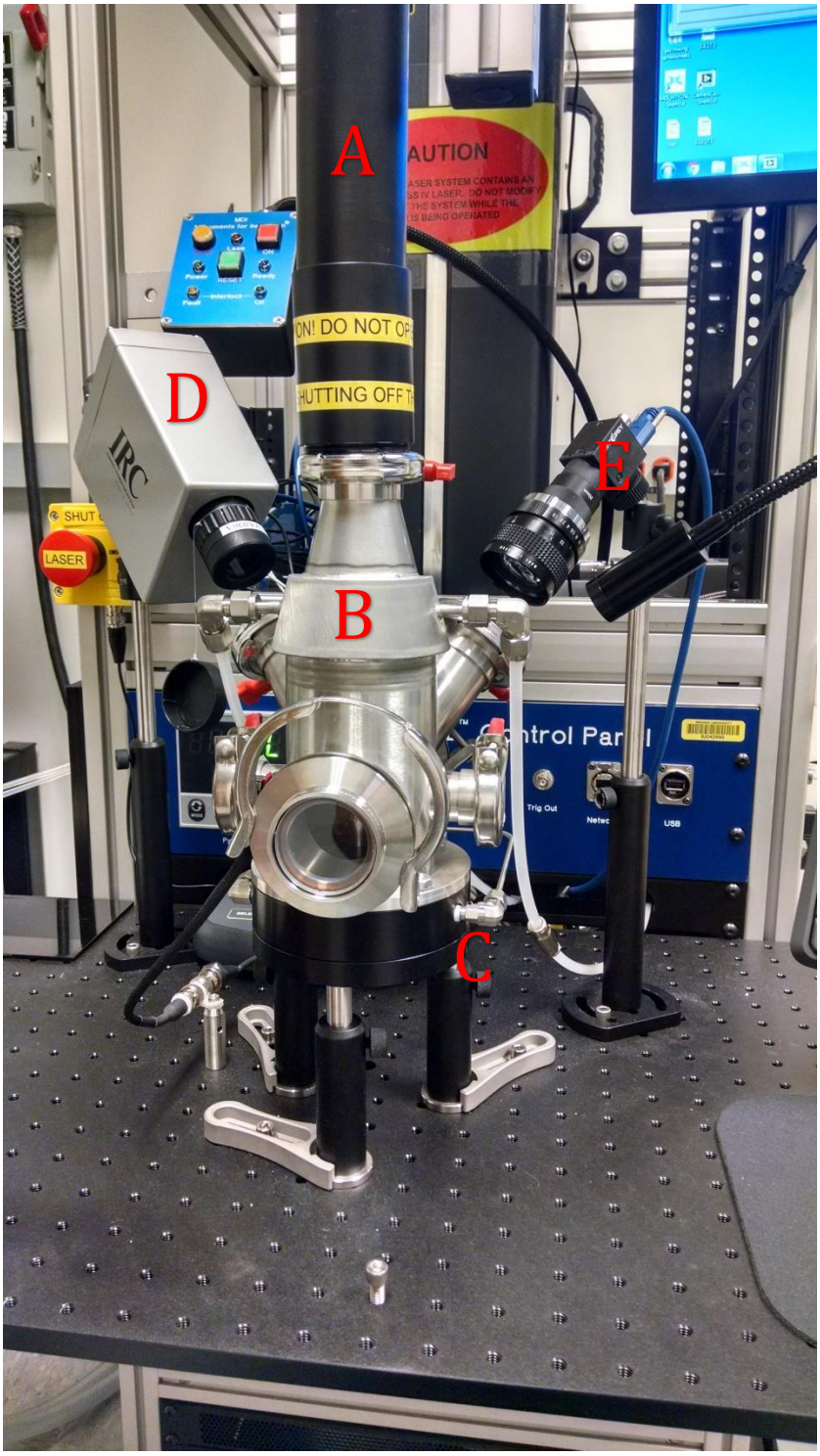

Fig. 4. Aerodynamic levitation laser furnace comprised of: (A) continuous wave CO_2 laser; (B) levitation chamber; (C) gas mixing valve; (D) optical pyrometer; (E) video camera.

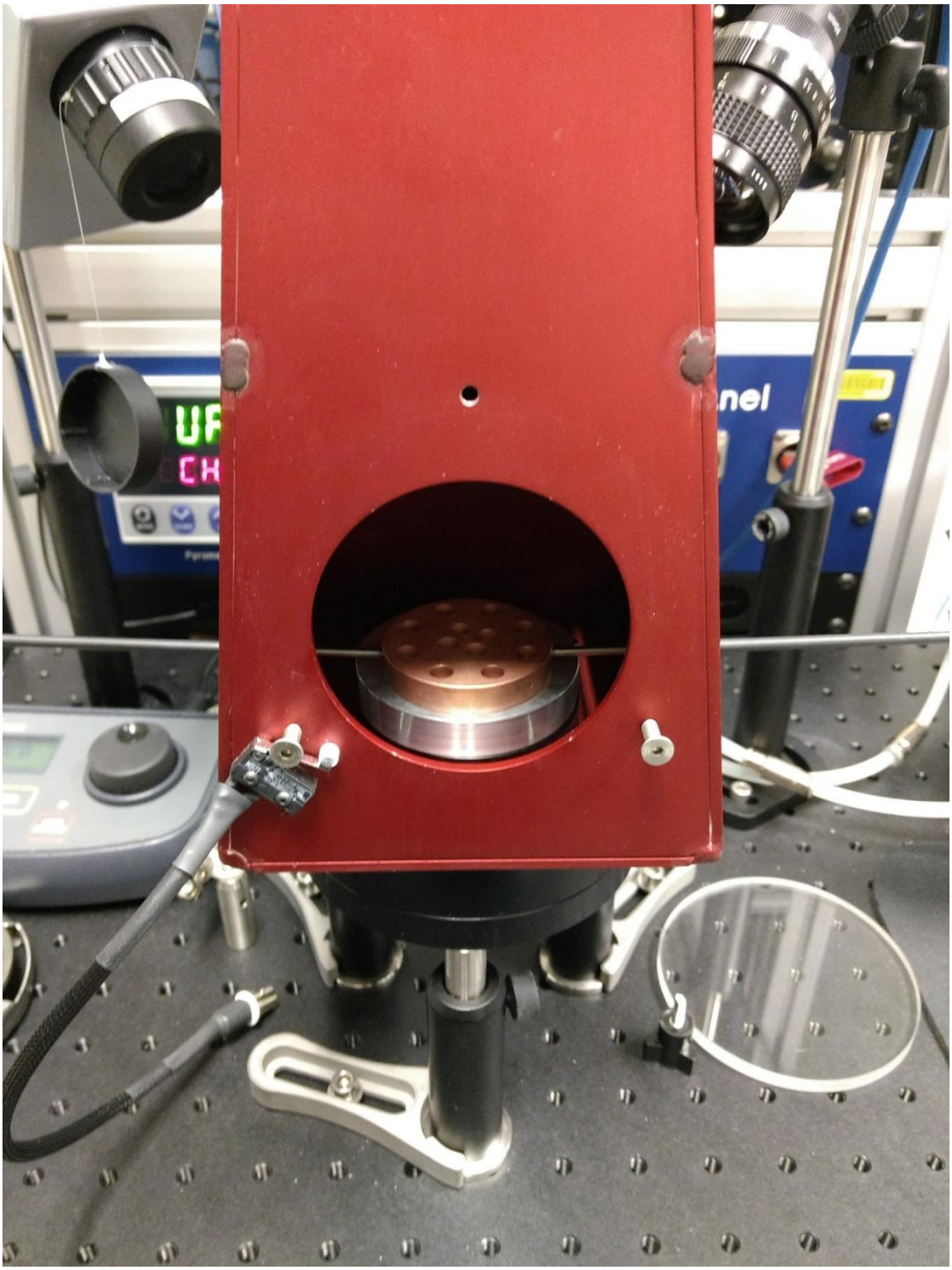

Fig. 5. Copper hearth plate with concave depressions situated in laser hearth chamber of aerodynamic levitation laser furnace. Hearth rods extending to left and right out from hearth plate and through slits of laser hearth.

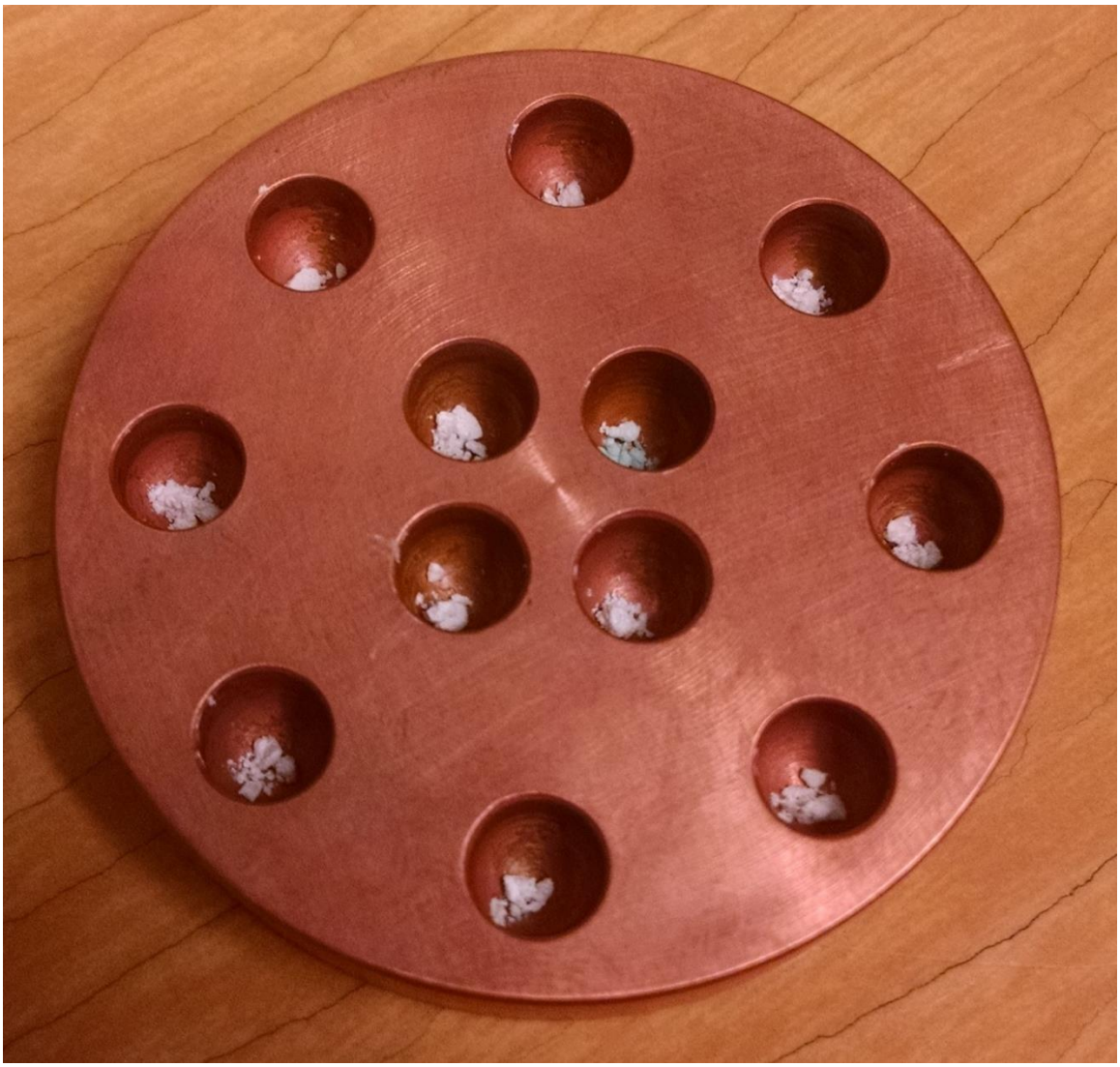

Fig. 6. Copper hearth plates used in laser hearth during laser fusing process of glass synthesis methodology, producing spheres 0.5 – 3.0 mm in diameter. The concave depressions contain ~4 mg aliquots of $MgSiO_3$ powder and the curve of the depressions encourages the powder to fuse in a spherical form as it is heated by the laser.

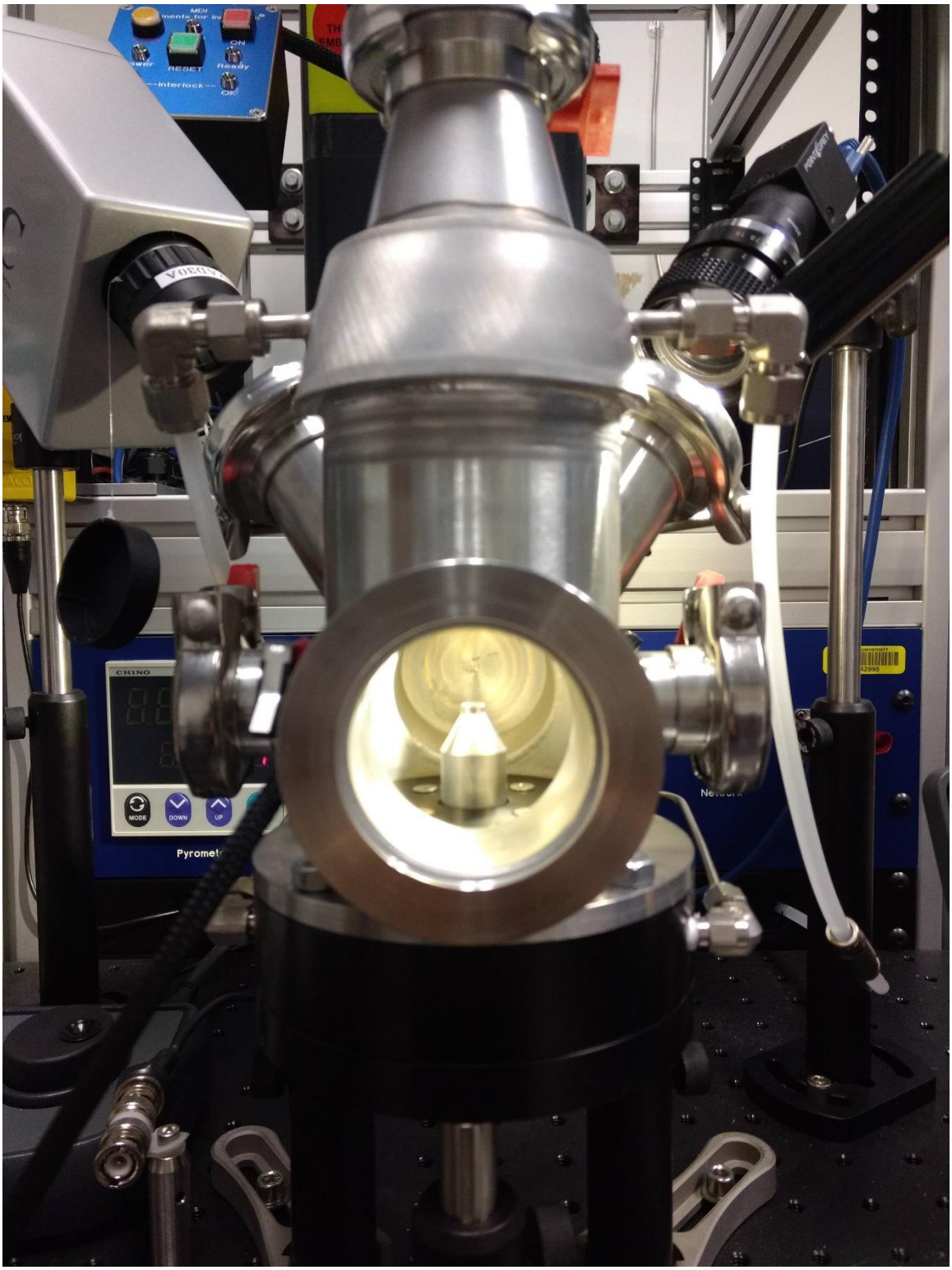

Fig. 7. Levitation chamber situated in aerodynamic levitation laser furnace with aluminum alloy conical nozzle capable of directing concentrated gas flows centered within chamber.

A B

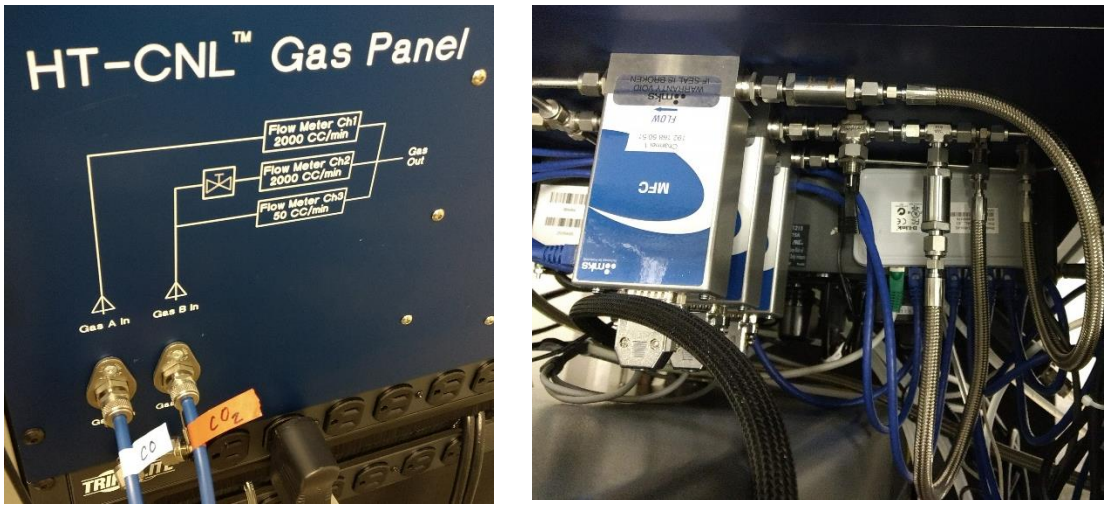

Fig. 8. Gas mixing valves combine (A) the individual gases and (B) regulate the gas flow rate of the final mixture.

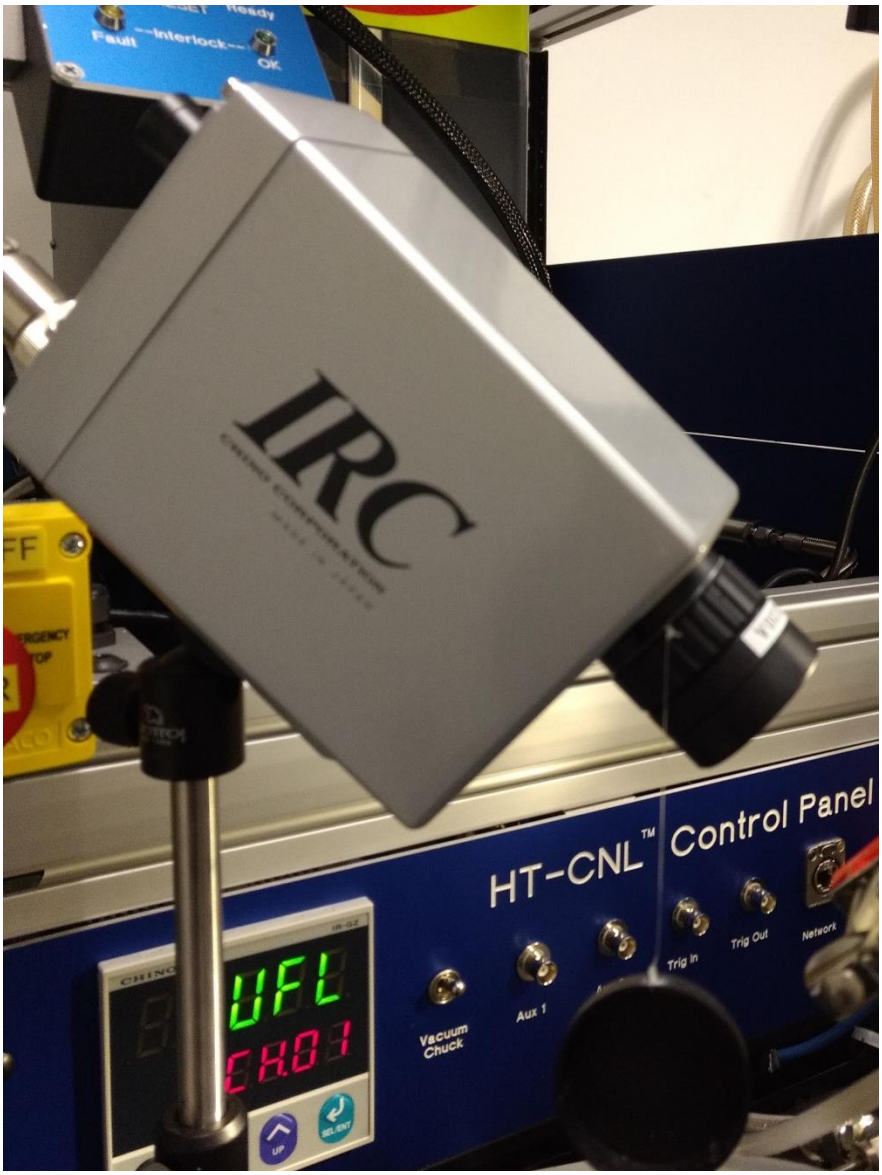

Fig. 9. An integrated Chino IR-CAS near-infrared optical pyrometer measures the sample surface temperature through a window looking into the levitation chamber. The pyrometer readout is sent directly to the laser furnace software, which tracks both the apparent and absolute (corrected) temperatures.

Fig. 10. Point Grey digital video camera adjusts contrast in order to maintain visibility of molten samples giving off extreme light emissions, which would be dangerous to view with the naked eye.

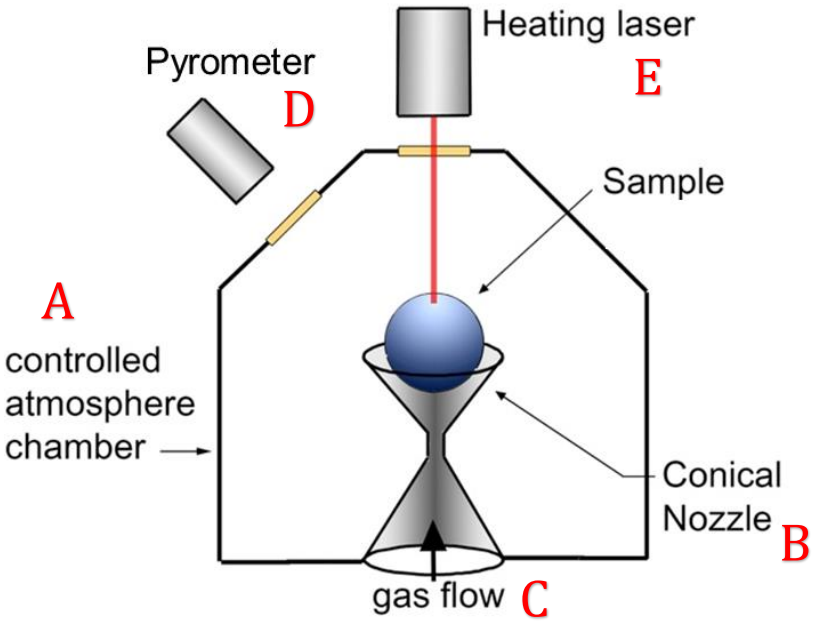

Fig. 11. Simplified layout for the levitation chamber of the aerodynamic levitation laser furnace. (A) The sealed levitation chamber keep external gases or contaminants from affecting the sample. (B) A conical nozzle with an aperture diameter of either 0.7 mm or 1.0 mm and orifice angles of either 60° or 90°, within which the spherical sample levitates. (C) A single gas flow, which is either a single gas composition or a set ratio of 2 compositions, passes vertically through the conical nozzle. As the flow passes around the sample, it acts upon it and both contains and suspends it. (D) The pyrometer measures the sample temperature by its light emissions, viewed through a glass lens. (E) A 400 W continuous wave CO_2 laser beam is directed at the sample from directly above it (Edited from University of Bristol, UK, Physics Department).

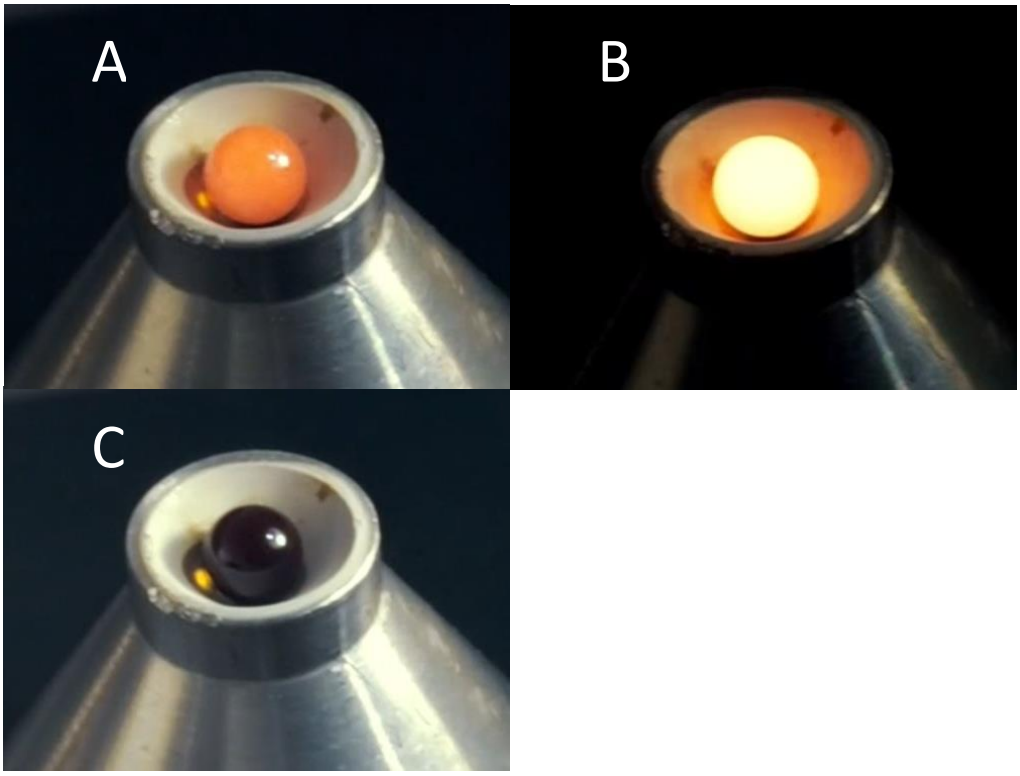

Fig. 12. Sample levitating in conical nozzle and being heated by continuous wave CO_2 laser. The three individual images show snapshots of the same sample taken seconds apart at different temperatures. (A) Heated sample at temperatures approaching liquidus. (B) Sample at temperature above liquidus. (C) Supercooled and vitreous sample (Briggs, 2018).

Fig. 13. Polytetrafluoroethylene washers adhered to double-sided carbon tape in an aluminum dish. Two mm-sized glass spheres are held in place by the carbon tape, positioned within the bounds of the washers prior to the addition of the temporary epoxy.

A B

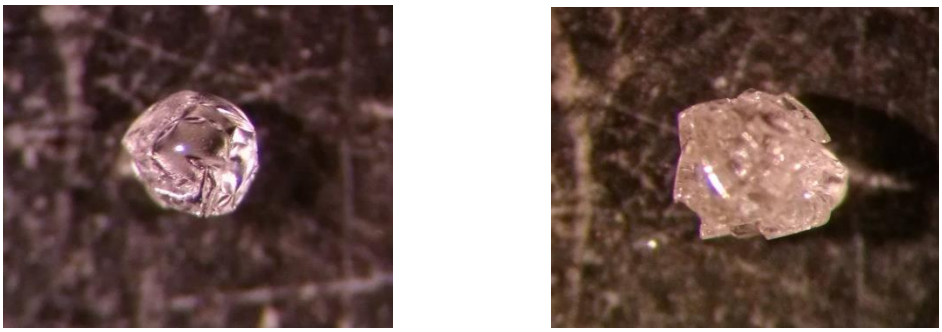

Fig. 14. Forsterite partially vitrified samples exhibiting “crumpled” exterior. (A) Sample 10.6.17.6. (B) Sample 10.6.17.8.

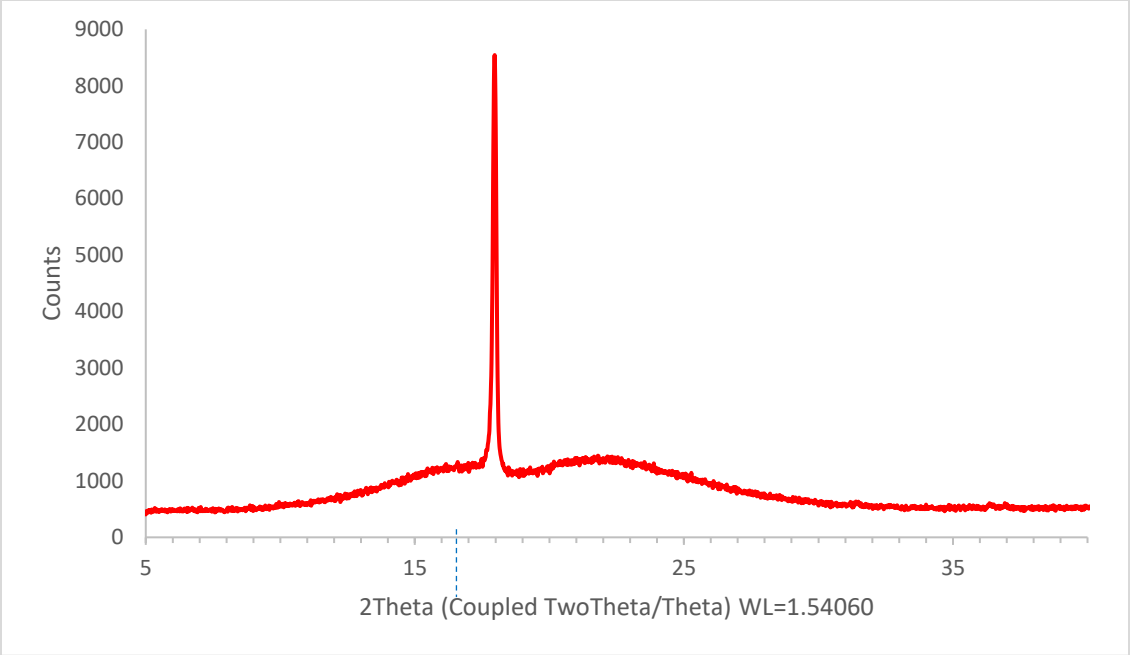

Fig. 15. XRD Vantec graphical output of Mg_2SiO_4 (forsterite) sample 10.6.17.6, showing crystalline Bragg's peak within an otherwise amorphous structure.

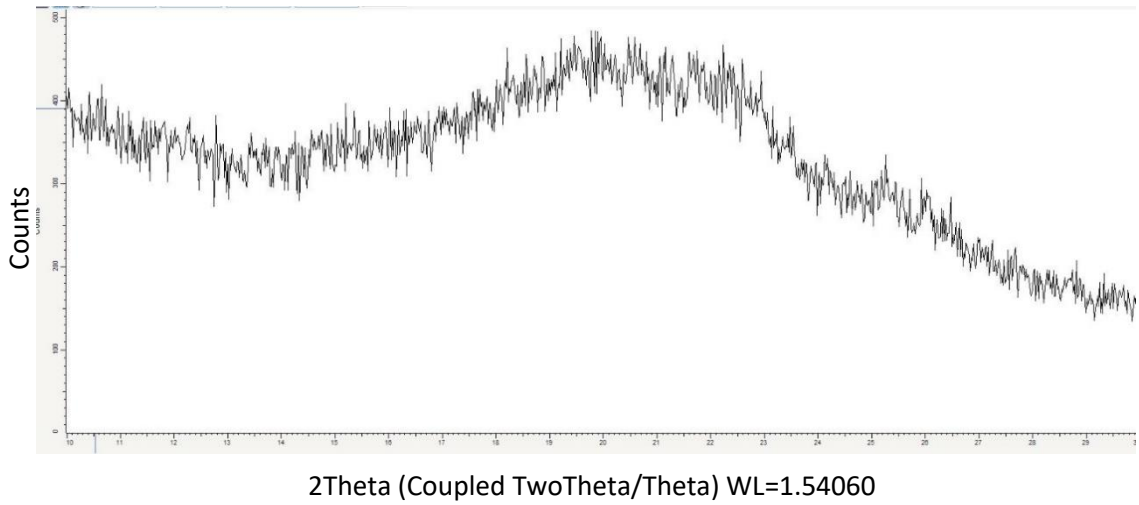

Fig. 16. XRD LynxEye graphical output of Mg_2SiO_4 (forsterite) sample 10.6.17.20, showing an amorphous structure with a complete lack of crystalline Bragg's peaks.

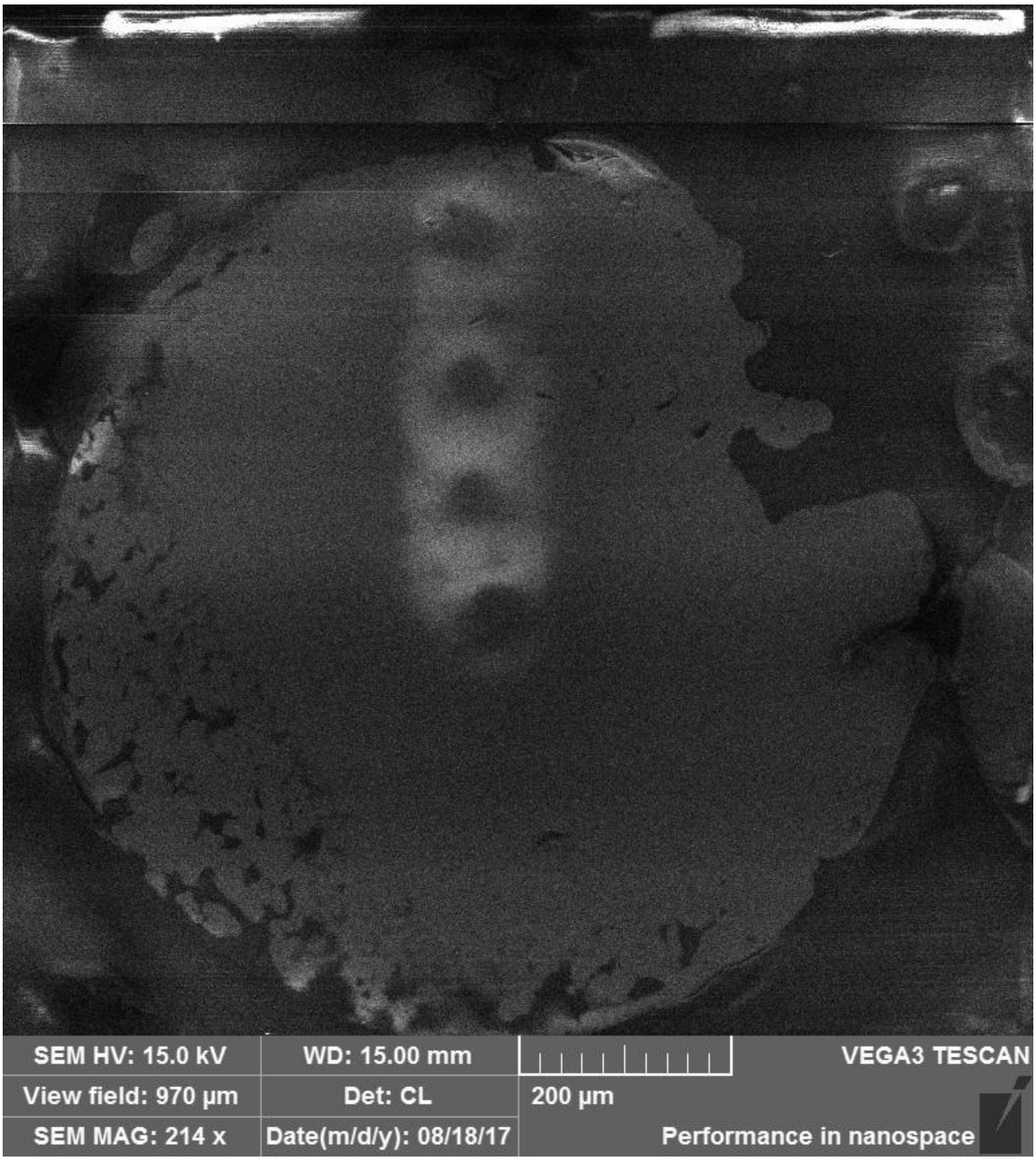

Fig. 17. SEM EDS spot analysis locations as shown on BSE images of polished forsterite glass sample.

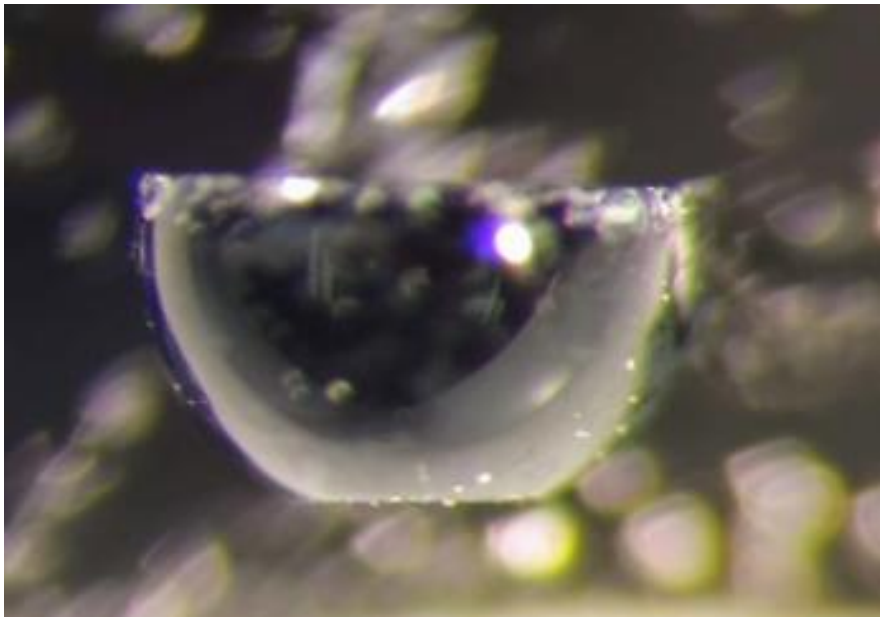

Fig. 18. Dual polished 1.1 mm diameter glass sample with Mg-Fe pyroxene composition. Sample has coarse-grind on base plane and 0.25μm polish on top plane.

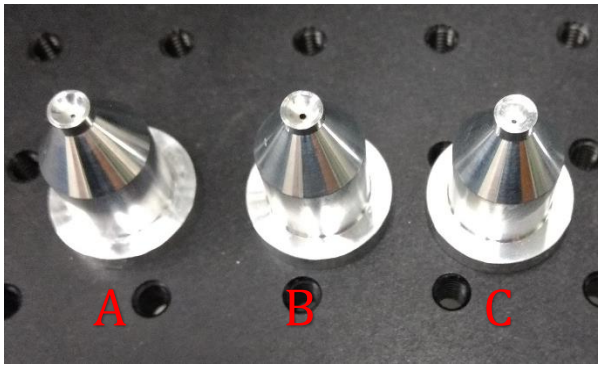

Fig. 19. Aluminum alloy conical nozzles used in levitation chamber of aerodynamic levitation laser furnace. (A) 90° / 0.7 mm nozzle; (B) 90° / 1.0 mm nozzle; (C) 60° / 0.7 mm nozzle.

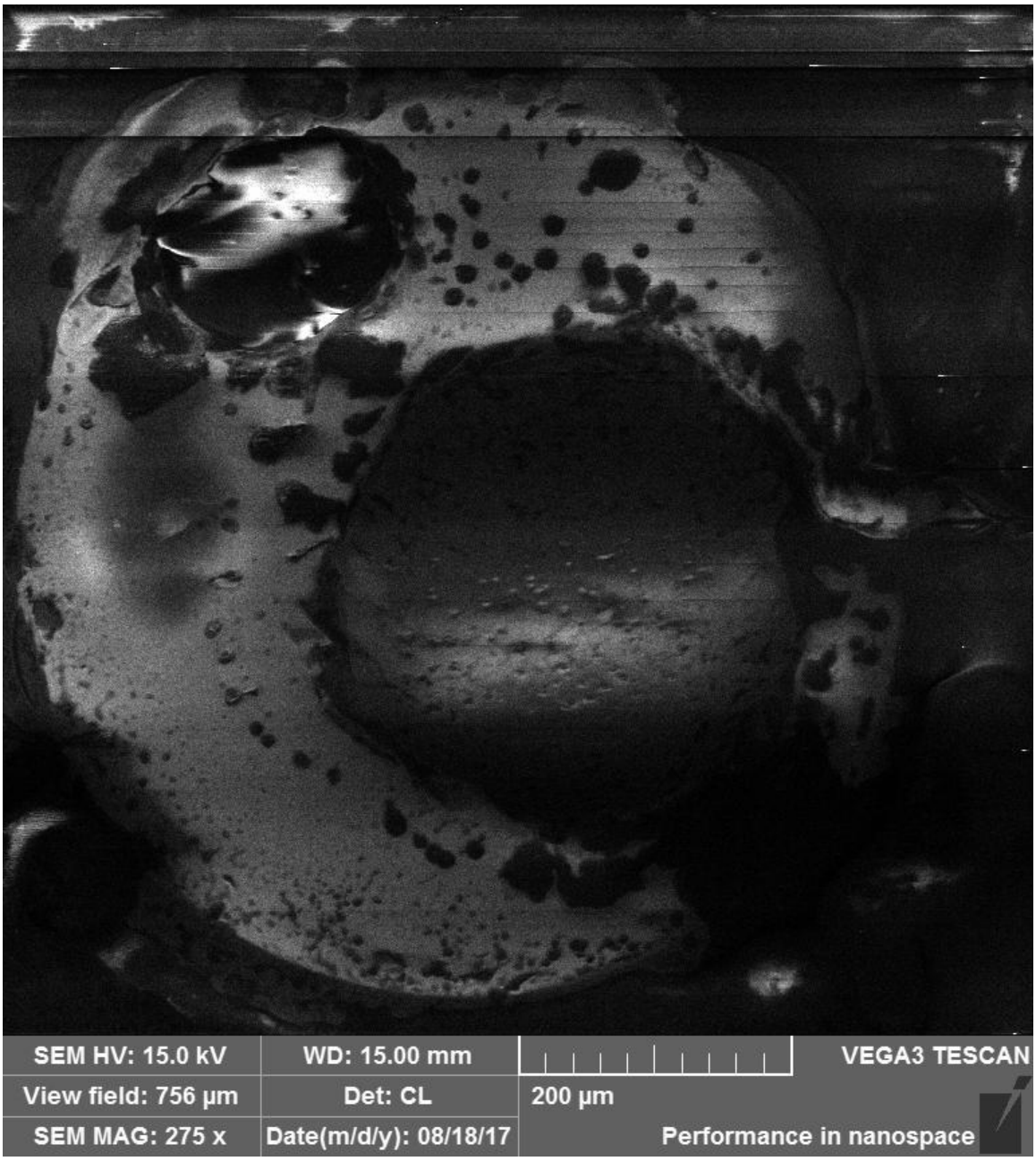

Fig. 20. SEM BSE image of polished forsterite glass sample with internal shrinkage void (bubble).

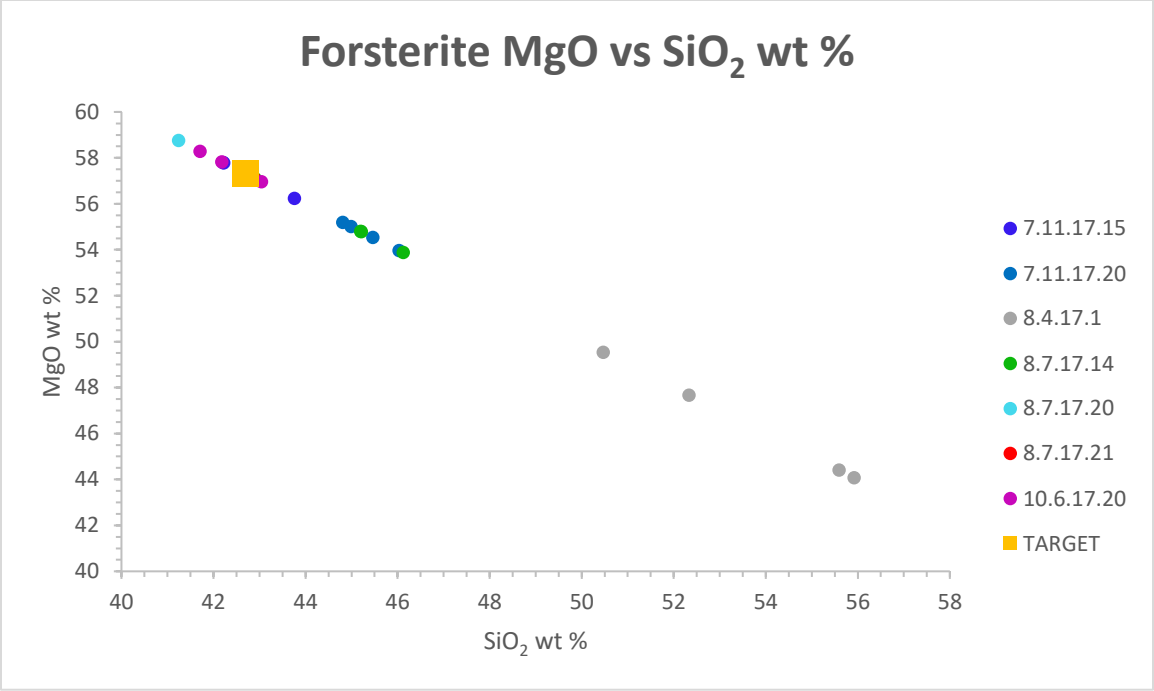

Fig. 21. Graph showing experimental MgO vs SiO_2 weight percentages of forsterite SEM EDS spot analyses relative to the theoretical forsterite weight percentages (TARGET).

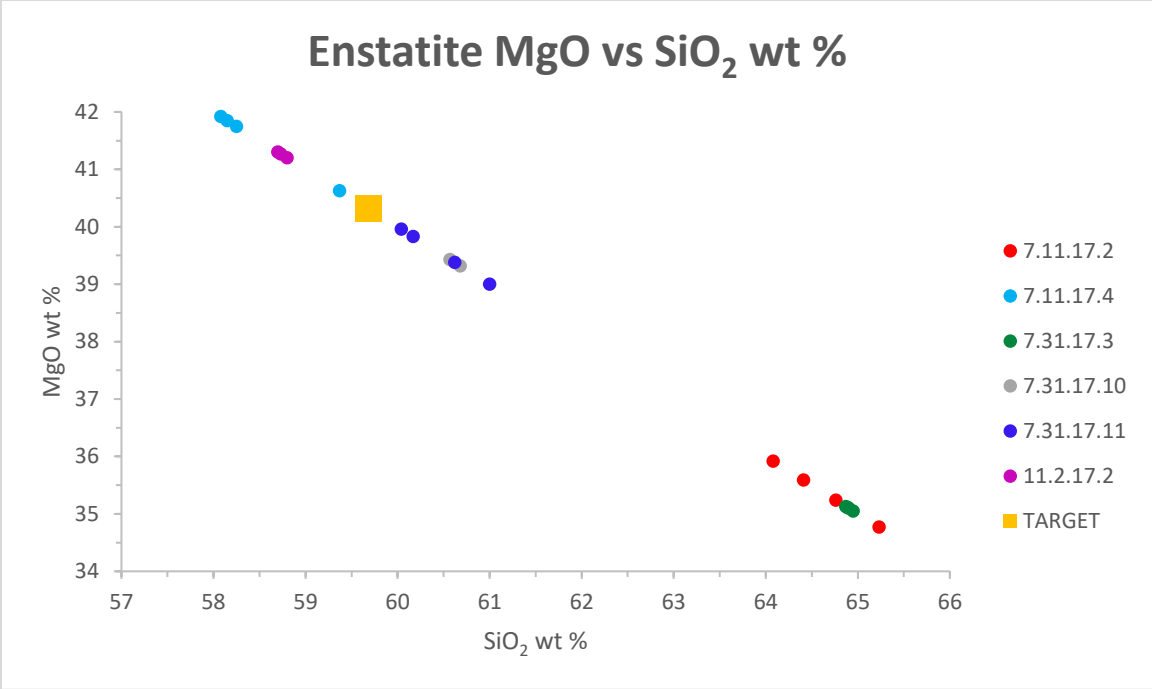

Fig. 22. Graph showing experimental MgO vs SiO_2 weight percentages of enstatite SEM EDS spot analyses relative to the theoretical enstatite weight percentages (TARGET).

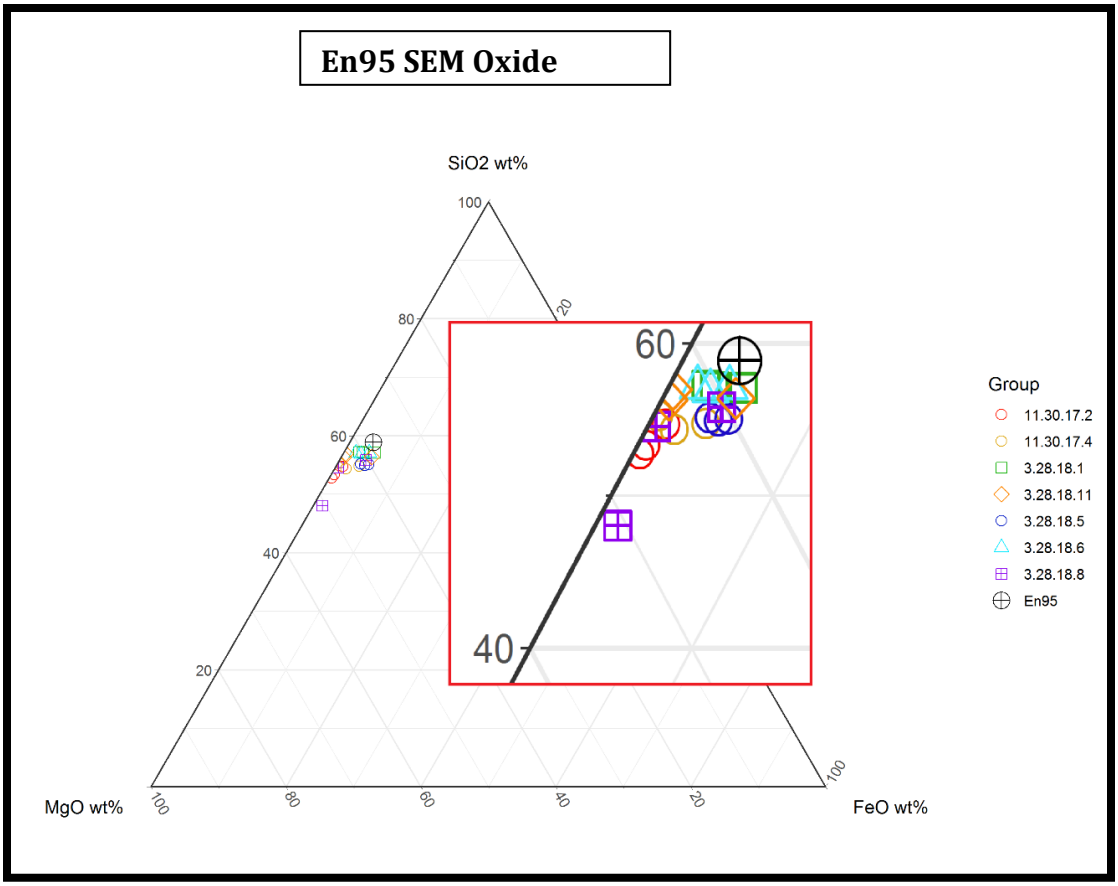

Fig. 23. Ternary diagram representing SEM multiple spot analyses for 7 $(Mg_{0.95}Fe_{0.05})SiO_3$ pyroxene samples compared against the target intended weight % (En95). For sample levitation conditions: (**circle**) 100% O_2; (**square**) 100% Ar; (**diamond**) 100% 5% CO in Ar; (**triangle**) 100% 5% CO_2 in Ar; (**square with crosshairs**) 50% Ar + 50% O_2.

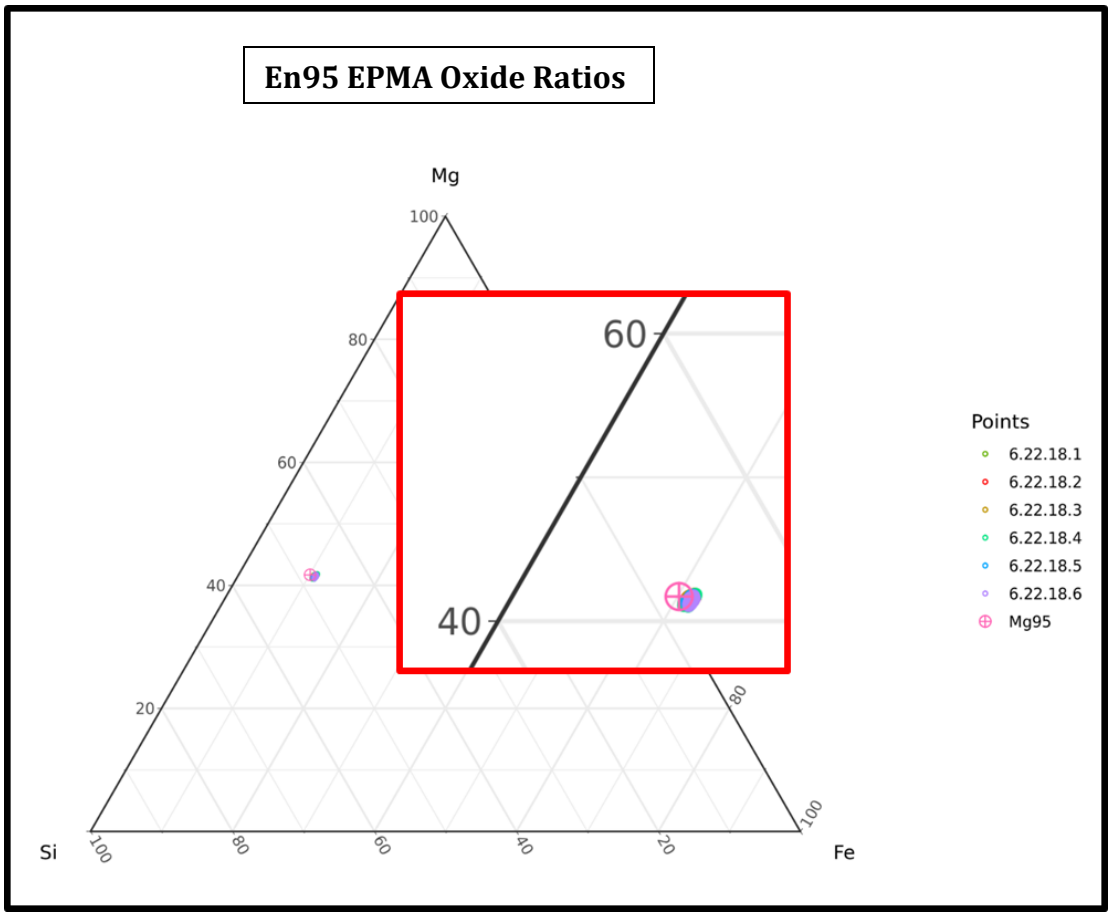

Fig. 24. Ternary diagram representing SEM multiple spot analyses for 2 $(Mg_{0.9}Fe_{0.1})SiO_3$ pyroxene samples compared against the target intended weight % (En90). Both samples levitated in 100% O_2.

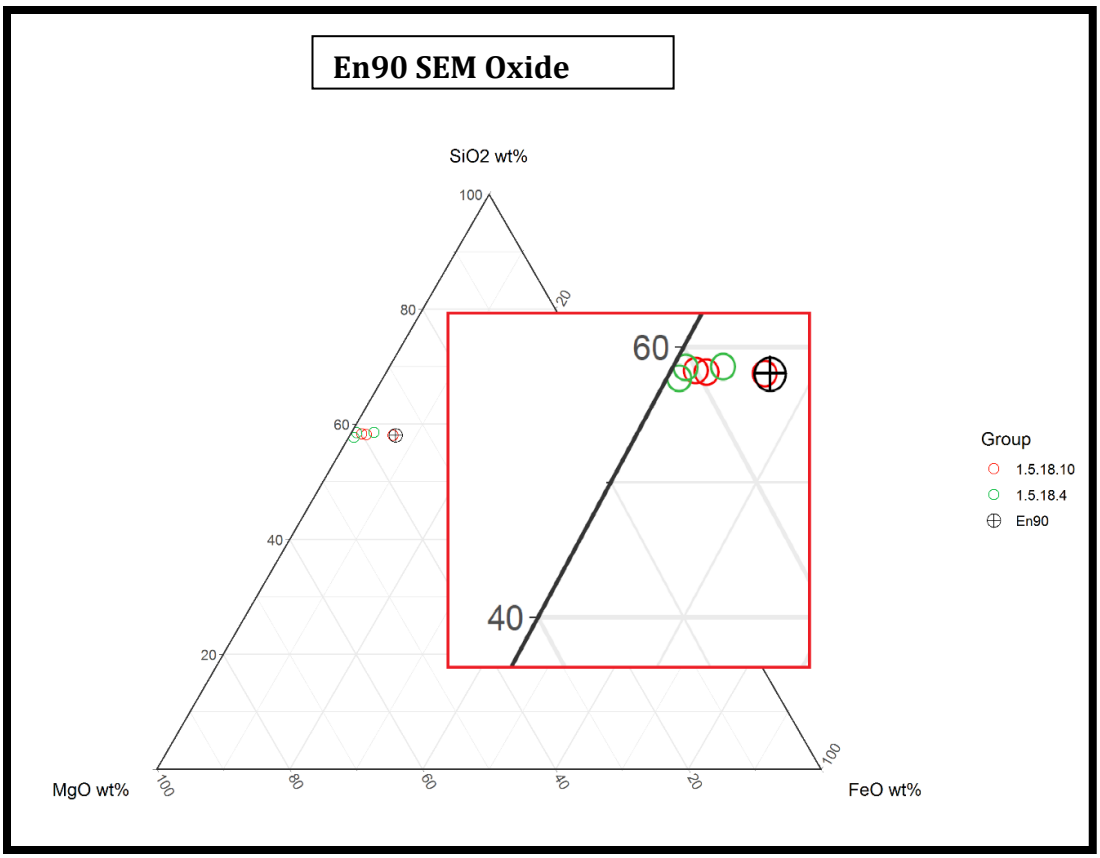

Fig. 25. Ternary diagram representing EPMA multiple spot analyses for 3 $(Mg_{0.9}Fe_{0.1})SiO_3$ pyroxene samples, compared against the target intended weight %.

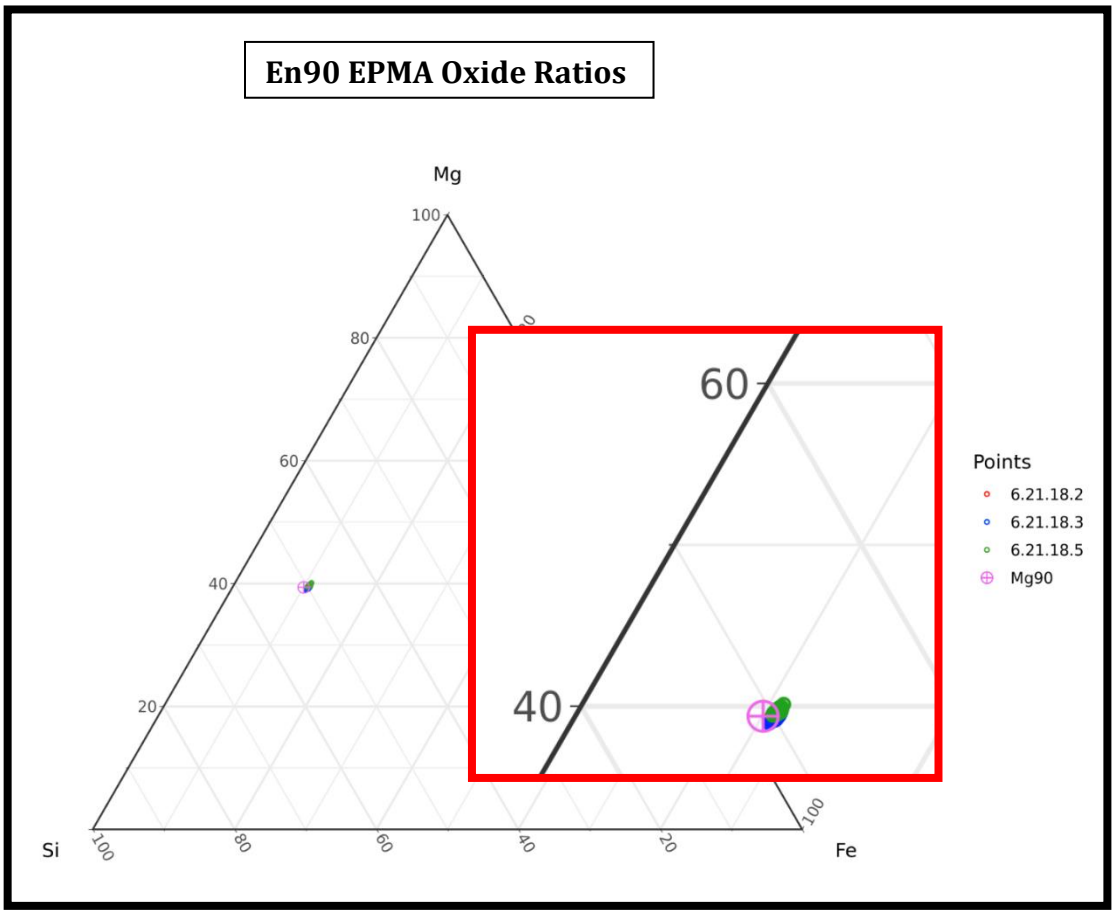

Fig. 26. Ternary diagram representing EPMA multiple spot analyses for 6 $(Mg_{0.95}Fe_{0.05})(Si_{0.95}Fe_{0.05})O_3$ pyroxene samples, compared against the target intended weight %.

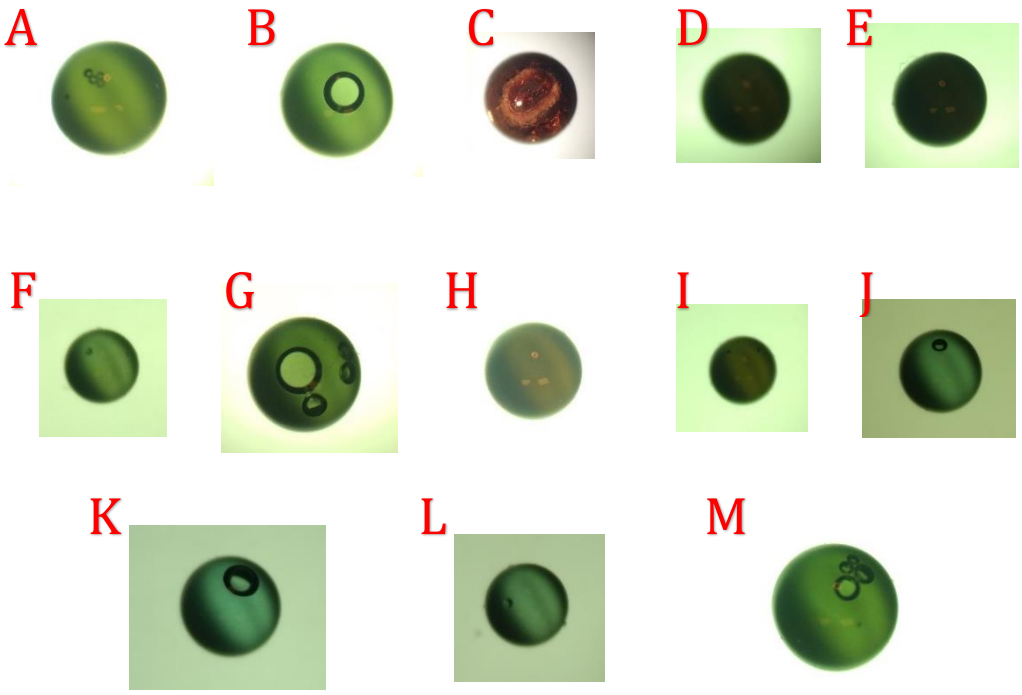

Fig. 27. The same En95 samples from Fig. 23, after vitrification, used in fugacity-constrained experiments: (A) 3.28.18.1 (Pure Ar); (B) 3.28.18.2 (Pure Ar); (C) 3.28.18.3 (Pure O_2); (D) 3.28.18.4 (Pure O_2); (E) 3.28.18.5 (Pure O_2); (F) 3.28.18.6 (Pure 5% CO_2 in Ar); (G) 3.28.18.7 (Pure 5% CO_2 in Ar); (H) 3.28.18.8 (50/50 O_2 and Ar); (I) 3.28.18.9 (50/50 O_2 and Ar); (J) 3.28.18.10 (Pure 5% CO in Ar); (K) 3.28.18.11 (Pure 5% CO in Ar); (L) 3.28.18.12 (50/50 5% CO in Ar and 5% CO_2 in Ar); (M) 3.28.18.13 (50/50 5% CO in Ar and 5% CO_2 in Ar). Image sizes do not reflect sample diameters, which can be found in Table 2.

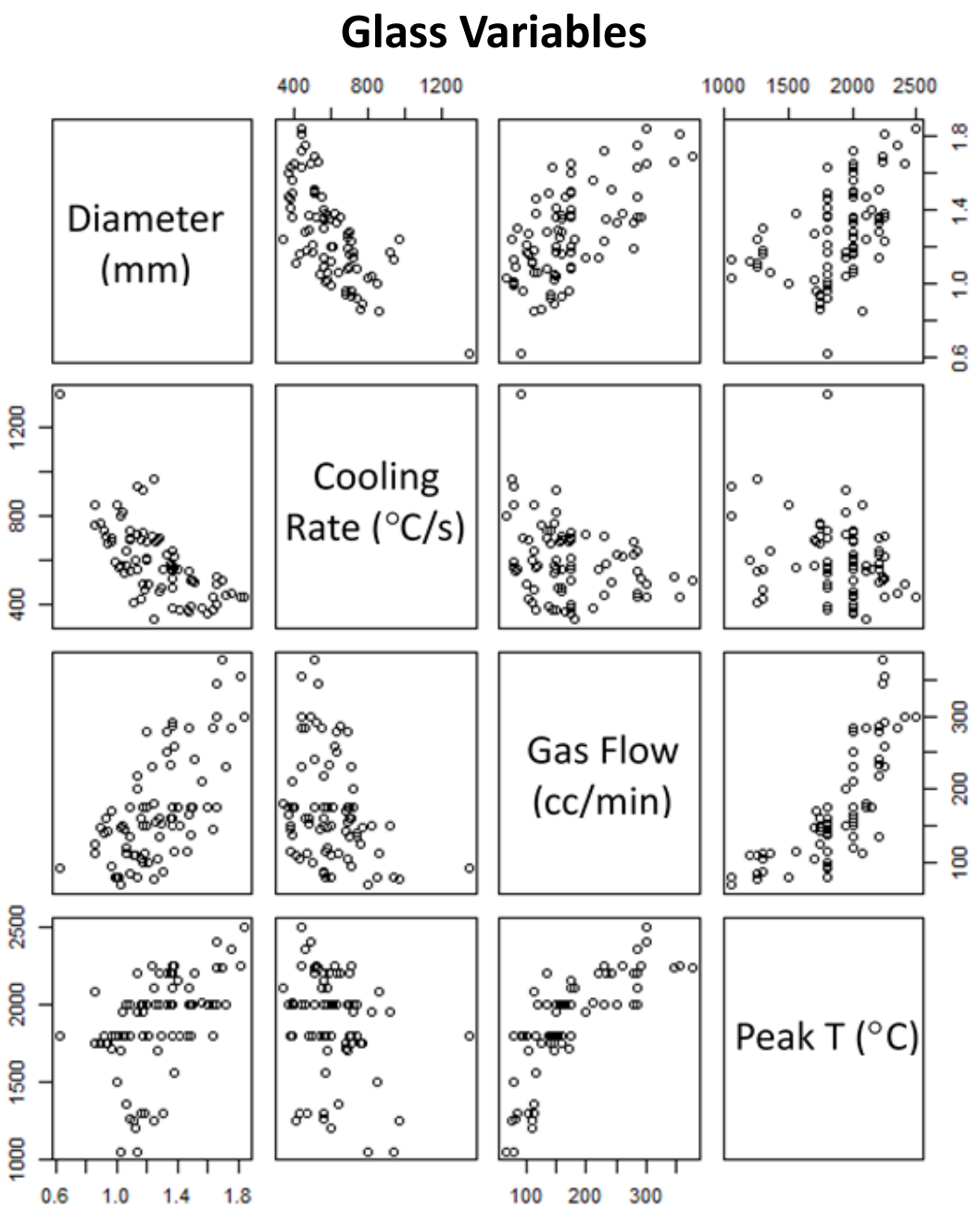

Fig. 28. Pairs plot of synthetic glasses variables, where each variable is plotted against every other variable. The variables shown from upper left to lower right are: sample diameter and the cooling rate, gas flow rate, and peak temperature reached during vitrification. The variable present in a given row represents the Y-axis and the variable present in a given column represents the X-axis.

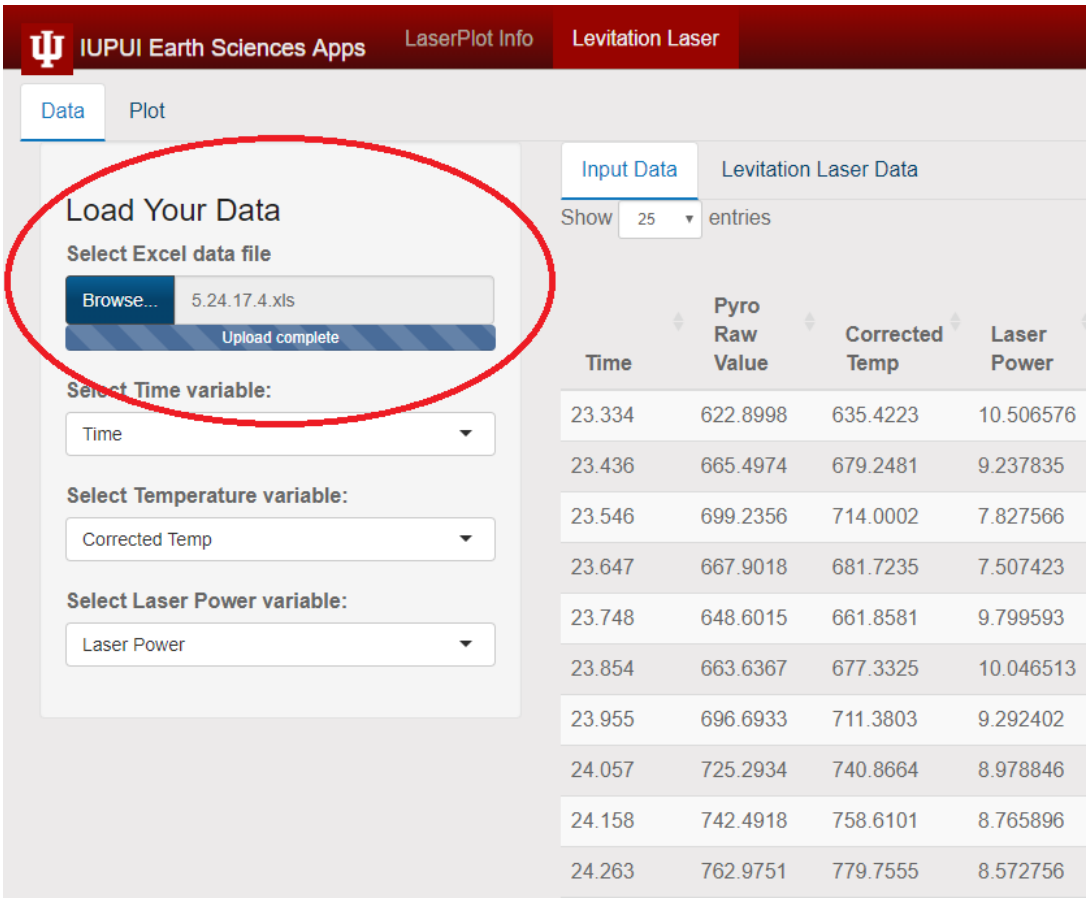

Fig. 29. Screenshot of data loading process taken from LaserPlot Data tab and highlighting location where user can upload Excel data output from aerodynamic levitation laser furnace.

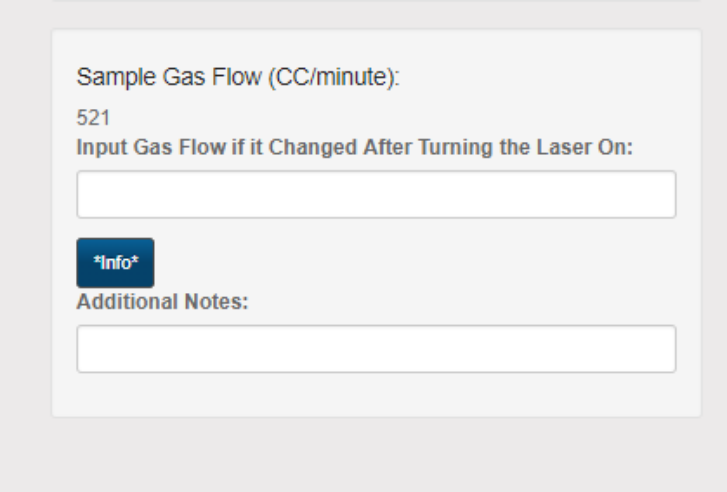

Fig. 30. Screenshot of plot controls taken from LaserPlot Plot tab and highlighting gas flow and additional notes.

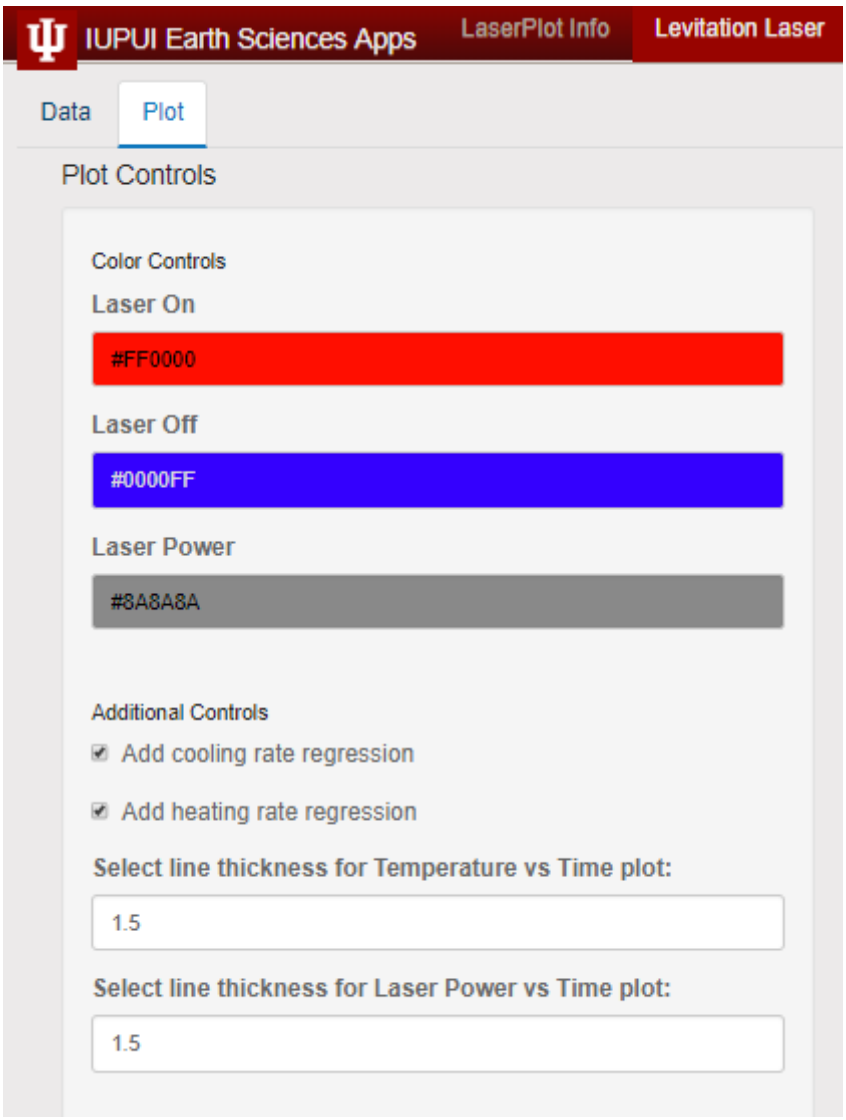

Fig. 31. Screenshot of plot controls taken from LaserPlot Plot tab and highlighting location where plot aesthetics can be controlled for both the temperature vs time and laser power vs time plots. Linear regressions for the heating and cooling rates can be toggled on/off here.

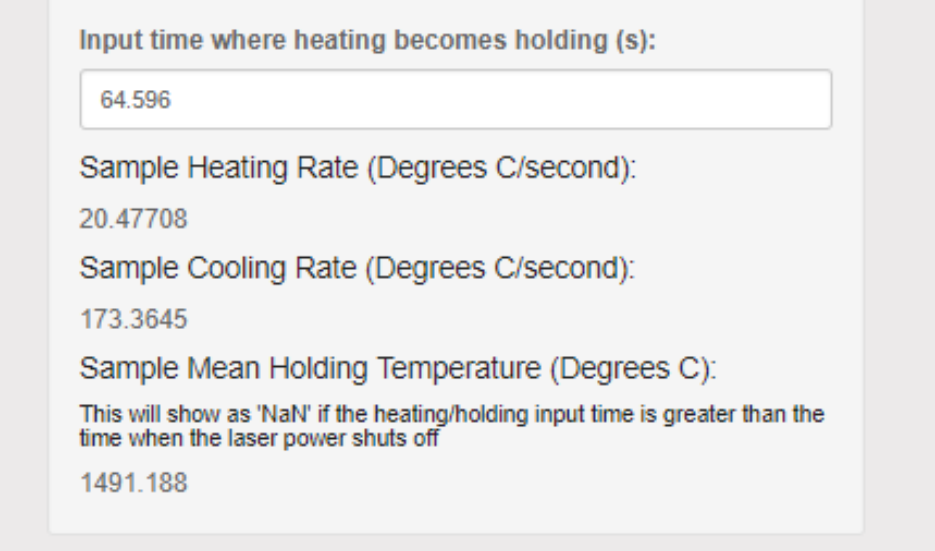

Fig. 32. Screenshot of plot controls taken from LaserPlot Plot tab and highlighting heat/hold time, which identifies the time that the sample temperature is no longer heating, but rather has begun holding at temperature. This point is necessary to calculate the heating rate, the holding temperature, and the holding duration.

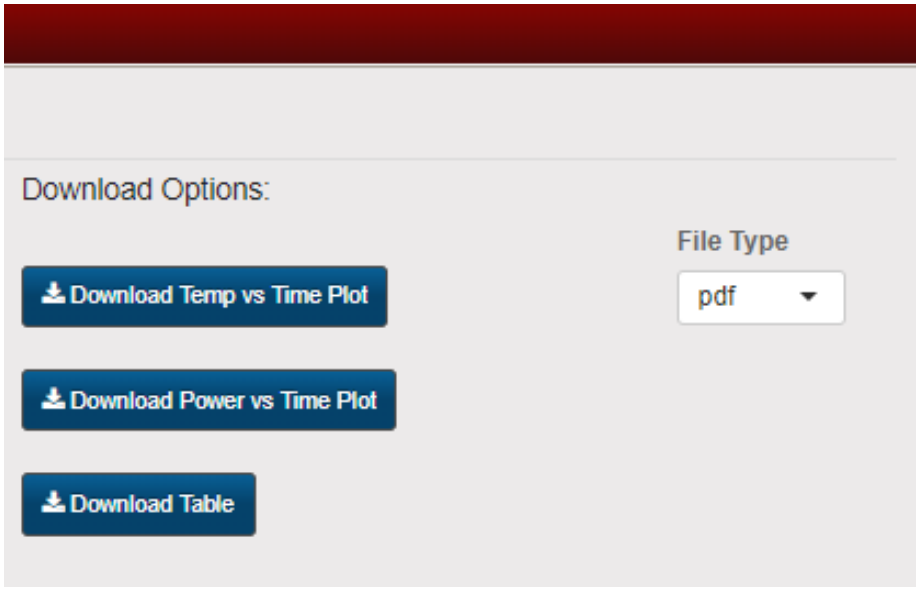

Fig. 33. Screenshot of plot controls taken from LaserPlot Plot tab and highlighting the download options, which includes the choice of plot output format (PNG or PDF), and the buttons for downloading the temperature vs time plot, the laser power vs time plot, and the table of data pulled from the loaded file and calculated by LaserPlot.

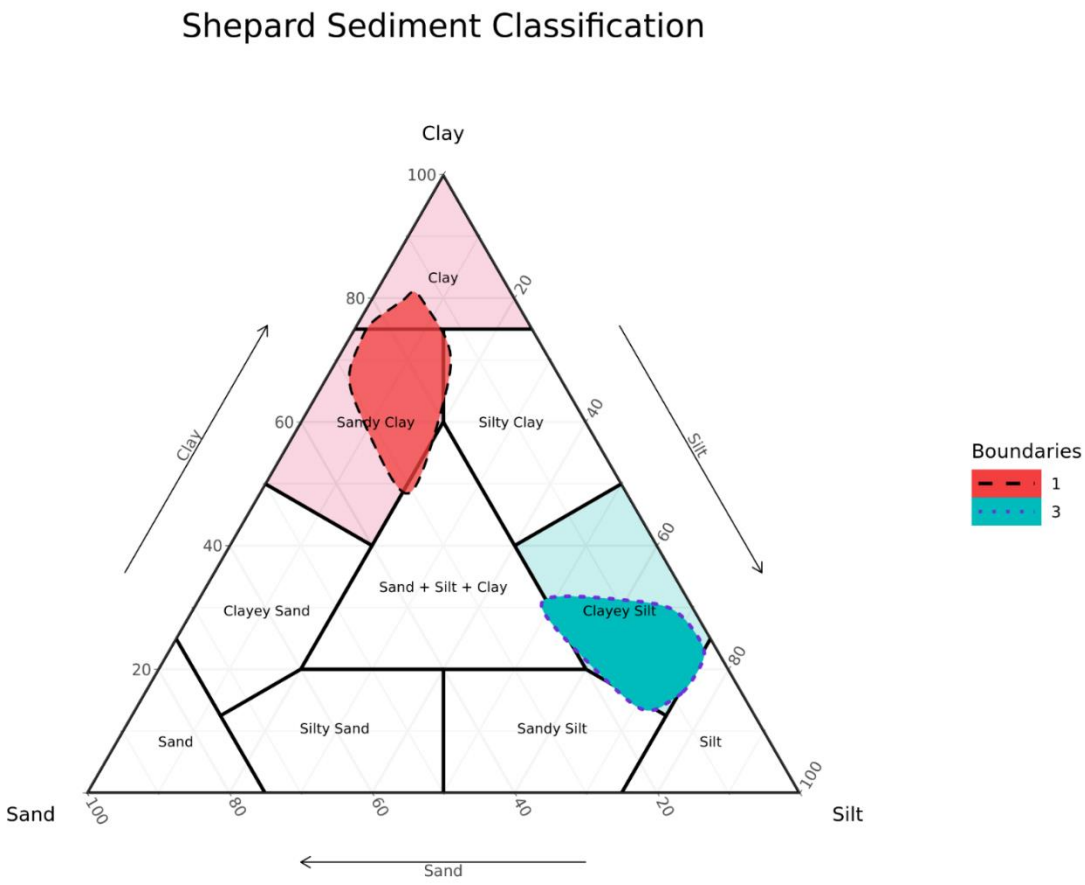

Fig. 34. Shepard sediment classification ternary discrimination diagram (Shepard, 1954) using example data points to highlight aesthetic controls. Plot was built in and downloaded from RockR!.

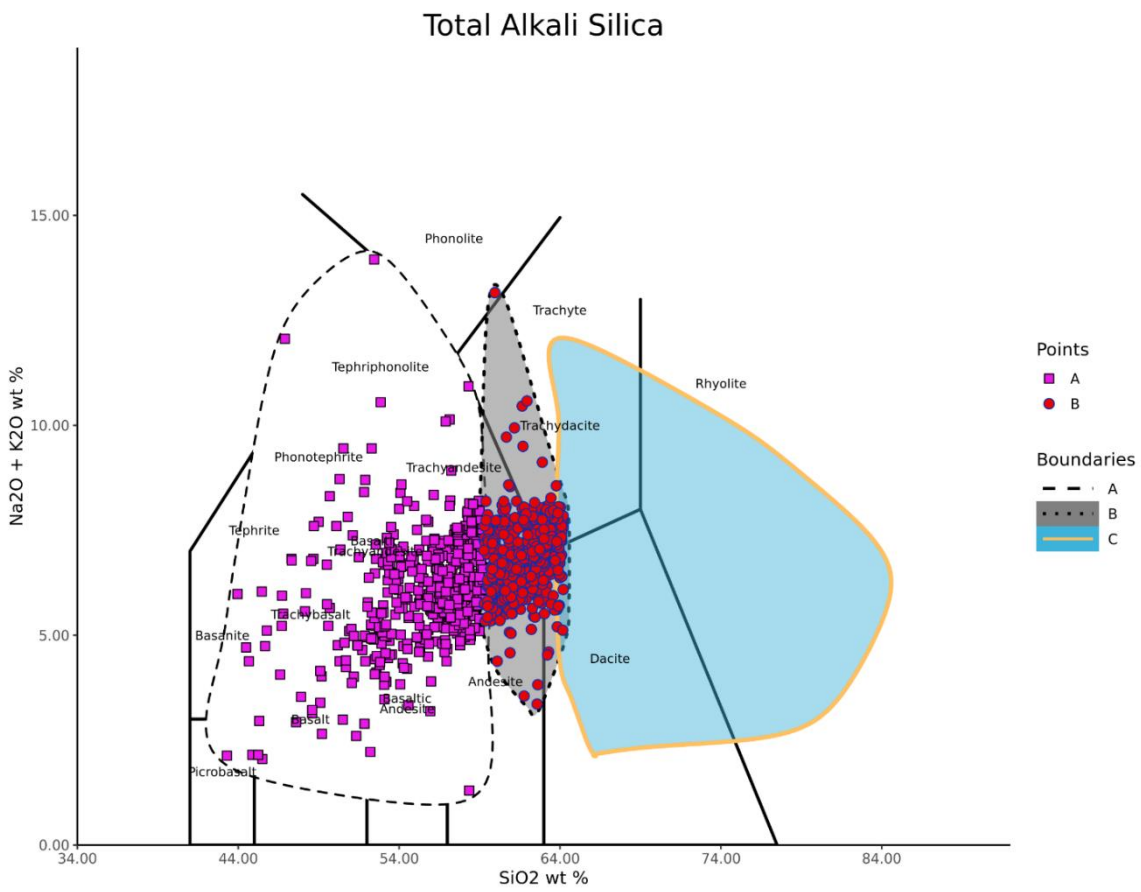

Fig. 35. Total Alkali vs Silica (TAS) (LeBas, 1986) bivariate discrimination diagram showing aesthetic control varieties using Andes example data set. Plot was built in and downloaded from RockR!.

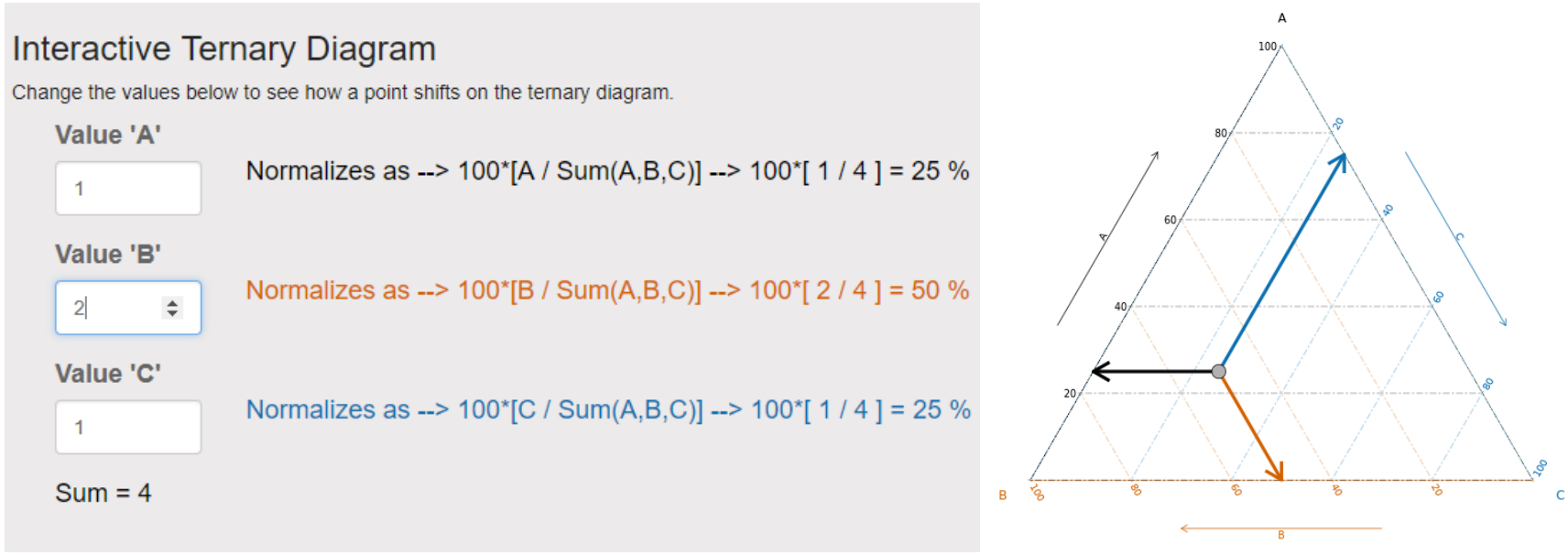

Fig. 36. Interactive ternary diagram, helping users visualize the calculation of normalized points on a ternary diagram. Changes to the endmember value is reflected in the plot to the right in real time, highlighting the relative portions in a three-axis system.

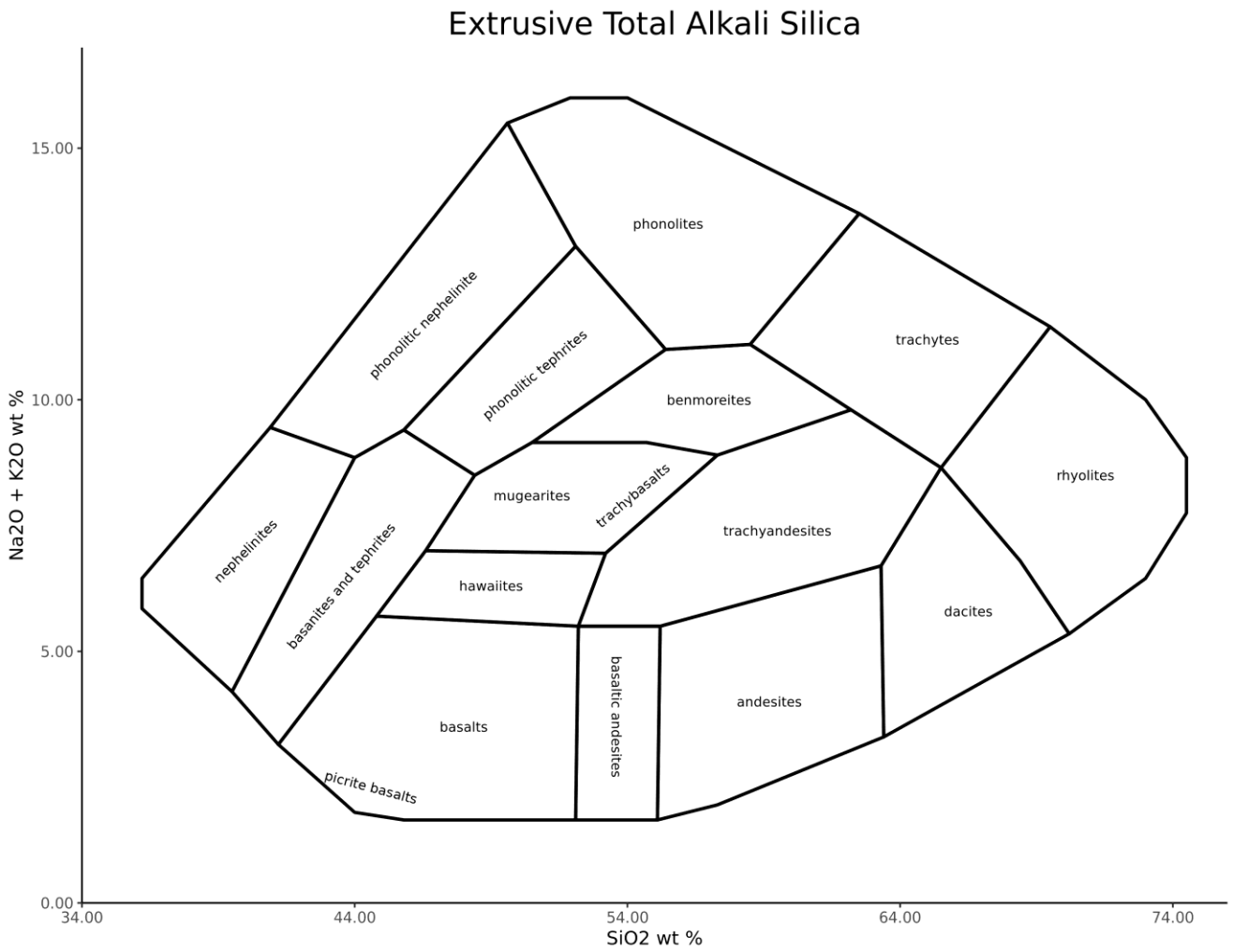

Fig. 37. Total Alkali vs Silica (TAS) (Cox, 1979) bivariate discrimination diagram built in and downloaded from RockR.

Appendix A

LaserPlot source code

(GitHub repository)

https://github.com/tzurloye/LaserPlot/

Appendix B

RockR source code

(GitHub repository)

https://github.com/RockRwebapp/RockR/

Curriculum Vitae

Thomas Edwards zur Loye

Education

Jun 2019 — Indiana University, College of Arts and Sciences, Indianapolis, IN
Master of Science in Geology, GPA 4.0/4.0
Thesis: Developing Levitation Laser-Fused Glasses as Proxies for Lower Mantle Experiments: A Methodological Approach

Dec 2018 — Indiana University, College of Arts and Sciences, Indianapolis, IN
Bachelor of Science in Geology, GPA 3.5/4.0

May 2010 — Indiana University, College of Arts and Sciences, Bloomington, IN
Bachelor of Arts in Anthropology, GPA 3.4/4.0

Experience

Geology Research and Teaching Experience

Graduate Research Assistant - IUPUI — May 2017-Apr 2019

- Utilized embedded class IV CO2 laser within aerodynamic levitation laser furnace under various conditions to create silicate glasses
- Created new procedures with various glass sample mixing, grinding, and polishing techniques
- Coded 2 new applications in R to improve data analysis and teaching capability

Graduate Teaching Assistant - IUPUI — Aug 2017-Dec 2017

- Instructed and assisted undergraduate students in optical spectroscopy and hand sample mineral identification techniques
- Prepared lab exercises and graded student homework/laboratory assignments
- Organized, cataloged, and detailed descriptions for approximately 400 mineral and rock thin section samples

Lab Assistant - IUPUI — Sep 2015-Mar 2016

- Performed hydroxide treatments of soil samples from lake sediment cores to remove carbon
- Operated centrifuge and isolated samples after acid and base treatments

Archaeological Experience

Archaeological Tech. - Alpine Archaeological Consultants, Inc. July 2012-Oct 2014

- Collaborated in teams of 3-5 people in sagebrush, desert, and alluvial conditions in Colorado, North Dakota, South Dakota, and Wyoming during summer to late fall seasons
- Completed pedestrian surveys of proposed pipeline transects and tracked GPS locations via Trimble unit
- Excavated auger tests, shovel tests, and archaic features including a basin house, hearths, and storage pits
- Profiled, photographed, and mapped feature profile bisects and plan views
- Determined Munsell values and textures of soils present in different levels of units and shovel tests

Crew Chief - Illinois State Archaeological Survey Sept 2011-June 2012

- Instructed new archaeologists in current company procedures and methodology
- Determined Munsell values and textures of soils present in specific zones
- Scribed feature limits in plan view and zone distinctions in profile view
- Compiled, reviewed, and prepared paperwork for digitizing for a field crew of 70 individuals
- Maintained and operated GPS total station to attain coordinates of mapping nails

Archaeological Tech. - Illinois State Archaeological Survey May 2010-Sept 2011

- Excavated Terminal Late Woodland and Early Mississippian Period features at a Phase III site in East St. Louis for the New Mississippi River Bridge project
- Processed faunal, floral, ceramic, and lithic cultural material recovered during excavation
- Consulted osteology/bioarchaeology experts regarding human remains

Archaeological Technician - Indiana University Aug 2009-May 2010

- Managed excavation of multiple shovel tests with volunteers at paleo site outside of Louisville, KY
- Washed, sorted, and cataloged artifacts from 5 sites in southern Indiana

Publications and Presentations

Nov 2018

zur Loye, Tom E., Macris, Catherine A., Farmer, Alison, Dorfman, Susannah M. (2018). Developing Levitation Laser-Fused Glasses as Proxies for Lower Mantle Experiments: A Methodological Approach. [Abstract] In: 130th Annual Geological Society of America Meeting. Nov 4-7. Indianapolis, IN.

Nov 2018

zur Loye, Thomas E., Mickey, Jeremiah L., Shukle, John T. (2018). RockR! A Petrographic Plotting Tool. [Abstract] In: 130th Annual Geological Society of America Meeting. Nov 4-7. Indianapolis, IN.

Mar 2018

J. Shukle, **T. zur Loye**, J. Mickey. (2018). RockR! A Petrographic Plotting App. Poster session presented at the Crossroads Conference at Indiana University, Bloomington, IN.

Dec 2017

C. A. Macris, E. D. Young, I. Kohl, and **T. E. zur Loye**. (2017). Evaporation Induced Oxygen Isotope Fractionation in Impact Ejecta [Abstract]. In: Proceedings of the 98th Annual Meeting of the American Geophysical Union. Dec 11-15. New Orleans, LA.

Apr 2009

C. A. Munson and **T. E. zur Loye**. (2009). Archaeology at the Hovey Lake Site. In: Proceedings of the 75th Annual Meeting of the Society of American Anthropologists. Apr 16. Saint Louis, MO.

Skills

Computer Software:

- Proficient use of Microsoft Word, Excel, and PowerPoint
- Proficient use of Adobe Illustrator and Acrobat
- Familiar with ArcGIS Desktop and ArcGIS Pro

Equipment Operation:

- Scanning Electron Microscope (SEM)
- Aerodynamic Levitation Laser Furnace
- X-Ray Defractor (XRD)

Programming Languages:

- Proficient in R and Shiny
- Familiar with HTML and CSS

Professional Affiliations

- Geological Society of America